University of Alberta

Detection of BPDE-DNA Adducts on Specific Genes

by

Chuan Wang

A thesis submitted to the Faculty of Graduate Studies and Research
in partial fulfillment of requirements for degree of

Doctor of Philosophy

Medical Sciences - Laboratory Medicine and Pathology

Spring 2014
Edmonton, Alberta

Abstract

Benzo[a]pyrene diol epoxide (BPDE), a known carcinogen, is a reactive metabolite of benzo[a]pyrene (BP). BP is usually formed during combustion of organic substances, such as cigarette smoke, automobile emission exhaust, and industrial waste burning. BPDE can covalently bind to the nucleobases of DNA. The investigation of the formation of BPDE-DNA adducts in the *p53* gene revealed a correlation between the profiles of adduct hotspots and *p53* mutation hotspots in cancers, suggesting a probable cancer-related mutation caused by BPDE-DNA adducts. Detection of BPDE-DNA adducts on specific genes is important for monitoring human exposure to this carcinogen and for studying environmental carcinogenesis.

In this thesis, two binding-induced DNA assembly (BINDA) assays for BPDE-DNA were developed to quantify the BPDE-DNA adducts in the specific *p53*-exon7. The focus on this gene was because of its relevance to cancer. In a homogeneous BINDA assay, two probes were constructed by attaching one DNA motif to an antibody against BPDE and another DNA motif to a hybridization sequence of *p53*-exon7. Cooperative binding of the two probes with the *p53*-exon7 containing BPDE adducts triggered the assembly of the two DNA motifs. Real-time qPCR quantification of the assembled DNA motifs enabled the detection of BPDE adducts in the specific gene. The second BINDA assay involved the immobilization of one DNA motif and the BPDE antibody on magnetic beads. Taking advantage of the pre-concentration and washing procedures of magnetic beads, this assay was able to achieve higher sensitivity.

Both the homogeneous BINDA and the magnetic bead-mediated BINDA assays were coupled with solid-phase extraction to analyze the BPDE-DNA adducts in the presence of complex genomic DNA. The magnetic bead-mediated BINDA assay was also applied to the detection of the BPDE-DNA adducts in the *p53*-exon7 of cells treated with BPDE. The results demonstrated the potential of the new assays for detection of DNA adducts on specific genes. The ability to quantify the DNA adducts formed on a specific sequence, rather than the overall adducts on the whole genome, opens up opportunities for further investigation into the specific DNA damage and its involvement in environmental carcinogenesis.

Acknowledgements

Without the help I received during my PhD study from the people all around me, I am sure I would not be able to finish this thesis.

My first sincere “thank you” goes to my supervisors Dr. Xing-Fang Li and Dr. X. Chris Le. Their wisdom, insightful suggestions, and guidance ensured my progress in research, writing, and logical thinking. In the past six years they helped me not only in the academic world, but also in daily life. I have learned a lot, but there is still a lot more to learn from them.

I would like to sincerely thank Dr. Hongquan Zhang for his continuous guidance on my research work. He is very energetic and is always happy to discuss my experiments. All these discussions drived me forward. I would also like to thank my supervisory committee members, Dr. Gregory Tyrrell and Dr. Liang Li, for their invaluable comments and advices throughout my study.

A special “thank you” goes to Ms. Katerina Carastathis and Ms. Dianne Sergy for their tireless administrative assistance all the time. The special “thank you” also goes to Ms. Cheryl Titus for her help in my graduate program. I want to thank all the AET Division members, particularly Dr. Yanming Liu, Dr. Shengwen Shen, Ms. Xiufen Lu and Dr. Hailin Wang. It will always be a great memory for me that I have once studied and worked with these people in the AET division.

Last but not least, I would like to say “thank you” to all my family. My parents, my grandparents, my sisters, my uncle, and all other family members have been encouraging, stimulating, and supporting me throughout my graduate study. Their love is an invaluable treasure for me in my life.

Table of Contents

List of Tables

List of Figures

List of Abbreviations

AgNC	silver nanocluster
ATP	adenosine triphosphate
AuNP	gold nanoparticle
BER	base excision repair
BP	benzo[a]pyrene
BINDA	binding induced DNA assembly
BPDE	benzo[a]pyrene diol epoxide
BSA	bovine serum albumin
CE	capillary electrophoresis
CIA	chemiluminescence immunoassay
Ct	threshold cycle
DAD	diode array spectrophotometric detector
DELFIA	dissociation-enhanced lanthanide fluoroimmunoassay
DNA	deoxyribonucleic acid
dNDP	deoxyribonucleoside diphosphate
dNMP	deoxyribonucleoside monophosphate
ECPA	electrochemical proximity assay
ELISA	enzyme-linked immunosorbent assay
FAM	carboxyfluorescein
FBS	fetal bovine serum
FRET	fluorescence resonance energy transfer
HPLC	high performance liquid chromatography

IARC	International Agency for Research on Cancer
Kd	dissociation constant
kDa	kilo daltons
LIF	laser-induced fluorescence
NER	nucleotide excision repair
NFQ	non-fluorescent quencher
n.t.	nucleotide
PAH	polycyclic aromatic hydrocarbon
PBS	phosphate buffered saline
PCR	polymerase chain reaction
PDGF	platelet-derived growth factor
PLA	proximity ligation assay
PSA	prostate-specific antigen
RCA	rolling circle amplification
RPMI	Roswell Park Memorial Institute medium
SD	standard deviation
SDS-PAGE	sodium dodecyl sulfate polyacrylamide gel electrophoresis
TEA	triethylamine
TG	tris-glycine
T_m	melting temperature
THF	tetrahydrofuran
TWJ	three way junction
UV	ultraviolet

Chapter One[1]

Introduction

1.1 General introduction

DNA damage is the underlying cause of mutations and a major cause of various cancers (*1*). The purine and pyrimidine bases are critical targets for various oxidizing or alkylating carcinogens or their active metabolites. Some of these chemicals can react with DNA to form covalently bound products that are known as DNA adducts. Adduct formation at specific sites is demonstrated to activate oncogenes or suppress tumor suppressor genes. For example, the P53 protein (or TP53, which specifically refers to the human P53 protein) encoded by the tumor-suppressor gene *p53*, is a transcription factor that inhibits cell growth and initiates cell death upon cellular stresses (*2–4*). The *p53* gene is frequently mutated in somatic cancers (*5*, *6*). Mutants of the P53 protein were not capable of binding to a specific DNA sequence and thus could not activate the downstream regulation pathway (*7*, *8*). More than 70% of mutations are missense mutations (International Agency for Research on Cancer, IARC) (*5*).

Benzo[a]pyrene diol epoxide (BPDE) is a potent carcinogen; it is the bio-transformed metabolite of benzo[a]pyrene (BP), which usually results from cigarette smoking, automobile emission exhaust and industrial waste combustion (*9*). BPDE can covalently bind to the N2 position of a guanine base and distort the

[1] A portion of this chapter has been published in H. Zhang, F. Li, B. Dever, C. Wang, X.-F. Li, X. C. Le, Assembling DNA through Affinity Binding to Achieve Ultrasensitive Protein Detection, *Angew. Chem. Int. Ed. Engl.*, 10698–10705 (2013)

DNA structure (*10*). The mapping of BPDE-*p53* adduct hotspots revealed that they were very similar to the profile of lung cancer mutation hotspots (*11*). The leading type of *p53* missense mutations is a G:C to T:A transversion, a hallmark of the BPDE induced mutation pattern (*12–14*), suggesting a probable direct cause of cancer-related mutation by BPDE-adducts (*11*, *15–17*). Detection of BPDE-DNA adducts is therefore an effective tool for monitoring human exposure to this carcinogen and for assessing cancer risk.

This chapter reviews (1) the correlation of BPDE-DNA adducts and *p53* mutations database; (2) currently available analytical techniques or assays for the detection of BPDE-DNA adducts and their limitations; (3) recently developed bio-analytical assays using the principle of binding-induced DNA assembly (BINDA).

BINDA has been used to develop sensitive and specific assays and many of these assays have been widely applied to the detection of macromolecules. BINDA could be potentially used to develop an assay for BPDE-DNA adducts formed on specific genes or sequences.

1.2 BPDE-DNA adducts background: mutation hotspots and cancer implication

1.2.1 DNA damage and cancer

DNA is represented by only one copy in most cells (considering the maternal and paternal DNA to be distinct). It is also the only biological molecule that cannot be any remanufactured and relies only on the repair of existing molecules (*1*). The integrity of DNA is mainly infringed in three way: spontaneous reactions

(*18*), endogenous metabolites, such as reactive oxygen species or reactive carbonyl species (*19*), and exogenous physical and chemical agents. Various DNA repair pathways are present in the cell, including but not limited to, base excision repair (BER, removes small modifications), nucleotide excision repair (NER, removes helix-distorting DNA damage), non-homologous end joining and homologous recombination (repair double strand breaks), and translesion synthesis (saves stalled replication) (*1*). The BPDE-DNA adducts are mainly repaired by nucleotide excision repair, which consists of global genome NER and transcription-coupled NER. Damaged DNA caused by those factors could generate mutations if they are not repaired in time.

DNA damage is highly correlated to the initiation of carcinogenesis by induction of mutations. Mutations of many genes could cause cancers. These genes include oncogenes, tumor suppressor genes, and repair genes (*3*).

Benzo[a]pyrene is present at 20 ng to 40 ng per cigarette (*20*). Its biotransformation form, benzo[a]pyrene diol epoxide, is highly electrophilic and reactive (*21*). Although many reports showed that BPDE could covalently bind to various cellular macromolecules, formation of adducts with DNA is the major reason for damage caused by BPDE (*21–25*). The hallmark G-T transversion mutation caused by BPDE-DNA adducts in lung tumors from smokers is different from the mutation in tumors from nonsmokers (*26*), indicating that BPDE produced through cigarette smoking is a type of carcinogenic lesion.

1.2.2 *p53* mutation hotspot and correlation to cancer mutation hotspots

p53 is one of the most studied tumor suppressor genes. The International

Agency for Research on Cancer (IARC) compiles all the genetic variations reported in p53 into the TP53 database (*27*). The mutated codon distribution is illustrated in Figure 1.1. It can be concluded from Figure 1.1 that not all 393 codons of the *p53* gene are mutated with equal opportunity. Instead, several codons mutate with a much higher incidence than all the other codons, such as codons 175, 248 and 273. It had been known that the G-T transversion caused by BPDE-DNA adducts is very common in lung cancer cases, but it was unclear whether the transversion was directly induced by BPDE. To investigate this problem, Pfeifer and coworkers used ligation-mediated PCR to map the distribution of BPDE-*p53* reaction hotspots (*11*) (Figure 1.2 lower graph). The incidence of adduct formation on each codon is expressed as relative intensity compared to codon 157. Surprisingly, these two hotspots profiles were highly correlated (Figure 1.2). This coincidence strongly suggested that BPDE was directly involved in the transformation of lung tissue. Therefore, detecting the BPDE-DNA adducts in human tissues or blood samples is of great importance in monitoring the exposure to this carcinogen and assessing the risk of developing a cancer.

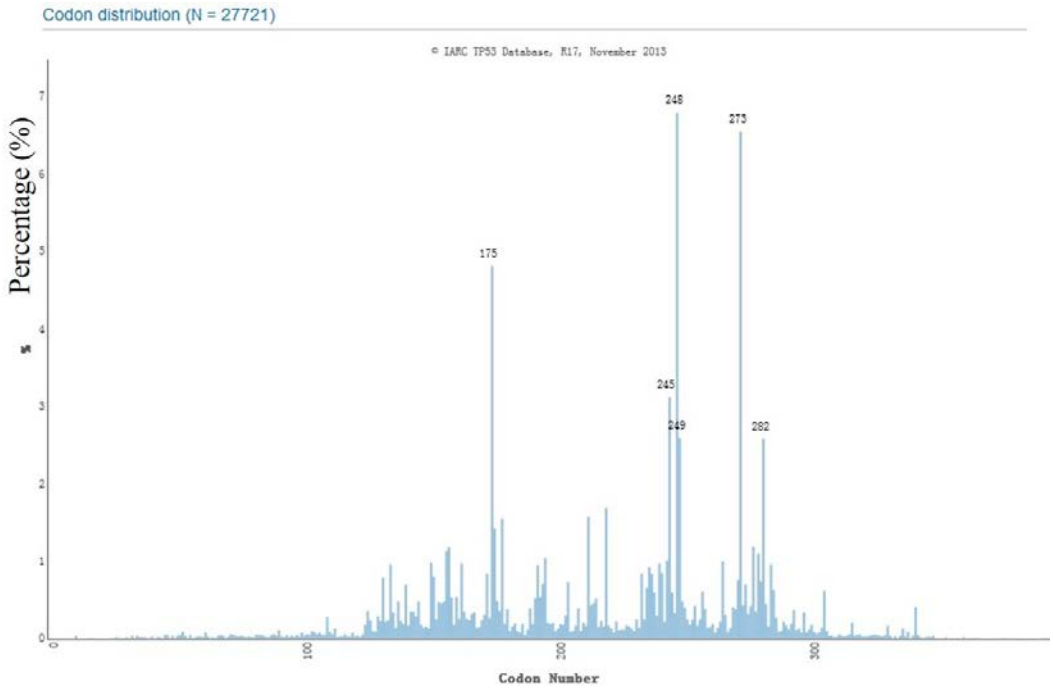

Figure 1.1 Mutation codon distribution of the *p53* gene in somatic cancers (IARC TP3 database, updated in November 2013).

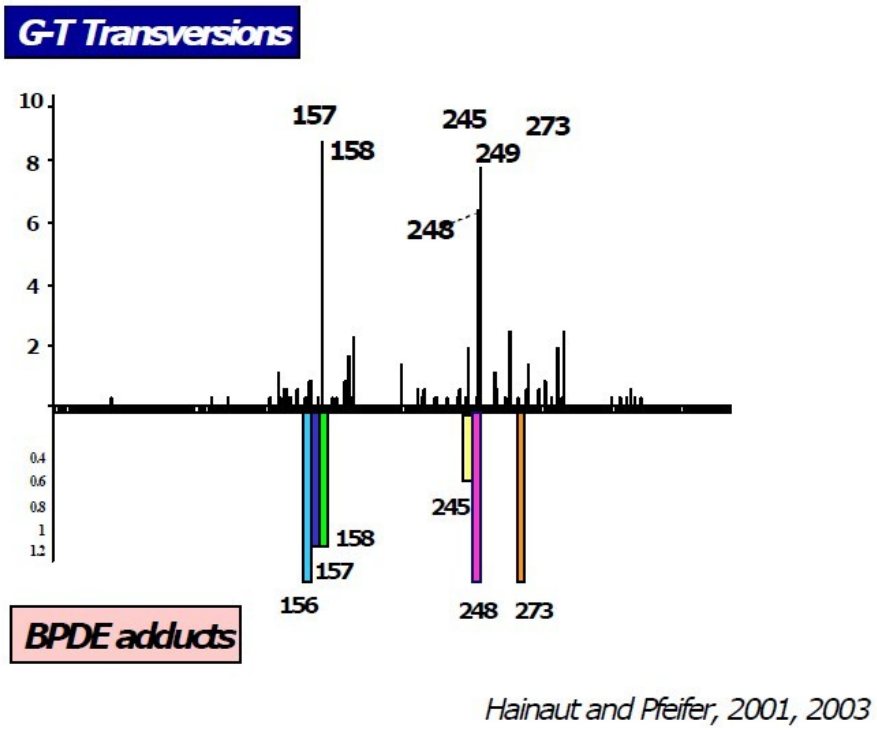

Figure 1.2 Correlation between mutation hotspots and adduct hotspots. The upper graph: G-T transversion induced by BPDE. The Y coordinate represents the percentage of transversions at that codon in all transversions. The lower graph: BPDE-*p53* adduct hotspots in BPDE-treated cells. The Y coordinate represents the relative quantity of adducts at that codon compared to codon 157.

1.3 Analytical methods for BPDE-DNA adducts

Several analytical techniques have been developed for quantification of DNA adducts, including ^{32}P-postlabeling (*28–30*), enzyme-linked immunosorbent assays (ELISA) (*31–33*), dissociation-enhanced lanthanide fluoroimmunoassay (*34*, *35*), chemiluminescence immunoassay (*36*), capillary electrophoresis–laser induced fluorescence immunoassays (*37–39*), and comet assay (*40*). However, all

these techniques are unable to provide information on the position of adducts.

On the other hand, DNA modification mapping assays, such as ligation-mediated PCR and transferase-dependent PCR, are capable of rendering sequence information of adduct sites and have already successfully explored the distribution of methylation (*41*), pyrimidine (6-4) pyrimidone photoproducts (*42*), BPDE-adducts (*11*), and acrolein-DNA adducts (*43*). However, their application is highly limited due to their low sensitivity, and their time-consuming and laborious procedures. Moreover, ligation-mediated PCR is not quantitative.

1.3.1 Enzyme-Linked Immunosorbent Assay

Weistein and coworkers used ELISA for detection of BPDE-DNA adducts (*31–33*). They coated denatured BPDE-modified calf thymus DNA on the microtiter plate and employed rabbit antiserum for the BPDE-DNA recognition. Alkaline phosphatase conjugate was used as the enzyme for signal output. DNA samples prepared from human lung tissue, tumor tissue or peripheral blood cells were added to the competitive ELISA for quantification. A detection limit of 0.08-0.10 fmol/μg DNA was achieved. This equals to 1 adduct in 10^5 nucleotides.

1.3.2 Nuclease P1 mediated ^{32}P Post-labeling

Randerath and coworkers reported a ^{32}P post-labeling assay for BPDE-DNA quantification (*29*). The BPDE-DNA sample was first enzymatically digested to single dNMPs, and then converted to [5'-^{32}P]dNDPs by T4 polynucleotide kinase-catalyzed [^{32}P] transfer from [γ-^{32}P]ATP. The ^{32}P-labeled BPDE-nucleotides could then be separated from the normal nucleotides by thin layer chromatography and quantified by autoradiography. The detection limit could reach 1 adduct in 10^8

nucleotides. Reddy and Randerath then modified the assay by adding nuclease P1 before ^{32}P-labeling (*30*). The P1 nuclease would cleave the monophosphate group of normal dNMPs, therefore reducing the background signal. This modification improved the sensitivity to 1 adduct in 10^{10} nucleotides.

1.3.3 Dissociation-enhanced Lanthanide Fluoroimmunoassay (DELFIA) and Chemiluminescence Immunoassay (CIA)

The Dissociation-Enhanced Lanthanide Fluoroimmunoassay (DELFIA) is also an immunoassay, adapted from the ELISA introduced in 1.3.1. Poirier and coworkers changed the signal output strategy from a alkaline phosphatase-catalyzed substrate reaction to a biotin-europium-labeled streptavidin signal amplification system (*35*). Based on this new signal generation strategy, they achieved a detection limit of 4 adducts in 10^8 nucleotides, if using 35 μg of DNA samples per microtiter plate well. Chemiluminescence immunoassay (CIA) was another modification of ELISA by incorporating chemiluminescence as the signal readout. The detection limit was further increased by 10-fold, compared to the DELFIA (*36*).

1.3.4 Capillary Electrophoresis Laser Induced Fluorescence

Le and coworkers combined the immuno-affinity with the capillary electrophoresis laser induced fluorescence for sensitive BPDE-DNA adduct detection (*37*, *38*). In this assay, the primary antibody was used to recognize BPDE-DNA adducts and the secondary antibody was labeled with a fluorophore bound to the primary antibody. The mass charge ratio of the DNA-antibody complex was larger than the secondary antibody and primary-secondary antibody

complex, and therefore three components were resolved in the CE column. The fluorescently labeled secondary antibody served as the signal readout for laser induced fluorescence quantification. Wang and coworkers further improve the detection limit (6.6×10^{-21} mol in absolute quantity and 120 fM in concentration) by incorporating quantum dots with excellent fluorescence properties (*39*).

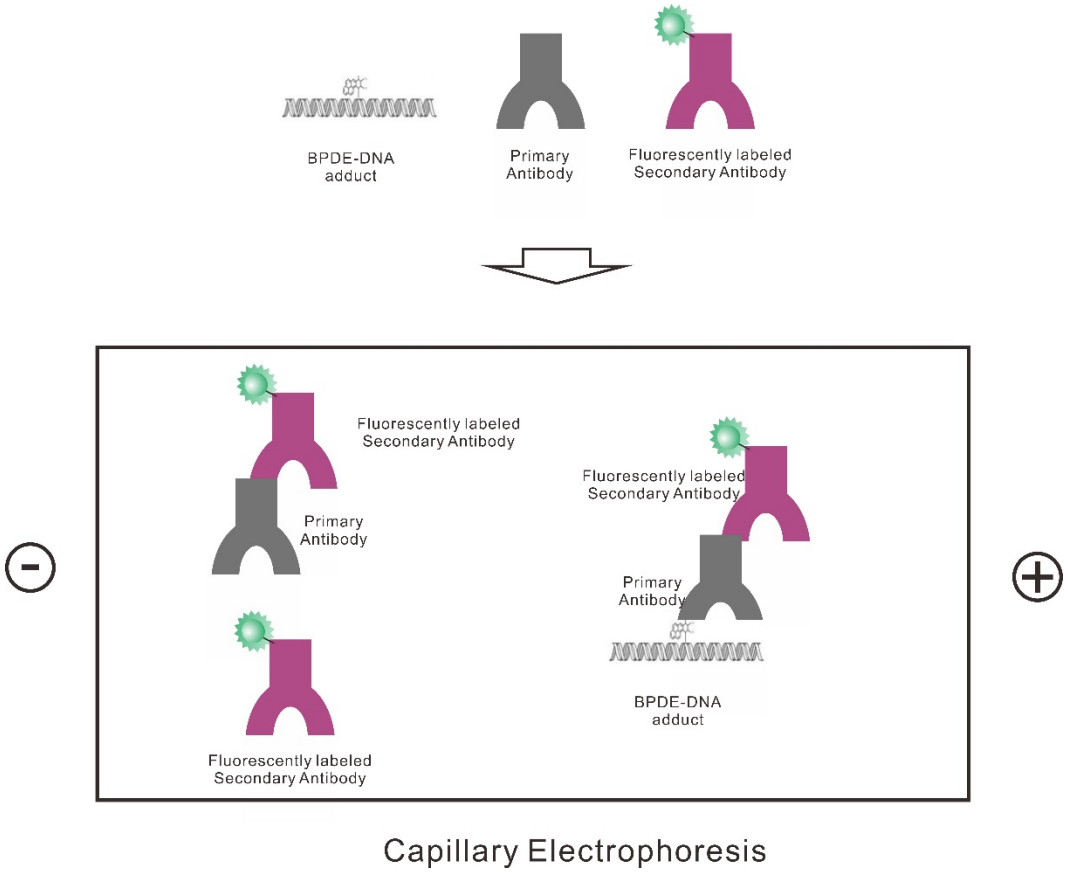

Figure 1.3 Schematic of capillary electrophoresis–laser induced fluorescence immunoassays for BPDE-DNA adducts. Adapted from Ref (*39*). A primary antibody binds to the BPDE-DNA adduct and itself is then bound by a fluorescently labeled secondary antibody.

1.3.5 Ligation-mediated PCR

Pfeifer and coworkers initially introduced ligation-mediated PCR for methylation analysis (*41*). They later applied this assay for the mapping of BPDE-DNA adduct hotspots (*11*). In this assay, a chemical or an enzyme was first used to cleave the DNA sequences at multiple positions with chemical modifications (methylation, BPDE adduct, etc.) (Figure 1.4). After the incision, the DNA was denatured and a primer designed for the region close to one end of the DNA sequence was introduced for extension. The incision site now was a blunt end, allowing for the ligation of an adapter. Then the primer for extension and another primer designed for the adapter were added to the incubation for PCR amplification. The PCR products were finally separated on a sequencing gel (with single nucleotide resolution). Based on the length of the product, the site of modification could be obtained. Although the ligation-mediated PCR assay was sensitive in the detection of modifications, it was relative quantification. No absolute modified quantities could be derived from the data. Therefore, highly sensitive and easy-to-operate methods capable of determining the quantity of DNA adducts within specific genes are still required.

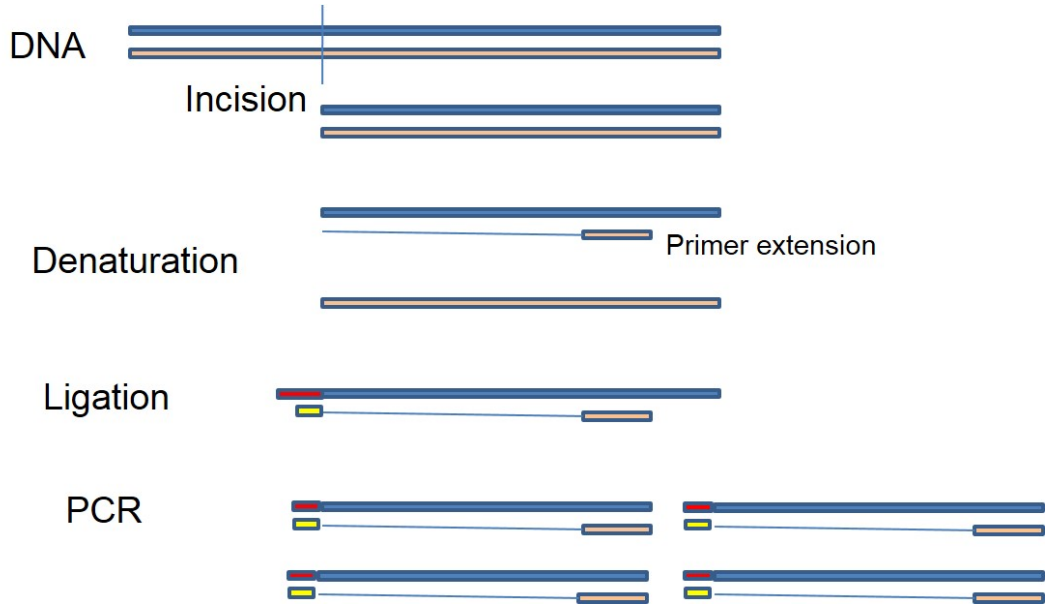

Figure 1.4 Schematic of ligation-mediated PCR. First a chemical or an enzyme was used to cleave the DNA sequences at positions with chemical modifications. After incision, the DNA was denatured and a primer designed for the region close to one end of the DNA sequence was introduced for extension. With a blunt end after the primer extension, an adapter was ligated at the modification site. Then the primer for extension and another primer designed for the adapter were added to the incubation for PCR amplification. The PCR products were finally resolved on a sequencing gel to reveal the modification sites.

1.4 Binding Induced DNA assembly

Combining target recognition with signal amplification is the main strategy for developing bio-analytical assays for macromolecules. In the 1990s, after the introduction of immuno-PCR (*44*), which used antibody for recognition and a DNA tag that conjugated on the antibody for subsequent signal amplification,

tremendous research work and applications based on this technique were reported (*45–47*). A major breakthrough of immuno-PCR is its high sensitivity, making use of the applicability for exponential amplification of DNA molecules. However, the operational complexity and background issue still drive researchers for better bio-analytical assays. In the past decade, methods taking advantage of affinity binding and DNA assembly have been developed (*48–53*). These assays were built on a "binding induced DNA assembly strategy". They shared a feature with immuno-PCR: target quantification was achieved by amplifiable DNA. On the other hand, two new features made these new assays different from immuno-PCR: (1) the DNA for detection was assembled after multiple affinity ligands (normally two) bind to one target molecule rather than a simple DNA tag conjugated to one affinity ligand; (2) these assays were homogeneous, without need for separation. In this section, the principle of binding induced DNA assembly and some assays related to this strategy are summarized.

1.4.1 Principle of binding induced DNA assembly

The term "DNA" usually refers to the double helix structure discovered by Watson and Crick in 1953 (*54*). The double helix structure is primarily maintained by two forces: hydrogen bonds between nucleotides and base-stacking interactions among aromatic nucleobases (*55*). However, the structure is highly associated with many other factors, such as salts in the solution and temperature. To better understand the thermodynamics of DNA, the melting temperature (T_m) is first introduced. T_m refers to the temperature at which half of the DNA molecules are in the random coil or single-stranded (ssDNA) state.

Suppose there are two short complementary sequences, 5'-GCCACG$(T)_{20}$-3' and 5'-$(T)_{20}$CGTGGC-3'. They could hybridize and form a duplex, with an estimated T_m of lower than 10˚C (estimated by IDT Oligo Analyzer 3.1, under parameters of 1 nM DNA, 1 mM Mg^{2+}, and 50 mM Na^{+}). This T_m indicates that the duplex between these two complementary sequences are unstable at room temperature. Now if we consider that the two sequences are linked together as a single oligonucleotide, 5'-GCCACG$(T)_{40}$CGTGGC-3', the complementary sequences at the two ends of this strand could hybridize and form a stem-loop (or hairpin) structure. The T_m for this hairpin structure is 53˚C, which is much higher than room temperature (Figure 1.5 A). Therefore, this hairpin structure formed by the same complementary sequences is stable at room temperature.

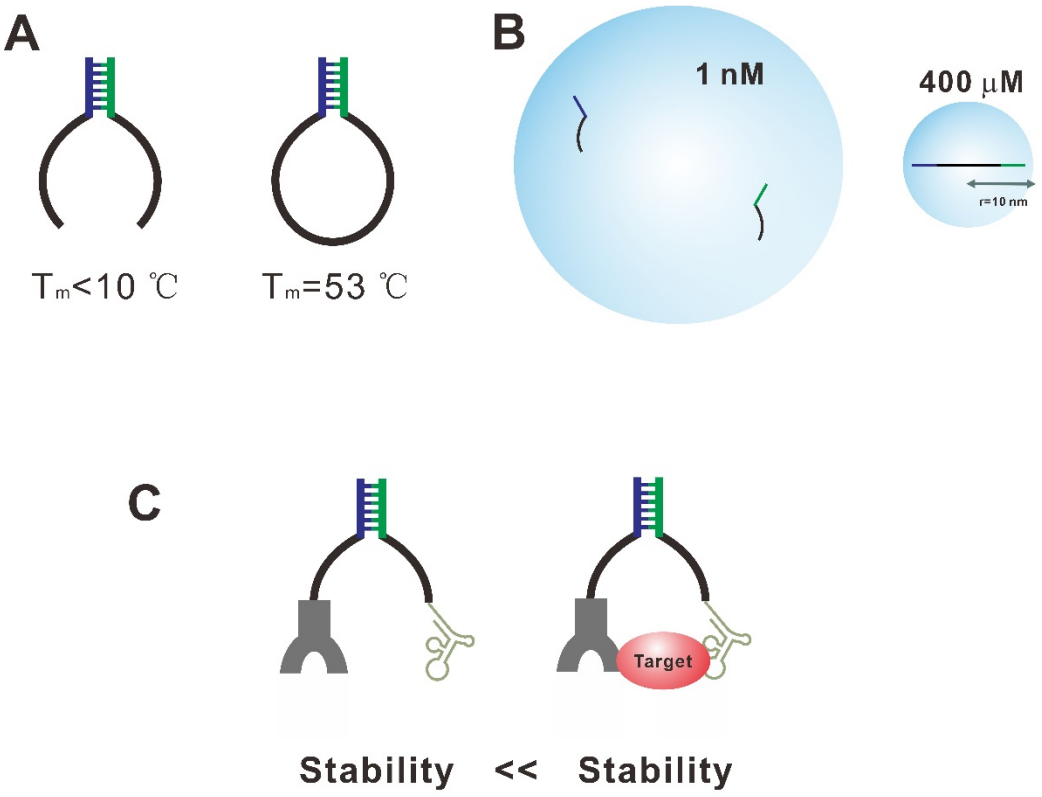

Figure 1.5 Increase of effective local concentration in intramolecular structure (adapted from Ref *56*). (A) The T_m of two short complementary sequences is much lower than the T_m of the hairpin structure of the same sequences linked by poly-T_{40}. (B) Effective local concentration is significantly increased in the intramolecular hairpin structure. (C) Expand the concept of hairpin structure to affinity ligand–target ternary complex. Antibody and aptamer were used to illustrate the affinity binding to the target molecule.

The reason for this significant increase of stability (quantitatively compared by T_m) is due to the enhancement of effective local concentration (*56*). Consider two complementary sequences, 5'-GCCACG$(T)_{20}$-3' and 5'-$(T)_{20}$CGTGGC-3', are dissolved at 1 nM in the solution. If the hairpin structure of two strands joined

by Poly-T_{40}, 5'-GCCACG$(T)_{40}$CGTGGC-3', is in the solution with the same concentration, the intra-molecular distance of two short complementary sequences is less than 20 nm (Figure 1.5 B). If we calculate the local effective concentration of two complementary DNA molecules within a sphere that contains one hairpin structure molecule, whose radius is 10 nm, these oligonucleotides have local concentrations of greater than 400 μM (*56*). This effective local concentration of the complementary sequences is 400,000 times the concentration of the two separate complementary sequences. At this concentration, the T_m for two separate complementary strands is 43˚C. The calculation revealed the most important reason for the increased stability of the hairpin structure: effective local concentration.

Based on this idea, the intramolecular hairpin structure can be expanded to affinity ligand–target complex (Figure 1.5 C). Each of the two complementary sequences is attached to an affinity ligand, forming two affinity probes that recognize different epitopes on the target molecule. Once the two affinity ligands bind to one target molecule, the affinity ligand–target ternary complex will change the concentration of two complementary sequences into intramolecular local concentration ($>10^5$-fold increase). On the other hand, the free complementary sequences in the solution are still at low concentration. In this way the duplex formed within the affinity ligand–target ternary complex is much more stable than the free complementary sequences. In other words, the complementary sequences can be assembled through target binding.

Many assays have been developed on this binding-induced DNA assembly

principle. Various designs of the DNA motifs and uses of different affinity ligands, such as antibodies and aptamers, have been reported (*56*, *57*).

1.4.2 Proximity Ligation Assay

Proximity ligation assays (PLA) use affinity binding to bring oligonucleotide probes into close proximity, enabling subsequent DNA ligation (*53*). The detection of a target macromolecule or complex is converted to the detection of new DNA strands that are formed by ligation (*58*). A pair of DNA probes, each conjugated to a specific affinity ligand recognizing the target, are brought into close proximity upon two binding events (*53*). Two DNA probes then hybridize with a connector oligonucleotide, facilitating the enzymatic ligation of the two DNA probes (Figure 1.6 A). Various techniques can then be used to amplify and detect the new ligated DNA strand (*58*). While the concentration of the connector oligonucleotide is usually more than 10,000-fold higher than the concentrations of the DNA in the affinity probes, hybridization of two DNA probes with the connector oligonucleotide only takes place when both affinity probes bind to the same target molecule. Essentially, through affinity binding the local concentrations of both DNA probes are greatly increased to favor stable hybridization with the connector oligonucleotide. Stable hybridization of the DNA probes with the connector is required for subsequent ligation to form a new DNA strand for amplification and detection. Background signal is generated from target-independent hybridization of two DNA probes with the connector. Therefore, the length of the connector oligonucleotide is crucial for controlling the signal-to-background ratio. Landegren and co-workers first used this strategy

in combination with real-time PCR to detect a homodimer of platelet derived growth factor (PDGF-BB) (*53*). Aptamers for PDGF-BB served as the affinity ligands and were extended to constitute the DNA probes. They successfully achieved a detection limit of 24,000 molecules of PDGF-BB in a 5 µL sample.

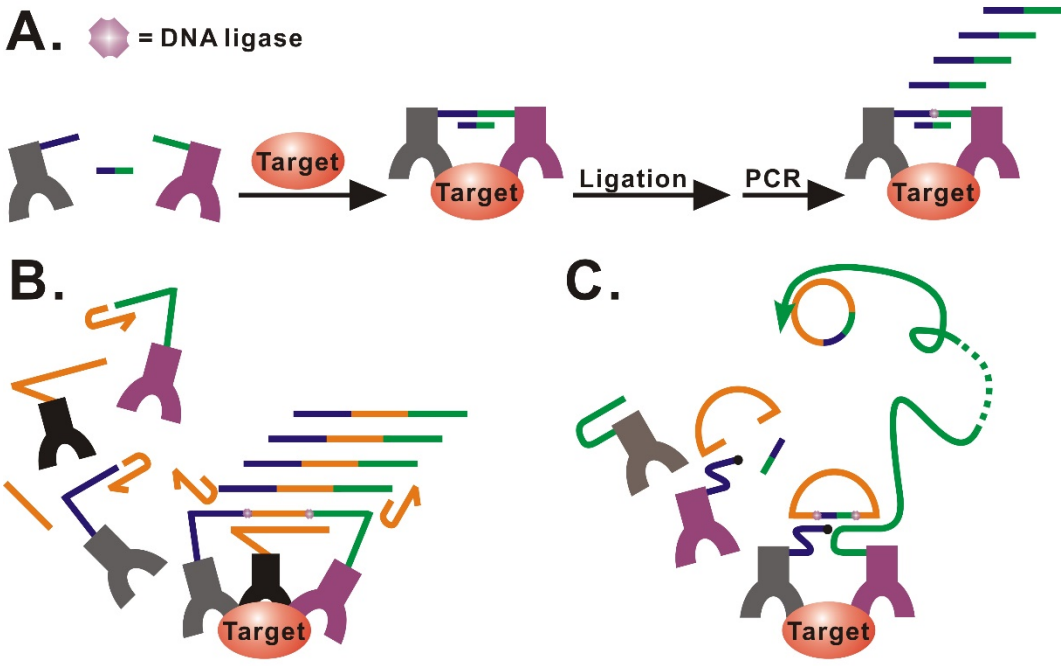

Figure 1.6 Proximity ligation assay and its variants (reprinted with permission from Ref *56*). (A) Principle of the proximity ligation assay. (B) 3PLA using an extra affinity ligand bearing the connecting oligonucleotide. (C) In situ PLA using a circularizable oligonucleotide for rolling circle amplification.

Another strategy was later introduced that involved a third affinity probe bearing the connector oligonucleotide (*59*). This variant was named 3PLA because it used three affinity probes, compared to the original assay (named 2PLA

thereafter) that used two affinity probes. In the 3PLA format, three monoclonal or polyclonal antibodies recognizing distinct epitopes of a target molecule were covalently conjugated to three oligonucleotides (two DNA probes and one connector oligonucleotide), forming three antibody–oligonucleotide probes. Binding of the three affinity probes to the same target molecule facilitated the hybridization of the two DNA probes to the connector oligonucleotide and a cassette oligonucleotide to result in two ligation events. The newly ligated DNA strand was then amplified and detected (Figure 1.6 B). The requirement of a target molecule binding to three affinity probes enhanced the specificity and reduced the background signal, thus improving the detection ~100-fold. Using 3PLA, a detection limit of 60 molecules of vascular endothelial growth factor (VEGF) in 5 µL buffer was achieved. Tavoosidana *et al*. (*60*) developed a 4PLA assay to detect prostasome, a microvesicle with a mean diameter of 150 nm, which is secreted by prostate cells. This 4PLA required the use of four antibodies to bind to four different proteins on the prostasome surface. Each antibody was conjugated to an oligonucleotide probe. Binding of the four probes to the prostasome vesicle was followed by two ligation events, generating a new DNA strand that was amplified for detection.

PLA has been combined with rolling circle amplification (RCA) (*61*) (Figure 1.6 C). Two affinity probes were incubated with fixed cells or tissue, and two binding events triggered the ligation between the circularizable probe and the connector oligonucleotide, forming a circular DNA product after ligation. The circular DNA served as the template for RCA to produce hundreds of repeating

units that subsequently hybridized with fluorescent probes, generating *in situ* signal for direct observation under a microscope. *In situ* PLA has been used to detect phosphorylated PDGF receptor β (*62*) and screen for inhibitors of PDGF receptor β in cells (*63*). *In situ* PLA has also been applied to study protein–protein interactions, DNA–protein interactions (*64*), and RNA–protein interactions (*65*). For example, MUC2 was demonstrated to be a major carrier of the cancer-related sialyl-Tn antigen in gastric carcinoma (*66*), and MUC1 extracellular domain subunit was confirmed to be associated with spliceosomes found in nuclear speckles (*67*). Coupling of *in situ* PLA with flow cytometry was used to study interactions between EGF receptor family members and HER2 as well as post-translational modification effects after stimulation by EGF in single cells (*68*).

Multiplexed PLA, which has been applied to high throughput screening, makes use of DNA probes as barcodes (*69–71*). These barcode sequences serve as primer sites for subsequent real-time PCR quantification (*69*). Solid-phase PLA has also been used for high throughput analyses (*72*, *73*), and could also detect target molecules in complex biological matrices (*74–76*). 2PLA has also been modified with a proximity extension assay (PEA), in which ligation is replaced with extension (*77*). Various formats of PLA have been used to detect proteins (*53*, *78*), protein complexes (*79*), and single virus particles (*80*), to screen for inhibitors of protein–protein interaction (*81*), and to determine the binding specificity of DNA binding proteins (such as P53, HNF-4α) to different double stranded DNA sequences (*82*).

1.4.3 Binding-Induced DNA Annealing Assays

Binding-induced DNA annealing assays are a series of assays developed for proteins based on DNA assembly upon target binding. Similar to what we discussed in Section 1.4.1, short complementary sequences were designed on the DNA probes such that the duplex formed under experimental concentration and temperature was unstable (T_m << experimental temperature) (Figure 1.7 A). Binding of two DNA probes to the same target molecule formed the probes–target ternary complex structure. The concentration of DNA probes within the ternary complex was the intramolecular concentration, which was also the local effective concentration. At this local effective concentration, the T_m of the two DNA probes was now much higher than the experimental temperature, making the duplex formed inside the probes–target ternary complex very stable. The detection of target molecules could then be converted to the quantification of annealed DNA probes.

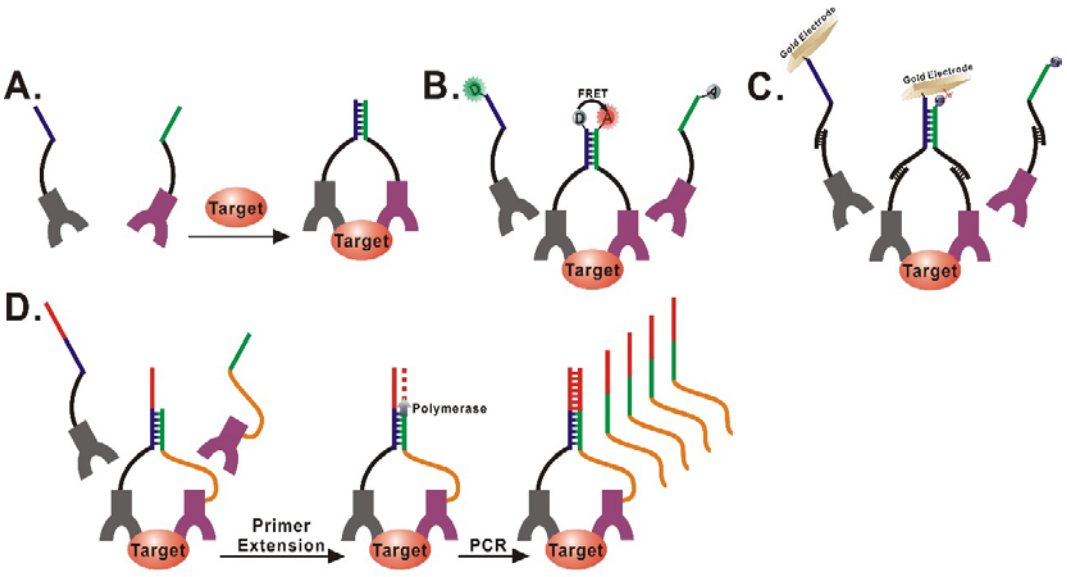

Figure 1.7 Binding-induced DNA annealing assays (reprinted with permission from Ref *56*). (A) Principle of the binding-induced DNA annealing assay. (B) FRET-based binding-induced DNA annealing assays (*52*, *83–87*). (C) Electrochemical binding-induced DNA annealing assay (*88*). (D) Binding-induced DNA annealing assay with primer extension and PCR amplification (*48*).

Heyduk and coworkers first reported a series of bio-sensors based on the principle of binding-induced DNA annealing and used fluorescence resonance energy transfer (FRET) to output the signal (Figure 1.7 B) (*52*, *84–87*, *89*). In these assays, a pair of short DNA oligonucleotide probes, one labeled with a fluorescence donor and one with a fluorescence acceptor were conjugated to a pair of affinity ligands that could bind to different epitopes on the surface of the protein target. Several types of affinity ligands, such as antibodies, peptides, and aptamers were used in their studies. No efficient FRET could occur at the

concentration of the two DNA probes used in the assay. Only when the fluorescence donor and acceptor were in close proximity (< 5 nm) could the FRET be observed and therefore this proximity could only be achieved upon the annealing of the two DNA probes. After the binding of two DNA probes to the target molecule, formation of probes–target ternary complex led to the stable duplex between the two DNA probes and the FRET signal output.

Heyduk and coworkers applied this assay for sensitive detection of thrombin (*52*), insulin (*84*), cardiac troponin I (*85*), and C-reactive protein (*86*), and a low pico-molar range of detection limits was obtained for these applications.

Besides FRET, other signal output methods were also developed for binding induced DNA annealing assays, such as electrochemical signal reading (*88*), polymerase chain reaction (PCR) (*48*), and rolling circle amplification (RCA) (*90*).

Easley and coworkers combined the binding-induced DNA annealing with electrochemical detection (Figure 1.7 C) (*88*). In their electrochemical proximity assay (ECPA), the gold electrode was modified by one DNA probe through a thiolated gold bond and the other DNA probe was conjugated to methylene blue (MB) which is an electron transfer donor. Both probes were connected to an affinity ligand. When two different DNA probe molecules bound to the same target molecule, close proximity of MB to the gold electrode leads to greatly enhanced electron transfer from MB to the gold electrode. This enhanced electron transfer was represented by the electrical current increase. Easley and coworkers used thrombin aptamer-modified DNA probes and insulin antibody-modified

DNA probes for the ECPA sensor construction and applied these sensors to detect thrombin and insulin, respectively. A detection limits of 50 pM for thrombin and 128 fM for insulin were obtained by this assay.

Liu and coworkers used DNA polymerase-mediated primer extension reaction followed by PCR to amplify the intramolecular DNA duplex formed in the binding-induced DNA annealing assay (Figure 1.7 D) (*48*). One DNA probe was extended by a long overhang sequence which provided the template for the primer extension reaction (shown in red in Figure 1.7 D). No primer extension reaction could occur because the complementary sequences of the two DNA probes were so short that the minimum stable duplex would be formed under experimental conditions. When target molecules were introduced to the system, binding-induced DNA annealing resulted in a stable intramolecular DNA duplex, allowing the primer extension reaction to start. The newly formed DNA strand from the primer extension reaction (red-green-orange color in Figure 1.7 D) was then amplified and quantified by PCR. Liu and coworkers first applied this assay for streptavidin analysis and then developed a multiplexed format for the identification of ligand–target pairs. A detection limit of 200 zeptomole for streptavidin was achieved. Their multiplex assay could differentiate a wide range of affinities for ligand–target pairs from protein/small molecule libraries.

King and coworkers applied the primer extension reaction and RCA to quantify the intramolecular DNA duplex (*90*). Two DNA aptamers for thrombin were modified to construct the affinity DNA probes. One aptamer was extended to form a circular DNA template, and the other aptamer was extended to a short 3'

overhang that could only hybridize with the circular aptamer when both aptamers were bound to the same thrombin molecule. After the formation of the aptamers–thrombin ternary complex, the annealed overhang and the circular aptamer triggered the RCA reaction which produced an elongated DNA consisting of repeat units of the template sequence. A detection limit of 30 pM was obtained for thrombin analysis by this strategy.

1.4.4 Assays based on binding-induced DNA assembly

Le and coworkers have developed the concept of binding-induced DNA assembly (BINDA) for protein detection (*91*, *92*). BINDA assays could also be applied to assemble functional nanostructures (*49*, *51*, *93*). The principle behind BINDA is similar to those of the proximity ligation assay (PLA) and binding-induced DNA annealing assay. Generally, specially designed DNA motifs were not able to assemble in the free solution under experimental conditions, due to the low T_m. Once the target molecules were introduced, the formation of an affinity probe–target ternary complex triggered the directed assembly of DNA motifs (Figure 1.8 A). The assembled DNA motifs could then be used for the following signal readout or signal transduction.

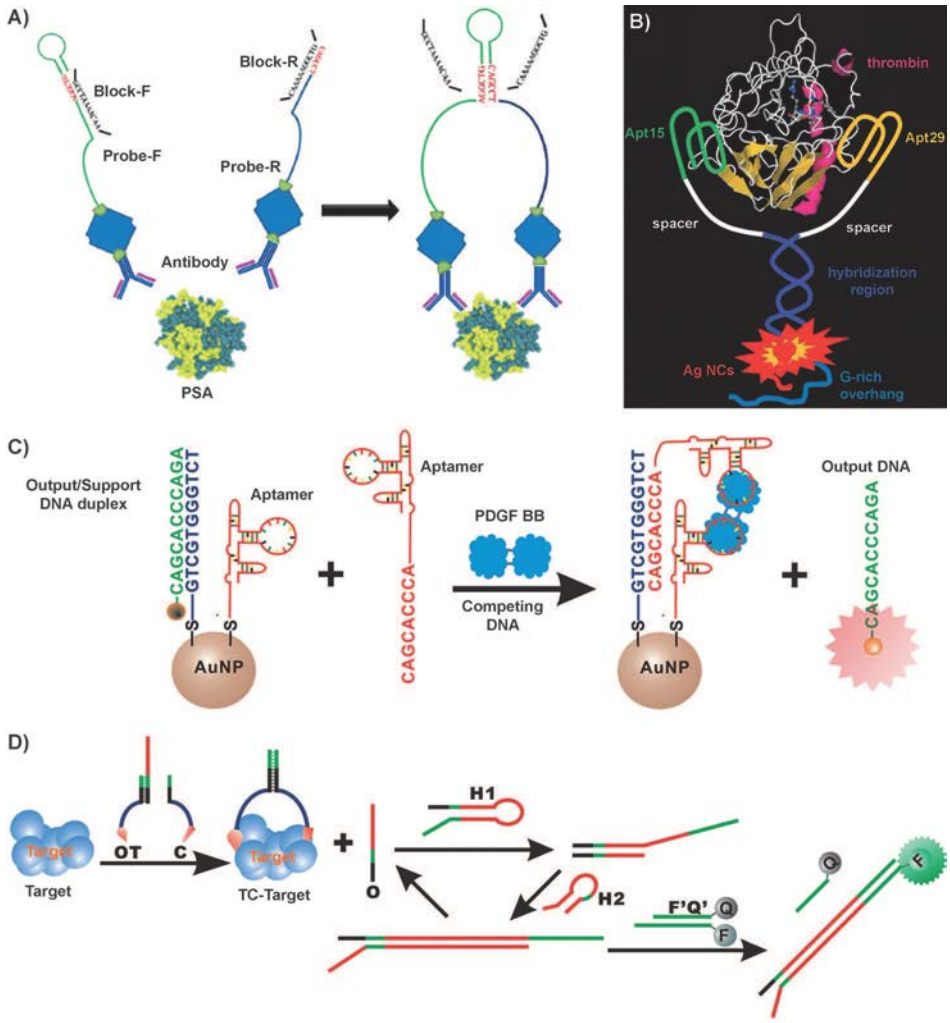

Figure 1.8 Assays based on binding-induced DNA assembly (BINDA) (reprinted with permission from Ref *56*). (A) BINDA assay for protein detection. PSA=prostate-specific antigen. Probe-F and Probe-R are DNA motif-tethered affinity ligands which recognize the target protein. Block-F and Block-R are blocking oligonucleotides that are used to minimize target-independent assembly. (B) Incorporation of BINDA to silver nanoclusters (AgNCs). The guanine-rich DNA sequence could enhance the fluorescence signal intensity. (C) Binding-induced molecular translator on a gold nanoparticle scaffold (AuNP). (D)

Binding-induced strand displacement with a catalytic DNA circuit for signal amplification of output DNA. F=fluorophore, Q=quencher, OT=output DNA motif, O=output DNA, C=competing DNA motif, T=support DNA, H1 and H2=DNA hairpins.

Le and coworkers first used the BINDA strategy and aptamers or antibodies conjugated DNA motifs for protein analysis (Figure 1.8 A) (*91*, *92*). Two DNA motifs contained complementary sequences that were too short to assemble at low concentration in the free solution due to the designed low T_m. To further reduce the target-independent DNA assembly, a pair of blocking oligonucleotides were introduced to compete with the hybridization between complementary sequences. The blocking oligonucleotides were designed to be longer than the complementary sequences in the DNA motifs (T_m of blocking oligonucleotides were higher than that of complementary sequences). Besides, much higher concentrations of blocking oligonucleotides than of the complementary sequences were used in the assay (~1000 fold). Combining these factors, the target-independent DNA assembly was minimized. In the presence of the target molecules, two DNA motifs were brought into proximity through target binding and the increased effective local concentration pushed up the T_m of the complementary sequences, allowing the DNA motifs to assemble at the experimental temperature (room temperature). DNA ligase was then introduced to the two DNA motifs to form a new DNA sequence for quantification by real-time qPCR.

Le and coworkers used this strategy for detection of streptavidin, platelet derived growth factor (PDGF), and prostate specific antigen (PSA) (*92*). Detection limits of yoctomole to zeptomole range and a dynamic range of over five orders of magnitudes were achieved.

Le and coworkers further applied BINDA to assemble functional nanomaterials (*49, 51, 93, 94*). They incorporated silver nanoclusters (AgNCs) into the BINDA for thrombin analysis (*93*). Guanine-rich DNA sequences could enhance the red fluorescence of AgNCs up to 500-fold when in proximate distance with AgNCs (*95*). Le and coworkers extended two aptamers by AgNCs nucleation sequence and G-rich sequence, respectively. A few complementary nucleotides that only hybridize in proximity were also added to the ends of each aptamer (Figure 1.8 B). When the AgNCs nucleated aptamer and G-rich aptamer were incubated with the thrombin, target binding-induced DNA assembly took place and the enhanced red fluorescence was used for thrombin quantification.

A binding-induced molecular translator was built by assembling DNA motifs on a gold nanoparticle (AuNP) scaffold and this molecular translator was successfully used for protein detection (Figure 1.8 C) (*49*). In this assay, one affinity ligand was conjugated to the AuNP and the other affinity ligand was conjugated to a competing DNA probe. A fluorophore-labeled output DNA was pre-hybridized to the supporting DNA on the AuNP scaffold and the fluorophore was quenched by AuNP. The competing DNA contained shorter complementary sequences to the supporting DNA than the output DNA. No output DNA was released from AuNP because the higher T_m led to preferential hybridization of

output DNA to the supporting DNA. After the incubation of the molecular translator with target molecules, binding of one target molecule to the two aptamer molecules brought the competing DNA onto the AuNP scaffold, greatly increased the local effective concentration of DNA probes and initiated DNA strand displacement between the competing DNA and the output DNA. The released fluorophore-labeled output DNA from the AuNP scaffold could then be used to indirectly quantify the target. Similarly, a DNA three-way junction (DNA TWJ) was constructed through target binding and the following strand displacement provided an indirect method for target detection (*94*).

In another study, the output DNA was directed to trigger a subsequent dynamic DNA assembly to further amplify the signals (Figure 1.8 D) (*51*). The signal was amplified through a binding-induced catalytic DNA circuit consisting of DNA hairpin H1 and H2. The H1 and H2 could not hybridize with each other because the complementary sequences were caged in the stems of hairpins (T_m in the hairpin was much higher). The released output DNA resulting from target binding opened the H1 hairpin through toehold-mediated strand displacement. Then the H1/H2 duplex triggered another strand displacement to release the output DNA for the next round. In this way, output DNA catalyzed the formation of H1/H2 duplexes and amplified signals for target detection.

1.5 Rationale and Scope of the thesis

Sensitive quantitative analytical techniques, such as ^{32}P-postlabeling (*28–30*), ELISA (*31*, *32*), DELFIA (*34, 35*), chemiluminescence immunoassay (*36*),

CE-LIF (*37*, *38*), and comet assay (*40*) are available for detection of BPDE-DNA adducts; however, these assays cannot provide information on the position of the adducts. While the ligation-mediated PCR (LM-PCR) could identify the adduct positions, it is unable to quantitatively measure the adducts. Therefore, we propose here to develop a unique technique that can provide highly sensitive and quantitative analysis of BPDE-DNA adducts and is capable of locating the position of the adducts on specific genes.

The recent developed binding induced DNA assembly (BINDA)-based assays have demonstrated sensitive and specific detection of many macromolecules, particularly proteins. Similar to immuno-PCR, the BINDA assay used DNA for the signal readout, providing an indirect measurement of unamplifable target proteins by amplifiable DNA. But unlike immuno-PCR, BINDA relies on the interactions of two or more different affinity probes with a single target molecule. The BINDA technique demonstrates two advantages over immuno-PCR: (1) the DNA for signal output is assembled by two probes, therefore no signal could be generated without the presence of the target; (2) the assembly of two probes occurs only when two probes bind to one target molecule, increasing the specificity of the affinity recognition. These advantages result in the homogeneous format of BINDA and low background signal compared to immuno-PCR (*53*). Homogeneous assays could also simplify the experimental procedures.

Consider the BPDE-DNA adduct as a macromolecule with two epitopes: one is the BPDE molecule for antibody recognition, the other is the DNA sequence

that could be recognized by a complementary sequence. Then a BINDA-based assay could be developed for the BPDE-DNA adducts if we construct two probes by attaching one DNA motif to an antibody against BPDE and the second DNA motif to a hybridization sequence for the target sequence. The objective of this thesis was to develop a BINDA-based assay for quantitative analysis of BPDE-DNA adducts on a specific gene. In this thesis, BPDE-*p53*-exon7 was used as a model target for method development.

This thesis consists of seven chapters. Chapter 1 reviews the biological implications of BPDE-DNA adducts, available analytical techniques for BPDE-DNA adduct detection and their limitations, and recent advances in BINDA assays and its basic principles. It was the advantages of the BINDA assay that inspired the concept of a BINDA-based assay for BPDE-*p53*-exon7 detection. Chapter 2 introduces the development of a TaqMan-based BINDA assay. Streptavidin was used as the target to develop the method. Chapter 3 demonstrates a homogeneous BINDA assay can be used to quantify the BPDE- *p53*-exon7 adducts. This homogeneous BINDA assay was developed on the basis of the TaqMan-based BINDA introduced in Chapter 2. BPDE-*p53*-exon7 was synthesized as the target standards to develop the assay. Chapter 4 describes a magnetic bead-mediated BINDA assay for BPDE-*p53*-exon7. In this new assay, one DNA motif and the antibody against BPDE were immobilized on the surface of magnetic beads. DNA motifs and antibodies on the magnetic beads provide an even higher effective local concentration after target binding. The detection limit achieved by magnetic bead-mediated BINDA assay was lower than that of the homogeneous BINDA

assay. Chapter 5 introduces the application of two BINDA assays for BPDE-*p53*-exon7 detection in genomic DNA. A solid-phase extraction was coupled to both BINDA assays to overcome the high background signal generated by the genomic DNA. Chapter 6 demonstrates that the solid-phase extraction coupled with magnetic bead-mediated BINDA assay could be used for real sample analysis. Cells were treated by BPDE and the DNA was extracted after treatment for assay analysis. The assay could detect BPDE-*p53*-exon7 from 10^7 treated cells. Chapter 7 discusses the conclusion and significance of the thesis as well as the future research.

1.6 References

1. J. H. J. Hoeijmakers, DNA damage, aging, and cancer, *N. Engl. J. Med.* **361**, 1475–85 (2009).

2. C. Prives, P. A. Hall, The P53 pathway, *J. Pathol.* **187**, 112–126 (1999).

3. B. Vogelstein, D. Lane, A. J. Levine, Surfing the *p53* network, *Nature* **408**, 307–10 (2000).

4. B. Vogelstein, K. W. Kinzler, Cancer genes and the pathways they control, *Nat. Med.* **10**, 789–99 (2004).

5. A. Petitjean, E. Mathe, S. Kato, C. Ishioka, S. V. Tavtigian, P. Hainaut, M. Olivier, Impact of Mutant *p53* Functional Properties on TP53 Mutation Patterns and Tumor Phenotype: Lessons from Recent Developments in the IARC TP53 Database, *Hum. Mutat.* **28**, 622–629 (2007).

6. M. Hollstein, B. Shomer, M. Greenblatt, T. Soussi, E. Hovig, R. Montesano, C. C. Harris, Somatic point mutations in the *p53* gene of human tumors and cell lines: updated compilation, *Nucleic Acids Res.* **24**, 141–6 (1996).

7. T. Unger, M. M. Nau, S. Segal, J. D. Minna, P53: a Transdominant Regulator of Transcription Whose Function Is Ablated By Mutations Occurring in Human Cancer, *EMBO J.* **11**, 1383–90 (1992).

8. S. E. Kern, J. A. Pietenpol, S. Thiagalingam, A. Seymour, K. W. Kinzler, B. Vogelstein, Oncogenic forms of *p53* inhibit p53-regulated gene expression, *Science* **256**, 827–30 (1992).

9. J. M. Waldman, P. J. Lioy, A. Greenberg, J. P. Butler, Analysis of human exposure to benzo(a)pyrene via inhalation and food ingestion in the Total Human Environmental Exposure Study (THEES), *J. Expo. Anal. Environ. Epidemiol.* **1**, 193–225 (1991).

10. D. E. Volk, V. Thiviyanathan, J. S. Rice, B. A. Luxon, J. H. Shah, H. Yagi, *et al.*, Solution Structure of a Cis-Opened(10R)-N6-Deoxyadenosine Adduct of (9S,10R)-9,10-Epoxy-7,8,9,10-tetrahydrobenzo[a]pyrene in a DNA Duplex, *Biochemistry* **42**, 1410–1420 (2003).

11. M. F. Denissenko, A. Pao, M. Tang, G. P. Pfeifer, Preferential Formation of Benzo[a]pyrene Adducts at Lung Cancer Mutational Hotspots in P53, *Science.* **274**, 430–432 (1996).

12. M. Mazur, B. W. Glickman, Sequence specificity of mutations induced by benzo[a]pyrene-7,8-diol-9,10-epoxide at endogenous aprt gene in CHO cells, *Somat. Cell Mol. Genet.* **14**, 393–400 (1988).

13. R. H. Chen, V. M. Maher, J. J. McCormick, Effect of excision repair by diploid human fibroblasts on the kinds and locations of mutations induced by (+/-)-7 beta,8 alpha-dihydroxy-9 alpha,10 alpha-epoxy-7,8,9,10-tetrahydrobenzo[a]pyrene in the coding region of the HPRT gene, *Proc. Natl. Acad. Sci. U. S. A.* **87**, 8680–4 (1990).

14. E. Eisenstadt, A. J. Warren, J. Porter, D. Atkins, J. H. Millert, Carcinogenic epoxides of benzo[alpyrene and cyclopenta [cd]pyrene induce base substitutions via specific transversions, *Proc. Natl. Acad. Sci. U. S. A.* **79**, 1945–1949 (1982).

15. P. Hainaut, G. P. Pfeifer, Patterns of p53 G→T transversions in lung cancers reflect the primary mutagenic signature of DNA-damage by tobacco smoke, *Carcinogenesis* **22**, 367–74 (2001).

16. P. Hainaut, M. Olivier, G. P. Pfeifer, TP53 mutation spectrum in lung cancers and mutagenic signature of components of tobacco smoke: lessons from the IARC TP53 mutation database, *Mutagenesis* **16**, 551–3; author reply 555–6 (2001).

17. G. P. Pfeifer, P. Hainaut, On the origin of G→T transversions in lung cancer, *Mutat. Res. Mol. Mech. Mutagen.* **526**, 39–43 (2003).

18. T. Lindahl, Instability and decay of the primary structure of DNA, *Nature* **362**, 709–715 (1993).

19. R. De Bont, Endogenous DNA damage in humans: a review of quantitative data, *Mutagenesis* **19**, 169–185 (2004).

20. M. J. Kaiserman, W. S. Rickert, Carcinogens in tobacco smoke: benzo[a]pyrene from Canadian cigarettes and cigarette tobacco, *Am. J. Public Health* **82**, 1023–6 (1992).

21. D. L. Busbee, C. O. Joe, J. O. Norman, P. W. Rankin, Inhibition of DNA synthesis by an electrophilic metabolite of benzo[a]pyrene, *Proc. Natl. Acad. Sci. U. S. A.* **81**, 5300–4 (1984).

22. K. Shinohara, P. A. Cerutti, Excision repair of benzo[a]pyrene-deoxyguanosine adducts in baby hamster kidney 21/C13 cells and in secondary mouse embryo fibroblasts C57bl/6J, *Proc. Natl. Acad. Sci. U. S. A.* **74**, 979–983 (1977).

23. M. C. MacLeod, A Kootstra, B. K. Mansfield, T. J. Slaga, J. K. Selkirk, Specificity in interaction of benzo[a]pyrene with nuclear macromolecules: implication of derivatives of two dihydrodiols in protein binding, *Proc. Natl. Acad. Sci. U. S. A.* **77**, 6396–400 (1980).

24. P. A. Cerutti, F. Sessions, P. V. Hariharan, P. V. Maridaran, A. Lusby, Repair of DNA Damage Induced by Benzo (a) pyrene Diol-epoxides I and II in Human Alveolar Tumor Cells Repair of DMA Damage Induced by Benzo (a) pyrene, *Cancer Epidemiol. Biomarkers Prev.* **38**, 2118–2124 (1978).

25. P. Brookes, M. R. Osborne, Mutation in mammalian cells by stereoisomers of anti-benzo[a] pyrene-diolepoxide in relation to the extent and nature of the DNA reaction products, *Carcinogenesis* **3**, 1223–6 (1982).

26. G. P. Pfeifer, A. Besaratinia, Mutational spectra of human cancer, *Hum. Genet.* **125**, 493–506 (2009).

27. A. Petitjean, E. Mathe, S. Kato, C. Ishioka, S. V. Tavtigian, P. Hainaut *et al.*, Impact of Mutant *p53* Functional Properties on TP53 Mutation Patterns and Tumor Phenotype : Lessons from Recent Developments in the IARC TP53 Database, *Hum. Mutat.* **28**, 622–629 (2007).

28. R. C. Gupta, Enhanced Sensitivity of 32P-Postlabeling Analysis of Aromatic Carcinogen: DNA Adducts Enhanced Sensitivity of 32P-Postlabeling Analysis of Aromatic Carcinogen: DNA, *Cancer Res.* **45**, 5656–5662 (1985).

29. R. C. Gupta, M. V. Reddy, K. Randerath, 32P-postlabeling analysis of non-radioactive aromatic carcinogen--DNA adducts, *Carcinogenesis* **3**, 1081–92 (1982).

30. M. V Reddy, K. Randerath, Nuclease P1-mediated enhancement of sensitivity of 32P-postlabeling test for structurally diverse DNA adducts, *Carcinogenesis* **7**, 1543–51 (1986).

31. F. P. Perera, M. C. Poirier, S. H. Yuspa, J. Nakayama, A. Jaretzki, M. M. Cumen *et al.*, A pilot project in molecular cancer epidemiology: determination of benzo[a]pyrene--DNA adducts in animal and human tissues by immunoassays, *Carcinogenesis* **3**, 1405–10 (1982).

32. J. Nakayama, S. H. Yuspa, M. C. Poirier, Benzo(a)pyrene-DNA Adduct Formation and Removal in Mouse Epidermis in Vivo and in Vitro: Relationship of DNA Binding to Initiation of Skin Carcinogenesis, *Cancer Res.* **44**, 4087–4095 (1984).

33. I. Hsu, M. C. Poirier, S. H. Yuspa, D. Grunberger, I. B. Weinstein, R. H. Yolken *et al.*, Measurement of Benzo(a)pyrene-DNA Adducts by Enzyme Immunoassays and Radioimmunoassay, *Cancer Res.* **41**, 1091–1095 (1981).

34. B. Schoket, D. H. Phillips, M. C. Poirier, I. Vincze, DNA adducts in peripheral blood lymphocytes from aluminum production plant workers determined by 32P-postlabeling and enzyme-linked immunosorbent assay, *Environ. Health Perspect.* **99**, 307–309 (1993).

35. B. Schoket, W. A. Doty, I. Vincze, P. T. Strickland, G. M. Ferri, G. Assennato *et al.*, Increased Sensitivity for Determination of Polycyclic Aromatic Adducts in Human DNA Samples by Lanthanide Fluoroimmunoassay (DELFIA), *Cancer Epidemiol. Biomarkers Prev.* **2**, 349–353 (1993).

36. R. L. Divi, F. A. Beland, P. P. Fu, L. S. V. Tungeln, B. Schoket, J. E. Camara *et al.*, Highly sensitive chemiluminescence immunoassay for benzo[a]pyrene-DNA adducts: validation by comparison with other methods, and use in human biomonitoring, *Carcinogenesis* **23**, 2043–9 (2002).

37. H. Wang, M. Lu, N. Mei, J. Lee, M. Weinfeld, X. C. Le, Immunoassays using capillary electrophoresis laser induced fluorescence detection for DNA adducts, *Anal. Chim. Acta* **500**, 13–20 (2003).

38. H. Wang, M. Lu, M. Weinfeld, X. C. Le, Enhancement of immunocomplex detection and application to assays for DNA adduct of benzo[a]pyrene, *Anal. Chem.* **75**, 247–54 (2003).

39. Z. Wang, M. Lu, X. Wang, R. Yin, Y. Song, X. C. Le *et al.*, Quantum dots enhanced ultrasensitive detection of DNA adducts, *Anal. Chem.* **81**, 10285–9 (2009).

40. U. A. Harréus, N. H. Kleinsasser, S. Zieger, B. Wallner, M. Reiter, P. Schuller *et al.*, Sensitivity to DNA-damage induction and chromosomal alterations in mucosa cells from patients with and without cancer of the oropharynx detected by a combination of Comet assay and fluorescence in situ hybridization, *Mutat. Res.* **563**, 131–8 (2004).

41. G. P. Pfeifer, S. D. Steigerwald, P. R. Mueller, B. Wold, A. D. Riggs, Genomic sequencing and methylation analysis by ligation mediated PCR, *Science* **246**, 810–813 (1989).

42. G. P. Pfeifer, R. Drouin, A. D. Riggs, G. P. Holmquist, In vivo mapping of a DNA adduct at nucleotide resolution: detection of pyrimidine (6-4) pyrimidone photoproducts by ligation-mediated polymerase chain reaction, *Proc. Natl. Acad. Sci. U. S. A.* **88**, 1374–1378 (1991).

43. Z. Feng, W. Hu, Y. Hu, M. Tang, Acrolein is a major cigarette-related lung cancer agent: Preferential binding at p53 mutational hotspots and inhibition of DNA repair, *Proc. Natl. Acad. Sci. U. S. A.* **103**, 15404–15409 (2006).

44. T. Sano, C. L. Smith, C. R. Cantor, Immuno-PCR: very sensitive antigen detection by means of specific antibody-DNA conjugates, *Science* **258**, 120–2 (1992).

45. H. Zhang, Q. Zhao, X.-F. Li, X. C. Le, Ultrasensitive assays for proteins, *Analyst* **132**, 724–37 (2007).

46. C. M. Niemeyer, M. Adler, R. Wacker, Immuno-PCR: high sensitivity detection of proteins by nucleic acid amplification, *Trends Biotechnol.* **23**, 208–16 (2005).

47. J. Barletta, Applications of real-time immuno-polymerase chain reaction (rt-IPCR) for the rapid diagnoses of viral antigens and pathologic proteins, *Mol. Aspects Med.* **27**, 224–53 (2006).

48. L. M. McGregor, D. J. Gorin, C. E. Dumelin, D. R. Liu, Interaction-dependent PCR: identification of ligand-target pairs from libraries of ligands and libraries of targets in a single solution-phase experiment, *J. Am. Chem. Soc.* **132**, 15522–4 (2010).

49. F. Li, H. Zhang, C. Lai, X.-F. Li, X. C. Le, A molecular translator that acts by binding-induced DNA strand displacement for a homogeneous protein assay, *Angew. Chem. Int. Ed. Engl.* **51**, 9317–20 (2012).

50. H. Zhang, X.-F. Li, X. C. Le, Binding-induced DNA assembly and its application to yoctomole detection of proteins, *Anal. Chem.* **84**, 877–84 (2012).

51. F. Li, H. Zhang, Z. Wang, X. Li, X.-F. Li, X. C. Le, Dynamic DNA assemblies mediated by binding-induced DNA strand displacement, *J. Am. Chem. Soc.* **135**, 2443–6 (2013).

52. E. Heyduk, T. Heyduk, Nucleic acid-based fluorescence sensors for detecting proteins, *Anal. Chem.* **77**, 1147–56 (2005).

53. S. Fredriksson, M. Gullberg, J. Jarvius, C. Olsson, K. Pietras, S. M. Gustafsdottir *et al.*, Protein detection using proximity-dependent DNA ligation assays, *Nat. Biotechnol.* **20**, 473–7 (2002).

54. J. Watson, F. Crick, A structure for deoxyribose nucleic acid, *Nature* **171**, 737–738 (1953).

55. P. Yakovchuk, E. Protozanova, M. D. Frank-Kamenetskii, Base-stacking and base-pairing contributions into thermal stability of the DNA double helix, *Nucleic Acids Res.* **34**, 564–74 (2006).

56. H. Zhang, F. Li, B. Dever, C. Wang, X.-F. Li, X. C. Le, Assembling DNA through Affinity Binding to Achieve Ultrasensitive Protein Detection, *Angew. Chem. Int. Ed. Engl.* , 10698–10705 (2013).

57. H. Zhang, F. Li, B. Dever, X.-F. Li, X. C. Le, DNA-mediated homogeneous binding assays for nucleic acids and proteins, *Chem. Rev.* **113**, 2812–41 (2013).

58. T. Conze, A. Shetye, Y. Tanaka, J. Gu, C. Larsson, J. Goransson *et al.*, Analysis of genes, transcripts, and proteins via DNA ligation, *Annu. Rev. Anal. Chem. (Palo Alto. Calif).* **2**, 215–39 (2009).

59. E. Schallmeiner, E. Oksanen, O. Ericsson, Sensitive protein detection via triple-binder proximity ligation assays, *Nat. Methods* **4**, 135–137 (2007).

60. G. Tavoosidana, G. Ronquist, S. Darmanis, J. Yan, L. Carlsson, D. Wu *et al.*, Multiple recognition assay reveals prostasomes as promising plasma biomarkers for prostate cancer, *Proc. Natl. Acad. Sci. U. S. A.* **108**, 8809–14 (2011).

61. O. Soderberg, M. Gullberg, M. Jarvius, K. Ridderstrale, K.-J. Leuchowius, J. Jarvius *et al.*, Direct observation of individual endogenous protein complexes in situ by proximity ligation, *Nat. Methods* **3**, 995–1000 (2006).

62. M. Jarvius, J. Paulsson, I. Weibrecht, K.-J. Leuchowius, A.-C. Andersson *et al.*, In situ detection of phosphorylated platelet-derived growth factor receptor beta using a generalized proximity ligation method, *Mol. Cell. Proteomics* **6**, 1500–9 (2007).

63. K.-J. Leuchowius, M. Jarvius, M. Wickstrom, L. Rickardson, U. Landegren, R. Larsson *et al.*, High content screening for inhibitors of protein interactions and post-translational modifications in primary cells by proximity ligation, *Mol. Cell. Proteomics* **9**, 178–83 (2010).

64. I. Weibrecht, M. Gavrilovic, L. Lindbom, U. Landegren, C. Wahlby, O. Soderberg, Visualising individual sequence-specific protein-DNA interactions in situ, *N. Biotechnol.* **29**, 589–98 (2012).

65. J. Jung, A. W. Lifland, C. Zurla, E. J. Alonas, P. J. Santangelo, Quantifying RNA-protein interactions in situ using modified-MTRIPs and proximity ligation, *Nucleic Acids Res.* **41**, e12 (2013).

66. T. Conze, A. S. Carvalho, U. Landegren, R. Almeida, C. A. Reis, L. David *et al.*, MUC2 mucin is a major carrier of the cancer-associated sialyl-Tn antigen in intestinal metaplasia and gastric carcinomas, *Glycobiology* **20**, 199–206 (2010).

67. P. Kumar, L. Lindberg, T. L. Thirkill, J. W. Ji, L. Martsching, G. C. Douglas, The MUC1 extracellular domain subunit is found in nuclear speckles and associates with spliceosomes, *PLoS One* **7**, e42712 (2012).

68. K.-J. Leuchowius, I. Weibrecht, U. Landegren, L. Gedda, O. Söderberg, Flow cytometric in situ proximity ligation analyses of protein interactions and post-translational modification of the epidermal growth factor receptor family, *Cytometry. A* **75**, 833–9 (2009).

69. S. Fredriksson, W. Dixon, H. Ji, A. C. Koong, M. Mindrinos, R. W. Davis, Multiplexed protein detection by proximity ligation for cancer biomarker validation, *Nat. Methods* **4**, 327–329 (2007).

70. S. Fredriksson, J. Horecka, O. T. Brustugun, J. Schlingemann, A. C. Koong, R. Tibshirani *et al.*, Multiplexed proximity ligation assays to profile putative plasma biomarkers relevant to pancreatic and ovarian cancer, *Clin. Chem.* **54**, 582–9 (2008).

71. M. Lundberg, S. B. Thorsen, E. Assarsson, A. Villablanca, B. Tran, N. Gee *et al.*, Multiplexed homogeneous proximity ligation assays for high-throughput protein biomarker research in serological material, *Mol. Cell. Proteomics* **10**, M110.004978 (2011).

72. M. Hammond, R. Y. Nong, O. Ericsson, K. Pardali, U. Landegren, Profiling cellular protein complexes by proximity ligation with dual tag microarray readout, *PLoS One* **7**, e40405 (2012).

73. S. Darmanis, R. Y. Nong, J. Vanelid, A. Siegbahn, O. Ericsson, S. Fredriksson *et al.*, ProteinSeq: high-performance proteomic analyses by proximity ligation and next generation sequencing, *PLoS One* **6**, e25583 (2011).

74. L. Zhu, H. Koistinen, P. Wu, A. Narvanen, E. Schallmeiner, S. Fredriksson *et al.*, A sensitive proximity ligation assay for active PSA, *Biol. Chem.* **387**, 769–72 (2006).

75. S. Darmanis, R. Y. Nong, M. Hammond, J. Gu, A. Alderborn, J. Vanelid *et al.*, Sensitive plasma protein analysis by microparticle-based proximity ligation assays, *Mol. Cell. Proteomics* **9**, 327–35 (2010).

76. M. Kamali-Moghaddam, F. E. Pettersson, D. Wu, H. Englund, S. Darmanis, A. Lord *et al.*, Sensitive detection of A b protofibrils by proximity ligation - relevance for Alzheimer' s disease, *BMC Neurosci.* **11**, 1–7 (2010).

77. M. Lundberg, A. Eriksson, B. Tran, E. Assarsson, S. Fredriksson, Homogeneous antibody-based proximity extension assays provide sensitive and specific detection of low-abundant proteins in human blood, *Nucleic Acids Res.* **39**, e102 (2011).

78. M. Gullberg, S. M. Gustafsdottir, E. Schallmeiner, J. Jarvius, M. Bjarnegard, C. Betsholtz *et al.*, Cytokine detection by antibody-based proximity ligation, *Proc. Natl. Acad. Sci. U. S. A.* **101**, 8420–4 (2004).

79. L. Zhu, H. Koistinen, U. Landegren, U.-H. Stenman, Proximity ligation measurement of the complex between prostate specific antigen and alpha1-protease inhibitor, *Clin. Chem.* **55**, 1665–71 (2009).

80. S. M. Gustafsdottir, A. Nordengrahn, S. Fredriksson, P. Wallgren, E. Rivera, E. Schallmeiner *et al.*, Detection of individual microbial pathogens by proximity ligation, *Clin. Chem.* **52**, 1152–60 (2006).

81. S. M. Gustafsdottir, S. Wennstrom, S. Fredriksson, E. Schallmeiner, A. D. Hamilton, S. M. Sebti *et al.*, Use of proximity ligation to screen for inhibitors of interactions between vascular endothelial growth factor A and its receptors, *Clin. Chem.* **54**, 1218–25 (2008).

82. S. M. Gustafsdottir, J. Schlingemann, A. Rada-Iglesias, E. Schallmeiner, M. Kamali-Moghaddam, C. Wadelius *et al.*, In vitro analysis of DNA-protein interactions by proximity ligation, *Proc. Natl. Acad. Sci. U. S. A.* **104**, 3067–72 (2007).

83. T. Heyduk, Practical biophysics: Sensors for rapid detection of biological targets utilizing target-induced oligonucleotide annealing, *Biophys. Chem.* **151**, 91–5 (2010).

84. E. Heyduk, M. M. Moxley, A. Salvatori, J. A. Corbett, T. Heyduk, Homogeneous Insulin and C-Peptide Sensors for Rapid Assessment of Insulin and C-Peptide Secretion by the Islets, *Diabetes* **59**, 2360–2365 (2010).

85. E. Heyduk, B. Dummit, Y.-H. Chang, T. Heyduk, Molecular pincers: antibody-based homogeneous protein sensors, *Anal. Chem.* **80**, 5152–9 (2008).

86. L. Tian, T. Heyduk, Antigen peptide-based immunosensors for rapid detection of antibodies and antigens, *Anal. Chem.* **81**, 5218–25 (2009).

87. E. Heyduk, T. Heyduk, Fluorescent homogeneous immunosensors for detecting pathogenic bacteria, *Anal. Biochem.* **396**, 298–303 (2010).

88. J. Hu, T. Wang, J. Kim, C. Shannon, C. J. Easley, Quantitation of femtomolar protein levels via direct readout with the electrochemical proximity assay, *J. Am. Chem. Soc.* **134**, 7066–72 (2012).

89. T. Heyduk, Practical biophysics: Sensors for rapid detection of biological targets utilizing target-induced oligonucleotide annealing, *Biophys. Chem.* **151**, 91–5 (2010).

90. D. A. Di Giusto, W. A. Wlassoff, J. J. Gooding, B. A. Messerle, G. C. King, Proximity extension of circular DNA aptamers with real-time protein detection, *Nucleic Acids Res.* **33**, e64 (2005).

91. X. C. Le, H. Zhang, X.-F. Li, Binding-induced hairpin detection system. U.S. patent application 61/238,368 filed on August 31, 2009. International Publication Number WO 2011/022820 A1. Published on March 3, 2011.

92. H. Zhang, X.-F. Li, X. C. Le, Binding-induced DNA assembly and its application to yoctomole detection of proteins, *Anal. Chem.* **84**, 877–84 (2012).

93. J. Li, X. Zhong, H. Zhang, X. C. Le, J.-J. Zhu, Binding-induced fluorescence turn-on assay using aptamer-functionalized silver nanocluster DNA probes, *Anal. Chem.* **84**, 5170–4 (2012).

94. F. Li, Y. Lin, X. C. Le, Binding-Induced Formation of DNA Three-Way Junctions and Its Application to Protein Detection and DNA Strand Displacement, *Anal. Chem.* (2013), doi:10.1021/ac402179a.

95. H.-C. Yeh, J. Sharma, J. J. Han, J. S. Martinez, J. H. Werner, A DNA--silver nanocluster probe that fluoresces upon hybridization, *Nano Lett.* **10**, 3106–10 (2010).

Chapter Two

TaqMan-based Binding-Induced DNA Assembly Assay (BINDA)

2.1 Introduction

Detection and quantification of trace amounts of target molecules, especially in the presence of complex sample matrices, is challenging. Converting the detection of non-amplifiable targets (such as proteins) to amplifiable DNA is a useful strategy to enhance sensitivity. Unlike the traditional enzyme-linked immunosorbent assays (ELISA) in which signal generation relies on the enzyme-substrate reaction and is usually linear amplification, DNA quantification based on PCR technology can produce exponential signal amplification and therefore is far more sensitive than ELISA (*1*). However, the high sensitivity of DNA amplification can also generate very high level of background due to non-specific binding. For this reason, multiple wash steps or other separation techniques (*2*, *3*) are usually incorporated in PCR-based detection assays.

To minimize the background signal arising from non-specific binding of DNA and to simplify experimental procedures, homogeneous assays based on dual-recognition were developed (*4*). Replacement of a single DNA as signal output by DNA assembly upon dual-recognition can greatly reduce the background and increase the specificity for target detection. A binding-induced DNA assembly assay (BINDA) was developed based on this concept (*5*). Two DNA probes that are conjugated to specific affinity ligands assemble preferentially only when the dual binding event is triggered upon target binding.

Then a highly stable hairpin structure is formed and the real-time qPCR detection technique can be used to quantify the assembled hairpin structure following a simple ligation step. This technique enables effective differentiation of the target-specific DNA assembly from the background target-independent DNA assembly.

A BINDA assay was previously developed using real-time qPCR with SYBR Green chemistry to quantify the assembled DNA. The SYBR Green dye binds to all double-stranded DNA. This format of real-time qPCR cannot be used in assays when other DNA is also present in addition to the designed probes. Therefore, to broaden the applicability of the assay, especially to samples containing other DNA, it is necessary to develop a BINDA assay using real-time qPCR with TaqMan chemistry for detection.

In this chapter, streptavidin was used as the target to develop a TaqMan based BINDA assay. Streptavidin is a 52.8-KDa protein purified from the bacterium *Streptomyces avidinii*. Homo-tetramers of streptavidin have an extraordinarily high affinity for biotin, with a dissociation constant (Kd) of $\approx 10^{-14}$ mol/L (*6*). Due to the high binding affinity and specificity of streptavidin and biotin, and the availability of a simple biotin-labeling method for proteins and DNA, streptavidin is an ideal model target for testing target-binding assays. The design of DNA elements in the BINDA system is similar to the SYBR Green-based assay. The main difference is the addition of a TaqMan probe hybridization sequence in one of the DNA probes. With the TaqMan chemistry in real-time qPCR detection, detection of multiple targets in one tube and in the presence of other DNA can be potentially achieved.

2.2 Experimental

2.2.1 Reagents and instruments

The oligonucleotides (listed in Table 2.1, except the TaqMan probe) were custom synthesized, labeled, and purified by Integrated DNA Technologies (IDT, Coralville, IA). Probe-F had a biotin group attached at the 5' end, and oligos of Probe-R were labeled with a phosphate group at the 5' end and a biotin group at the 3' end. The stem sequences are underlined in the Probe-F and Probe-R oligos. The stem sequences of Probe-R6, Probe-R7, and Probe-R8 oligos contain 6, 7, and 8 complementary bases, respectively. Block-R6 was used in the assay when Probe-R6 were added, while Block-R7 or Block-R8 were used when Probe-R7 or Probe-R8 was added. The underlined sequences of Block-F and Block-R are complementary to the corresponding sequences of Probe-F and Probe-R oligos, respectively. The TaqMan probe was custom synthesized and purified by Applied Biosystems (Foster City, CA). The TaqMan probe was labeled with a 5’ FAM reporter dye and a 3’ non-fluorescent quencher (NFQ). Streptavidin and biotin were obtained from Sigma-Aldrich (Oakville, ON). Platinum® qPCR SuperMix UDG (Cat. No. 11730) and T4 DNA Ligase (Cat. No. 15224) were purchased from Invitrogen (Carlsbad, CA). Phosphate buffered saline (1 × PBS) (137 mM NaCl, 10 mM phosphate, 2.7 mM KCl, pH 7.4) was diluted with deionized water from 10 × PBS buffer (Fisher Scientific, Nepean, ON). All other reagents were of analytical grade.

Table 2.1 Oligonucleotide probes and blocks designed for streptavidin detection.

Oligonucleotides	Sequences (5'→3')
Probe-F	ACT GTG TCT GGT GGT TGG TGT TCG TCG TCT GGT GTG TCA TTG TTT TAG GCT G*GT CGC TTT GTT TTG CGA C
Probe-R6	CAG CCT TTT TGT TTG TTT TGT TTT TTT TGA TGG AGC AGC TCT GAG ATC
Probe-R7	CAG CCT ATT TTG TTT GTT TTG TTT TTT TTG ATG GAG CAG CTC TGA GAT C
Probe-R8	CAG CCT AAT TTT GTT TGT TTT GTT TTT TTT GAT GGA GCA GCT CTG AGA TC
Primer-F	ACT GTG TCT GGT GGT TGG TG
Primer-R	GAT CTC AGA GCT GCT CCA TC
TaqMan probe	TCG TCG TCT GGT GTG TC
Block-F-1	TTT GCC TAA AAC** TTA
Block-F-2	TTT GCC TAA AAC ATA T
Block-F-3	TTT GCC TAA AAC AAA TT
Block-F-4	TTT GCC TAA AAC AAT TTT
Block-R6-1	TTT AAA AGG CTG T TT
Block-R6-2	TTT AAA AAG GCT GTT T
Block-R6-3	TTT CAA AAA GGC TGT TT
Block-R6-4	TTT ACA AAA AGG CTG TTT
Block-R7-1	TTT AAA TAG GCT GTT T
Block-R7-2	TTT AAA ATA GGC TGT TT
Block-R7-3	TTT CAA AAT AGG CTG TTT
Block-R7-4	TTT ACA AAA TAG GCT GTT T
Block-R8-1	TTT AAA TTA GGC TGT TT
Block-R8-2	TTT AAA ATT CGG CTG TTT
Block-R8-3	TTT CAA AAT TCG GCT GTT T
Block-R8-4	TTT ACA AAA TTC GGC TGT TT

*Stem sequences in Probe-F and Probe-R6, Probe-R7 and Probe-R8 are underlined.
**Blocking sequences in all the blocks corresponding to their respective probes are underlined.

A 7500 Fast Real-Time PCR system from Applied Biosystems was used to run all PCR experiments. A 96-well MicroAmp Fast Optical Plate (Cat. No. 4346906) with barcode, and MicroAmp Optical Adhesive Cover (Cat. No. 4360954) from Applied Biosystems compatible with this Real-Time PCR system were used in this study.

2.2.2 Procedures of binding-induced DNA assembly (BINDA) assay using streptavidin as a model target

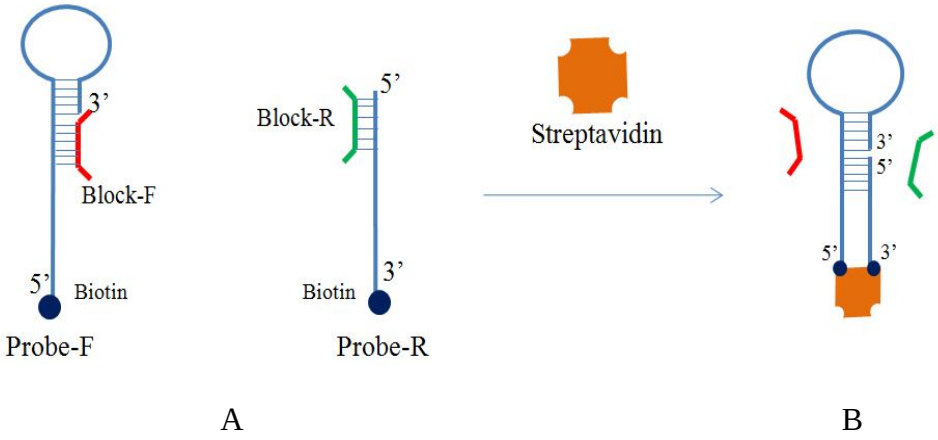

Figure 2.1 Detection of streptavidin by binding-induced DNA assembly assay. (A) Biotinylated Probe-F and Probe-R hybridize with corresponding blocks in the absence of streptavidin. (B) In the presence of streptavidin, concurrent binding of both Probe-F and Probe-R to the same streptavidin molecule forms binding-induced DNA assembly.

Figure 2.1 illustrates schematically the binding-induced DNA assembly assay for streptavidin. Biotinylated Probe-F and Probe-R hybridize with corresponding

blocks (Block-F and Block-R) when there is no streptavidin present in the incubation solution. When streptavidin is added, binding of both Probe-F and Probe-R to the same streptavidin molecule promotes the binding-induced DNA assembly. The assembled DNA can be ligated to form a longer DNA molecule (Probe-F + Probe-R = 118 nucleotides) and be amplified and quantified by real-time PCR. In this BINDA assay, the quantification of the target molecule is converted to the indirect quantification of the assembled and ligated DNA from Probe-F and Probe-R. The signal output from the real-time PCR is therefore proportional to the initial concentration of the target molecule, i.e., streptavidin, in this specific study.

The experimental procedures are described as follows. Probe-F and Probe-R were added to 50 μL 1×PBS solution to a final concentration of 100 pM. Block-F and Block-R were also added to a final concentration of 100 nM. A desired amount of streptavidin was then added to the mixture. The solution was incubated at 37˚C for 30 min followed by incubation at room temperature for another 30 min. Higher temperature (37˚C) allows the complete interaction between streptavidin and biotin while lower temperature increases the assembly between Probe-F and Probe-R. An aliquot (2 μL) of the above solution was then transferred into a 96-well real-time PCR reaction plate. After addition of the reagents for ligation and amplification, the final 20 μL reaction solution contained 100 μM ATP, 0.4 Unit T4 DNA ligase, 0.1 μM forward and reverse primers, 0.1 μM TaqMan probe, 0.25 μM ROX reference dye, and 10 μL Platinum® qPCR SuperMix UDG (including 2 × PCR buffer, DNA polymerase, Mg^{2+}, dNTP, dUTP,

uracil DNA glycosylase (UDG), and stabilizers). The PCR reactions were mixed well by vortexing of the plate followed by short centrifugation. After 10 min incubation at room temperature for the ligation reaction to occur, the 96-well plate was placed in the real-time PCR System. The PCR program consisted of 50˚C for 2 min, 95˚C for 2 min, followed by 50 cycles of 95˚C for 15 s and 60˚C for 30 s. All real-time qPCR experiments were carried out in triplicate.

2.2.3 Optimization of binding-induced DNA assembly (BINDA) assay

The objective of the optimization process was to achieve the maximum signal-to-background ratio from the assay. In this assay, signal was represented by threshold cycles (Ct). Therefore, the signal-to-background ratio was the difference in threshold cycles (ΔCt) between the analyses of the target at a particular concentration and the reagent blank (background). The parameters optimized in this section included the length of stem sequences (by combining Probe-F with different Probe-R), the length of Block-F and Block-R, the concentration ratio of the Probe over the Block, the ligation time, and the ligation and PCR procedures (combined in one-step or conducted in two separate steps).

2.2.4 Dynamic range of streptavidin analysis

Streptavidin at a series of concentrations was used to test the dynamic range under the optimized conditions. To prevent the absorption of extremely low concentrations of streptavidin on the sample tubes, the streptavidin was prepared in 1 × PBS containing 0.2% bovine serum albumin (BSA), or approximately 30 μM. This concentration of BSA (30 μM) was significantly higher than the streptavidin used in the analysis (1 fM to 100 pM).

2.3 Results and Discussion

2.3.1 Design of oligonucleotide probes

Probe-F contained a primer sequence, a TaqMan probe sequence, a stem sequence, and a hairpin structure sequence (Figure 2.2A). The primer region was used for PCR amplification; the TaqMan probe sequence was used to hybridize the TaqMan probe for real-time PCR detection; the stem sequence was used to hybridize the complementary sequence in Probe-R after both probes bound to a single target; and the hairpin sequence was used to provide a structure for the ligation between the 3' of Probe-F and the 5' of Probe-R.

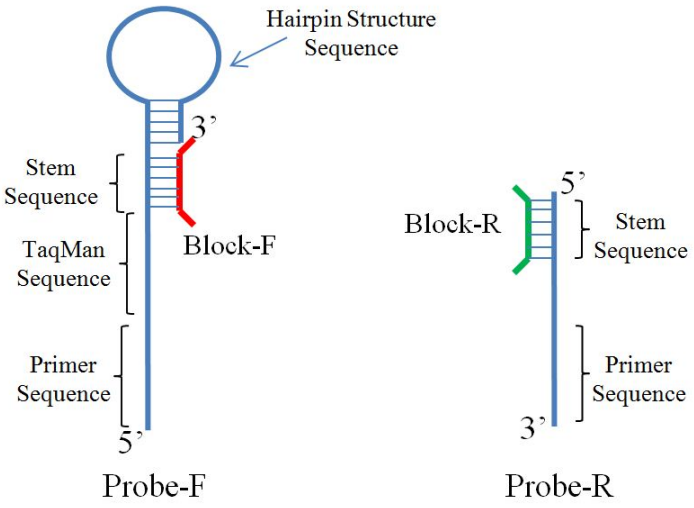

A B

Figure 2.2 Schematic showing the various components of the oligonucleotide probes used in the binding-induced DNA assembly assay. (A) Probe-F and Block-F; and (B) Probe-R and Block-R.

Probe-R contained a primer sequence and a stem sequence (Figure 2.2B). These sequences had the same function as the corresponding sequences within Probe-F.

Block-F and Block-R were used to block the stem sequence of Probe-F and Probe-F. These blocking sequences were used to prevent the hybridization between Probe-F and Probe-R in the absence of target binding.

The stem sequence was designed carefully to allow for maximum hybridization of two probes upon binding to the target, but minimum hybridization in the absence of the target binding. This design was guided by estimates of the melting temperature of the hybrid. The melting temperature (T_m) is defined as the temperature at which half of the double-stranded DNA dissociate to single-stranded DNA. In this study, the T_m of primers and TaqMan probes were analyzed using Primer Express 3.0 (Applied Biosystems), and the T_m of other oligos were analyzed using Oligo Analyzer 3.1 (Integrated DNA Technologies) under default settings. Here we used T_{m1} to quantitatively describe the hybridization between two oligos. We estimated the T_m of hairpins with a loop containing about 110 thymidines (T_{ma}) and the corresponding hybrids from separate nucleotides (T_{mb}).

A number of design criteria are described below. Since the reaction often takes place at room temperature (25˚C), the T_{ma} of the designed stem sequence should be higher than 25˚C, but not too high to allow target independent hybridization, usually below 35˚C. For the same reason, the T_{mb} should be as low as possible.

Use of high GC content would shorten the length of stem sequence to achieve the desired T_{ma}. Four GC out of 5 nucleotides result in a T_{ma} of around 27˚C, and 4 GC out of 8 nucleotides with a loop containing 110 thymidines result in a T_{ma} of around 38˚C, while 5–8 n.t. stem sequence keeps the T_{mb} below or around 10˚C. Therefore the length of stem sequence of 5–8 n.t. should be optimum.

The hairpin sequence was designed to provide a stable hairpin structure for the ligation of two probes. So the T_m should be high enough to maintain the hairpin. A hairpin containing 5 n.t. (include 4 G/C) and a loop of 8 thymidines have a T_m of around 55˚C, which is high enough to maintain the hairpin structure at room temperature.

The TaqMan probe (hydrolysis probe) was used to hybridize the template. It is cleaved to produce signal for real-time PCR detection. In TaqMan based real-time PCR, the T_m of primers should be 58–60˚C and of the TaqMan probe 68–70˚C (in Primer Express 3.0).

These oligonucleotides should not form a stable hetero-dimers with Probe-F or Probe-R, which would otherwise decrease the PCR efficiency. If the targets include DNA, the sequence of the target should also be considered so that no other sequence is amplified.

Each probe should not form hairpin structure (exclude the designed hairpin structure within Probe-F) that would affect the binding of stem sequences.

Probe-F and Probe-R should not have additional hetero-dimer sequences beside the stem sequence. Otherwise, this would lead to hybridization between

these two probes and thus significantly increase the background signal.

Block-F and Block-R help reduce the spontaneous binding of Probe-F and Probe-R. This is achieved by blocking partial or whole stem sequences when the probes are not binding to the target. Since the stem regions of Probe-F and Probe-R are complementary, there is an overlapping region between the corresponding Block-F and Block-R.

Here, T_{m1}, T_{m2}, and T_{m3} are referred to as the T_m of the block-pair overlapping region, block-region, and stem sequence in the form of binding-induced assembly, respectively.

The design of the block pair should satisfy:

$$T_{m1} << T_{m2} < T_{m3}$$

The main objective of the blocks is to provide enough blocking effect to prevent the hybridization of unbound Probe-F and Probe-R while not affecting the binding-induced DNA assembly between Probe-F and Probe-R when Probe-F and Probe-R bind to the target. The blocking segment containing 9, 10, 11, or 12 n.t. complementary to the probes would have a T_{m2} of ~20˚C, 25–26˚C, 29–30˚C, 33–35˚C, respectively. Although a longer complementary region (higher T_{m2}) is desirable for blocking, there is a compromise considering T_{m2} and T_{m3}. Too long a complementary region of the block could affect the binding-induced assembly, thus T_{m3} must be higher than T_{m2}.

According to the above principles and parameters, we have designed Probes-F/R and Blocks-F/R (Table 2.1). The T_m of the corresponding hybridization sequences are listed in Table 2.2.

Table 2.2 T_m of the hybridization sequences. (a) T_m between Probe-F and Probe-R (b) T_m between Probe-F and Block-F (c) T_m between Probe-R and Block-R

Table 2.2 (a) T_m between Probe-F and Probe-R

	Probe-R6	Probe-R7	Probe-R8
Probe-F	30.7 ˚C	33.5 ˚C	37.4 ˚C

Table 2.2 (b) T_m between Probe-F and Block-F

	Block-F-1	Block-F-2	Block-F-3	Block-F-4
Probe-F	19.7 ˚C	25.3 ˚C	28.5 ˚C	30.8 ˚C

Table 2.2 (c) T_m between Probe-R and Block-R

	Block-R6-1	Block-R6-2	Block-R6-3	Block-R6-4
Probe-R6	22.4 ˚C	26.3 ˚C	31.7 ˚C	35.6 ˚C
	Block-R7-1	Block-R7-2	Block-R7-3	Block-R7-4
Probe-R7	24.0 ˚C	27.4 ˚C	32.3 ˚C	35.9 ˚C
	Block-R8-1	Block-R8-2	Block-R8-3	Block-R8-4
Probe-R8	27.4 ˚C	35.9 ˚C	39.5 ˚C	42.4 ˚C

2.3.2 PCR efficiency and linear dynamic range of the target sequence

PCR efficiency and dynamic range could be affected by many factors, such as PCR inhibitors, non-specific PCR products, PCR reagents, and primer design. Since our method quantifies the target sequence (ligation product of Probe-F and

Probe-R) to indirectly determine the protein concentration, we first need to ensure the target sequence could be quantified accurately. Therefore, PCR efficiency and PCR dynamic range of the target sequence were first tested to ensure that the signal output of the real-time PCR represented the target sequence concentration.

To carry out the PCR efficiency and dynamic range experiment, the target sequences were first produced by conventional PCR. First, Probe-F and Probe-R6 (both at 1 nM) were mixed and incubated in 1 × PBS buffer without blocks. This was to maximize the hybridization between Probe-F and Probe-R6. After the incubation, 2 μL of the incubation solution was transferred to a PCR tube containing 5 units of T4 DNA ligase, 5 units of DNA polymerase, 0.1 μM forward and reverse primers, 100 μM ATP, 200 μM dNTP, and 3mM $MgCl_2$ in 1×PCR buffer. The PCR tube was gently vortexed and then kept at room temperature for 10 min before it was introduced to the PCR thermal cycler. The PCR program was set as: a denaturing step at 95˚C for 5 min; thermal cycle containing 95˚C for 30 s, 60˚C for 30 s and 72˚C for 30 s for a total of 40 cycles, before the final elongation step at 72˚C for 10 min.

The PCR product was visualized on a 12% native polyacrylamide gel electrophoresis (PAGE) gel (Figure 2.3). After purification of the target sequence from the gel, the products were quantified by measuring absorbance at 260 nm using NanoVue (GE). A series of 10-fold diluted solutions were used to test the PCR efficiency and dynamic range (Figure 2.4).

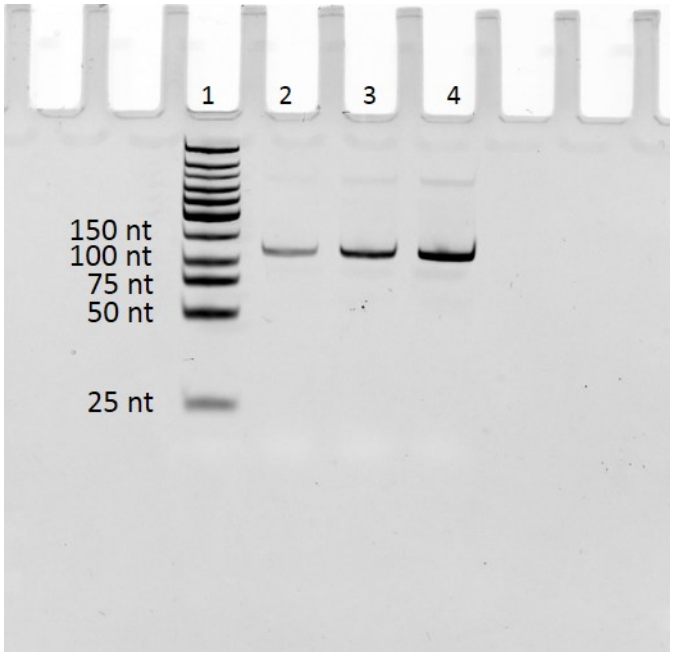

Figure 2.3 PCR product of target sequence (ligation product of Probe-F and Probe-R6) on 12% native PAGE gel. Lane 1: 100 bp DNA ladder, from bottom to top (25 bp, 50 bp, 75 bp, 100 bp, 150 bp, 200 bp, 300 bp, 400 bp, 500 bp, 600 bp, 700 bp). Lanes 2 to 4: 0.5 µL, 1 µL and 2 µL PCR products (118 bp).

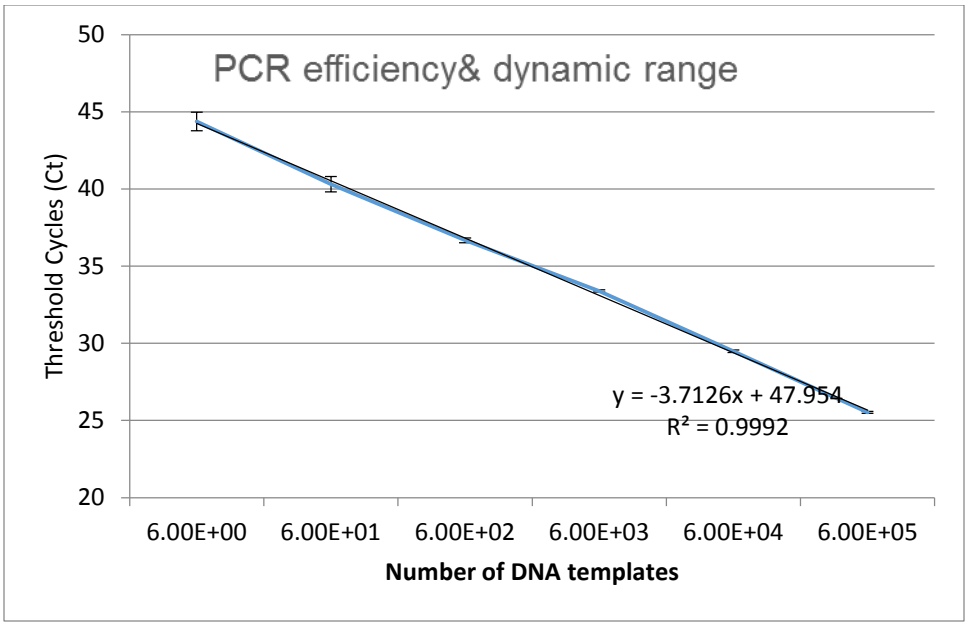

Figure 2.4 Threshold cycles from the real-time PCR analyses of 6, 60, 600, 6000, 60000, and 6000000 copies of the target sequence. Real-time qPCR experiments were carried out in triplicate and values are expressed as mean ± SD.

A wide linear dynamic range and high PCR efficiency are desirable for the binding-induced DNA assembly assay in order to quantitatively determine the target protein at a wide range of concentrations, including trace concentrations. The PCR efficiency could be determined using the equation: $E=10^{-1/slope}-1$. From Figure 2.3, the amplification of the target sequence by designed primers and PCR conditions could reach a high PCR efficiency (0.87) and a linear dynamic range of over 5 orders of magnitude ($R^2=0.9992$) including a copy number of less than 10. The results confirmed that our design of target sequences could be quantified by real-time PCR (from 6 copies to 6×10^5 copies).

2.3.3 Optimization of the assay

To test the design strategy of Probes-F/R and Blocks-F/R described in Section 2.3.1, we investigated the effect of the length of complementary stem sequences, from 6 nucleotides to 8 nucleotides. We used a combination of Probe-F with Probe-R6, Probe-R7, and Probe-R8. We also studied the effects of the complementary Blocks by using varying length of Blocks.

Firstly, Probe-F and Probe-R6 were studied (Figure 2.5). Streptavidin of 1 pM was used as the detection target in the testing group. The control group (blank) contained all reagents (but no streptavidin) and the same procedures were followed as for the testing group. Block-F-1 was used to study the effects of Block-R.

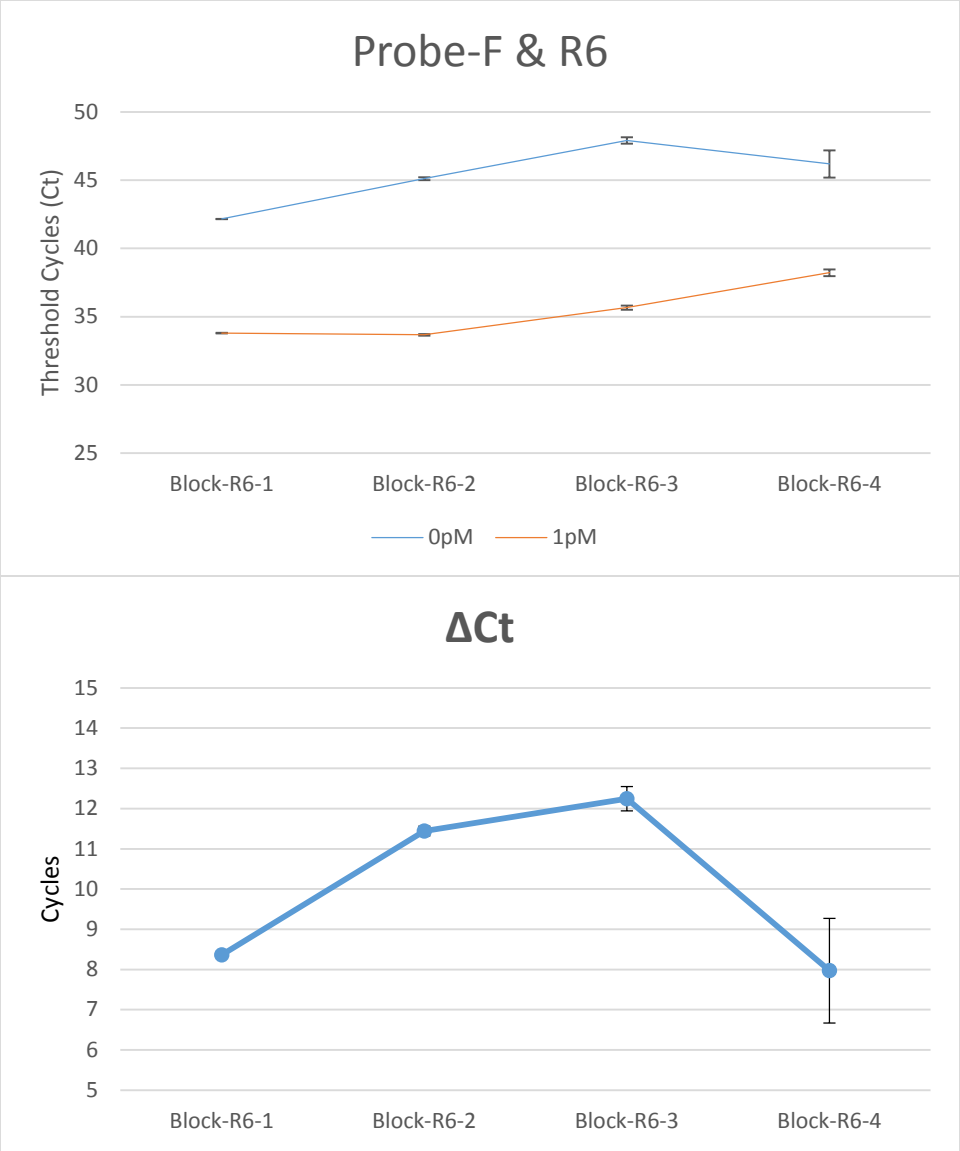

Figure 2.5 Probe-F and Probe-R6 with varying lengths of Block-R (From Block-R6-1 to Block-R6-4: 9 n.t., 10 n.t., 11 n.t., 12 n.t.). The upper graph shows threshold cycles (Ct) of both 1 pM streptavidin and the blank. The lower graph showed subtracted threshold cycles (ΔCt) of 1 pM streptavidin from the blank. Real-time qPCR experiments were carried out in triplicate and values are expressed as mean ± SD.

Results from Figure 2.5 showed a decreasing trend of signal from both 1 pM streptavidin and the blank sample with increasing Block-R length. We know that without target binding, the T_m between the Probe-F and Probe-R is below 10˚C. Under room temperature, most Probe-F and Probe-R will hybridize with their corresponding Blocks (T_m above 20˚C, see Table 2.2). When the target is present, binding of both Probe-F and Probe-R to the same target molecule will greatly enhance the T_m (above 30˚C) between the stem sequences of Probe-F and Probe-R. Therefore, competition will allow the Probes-F/R to dissociate from their Blocks and re-hybridize with each other. From Block-R6-1 to Block-R6-4, the T_m increases from 22.4˚C to 35.6˚C. When the T_m of a Block is above 30˚C, it would be much more difficult for Probe-F/R to dissociate from Blocks, because such a T_m is very close to the T_m of the Probe-F/R stem sequences or even higher than the T_m of Probe-F/R stem sequences. The decreasing trend is consistent with the calculation of T_m of the Blocks-R. When Block-R6-4 was used, the standard deviation of Ct (>1) was much larger than for shorter Blocks (Figure 2.5). This was because the copy numbers in each PCR reaction were less than 10 (Figure 2.4). In this situation, the variation of the template copy number could be very large due to such a small volume of solution (2 μL) transferred from the incubation buffer to the PCR reaction well. In some cases there could be more than 10 copies in that volume of solution while in other cases there could be no copies at all. Comparing the ΔCt from different Blocks we could conclude that Block-R6-3 generated the largest signal-to-background ratio.

Similarly, combining Probe-F/R7 with different Block-R7 and Probe-F/R8

with different Block-R8 was studied (Figure 2.6 and Figure 2.7). The decreasing trend of signal output from assembled Probe-F and Probe-R (R7 or R8) using increasing length of Block-R is consistent with the T_m calculation. Probe-F & Probe-R7 with Block-R7-3, and Probe-F & Probe-R8 with Block-R8-4 produced the highest ΔCt when Block-F-1 was used.

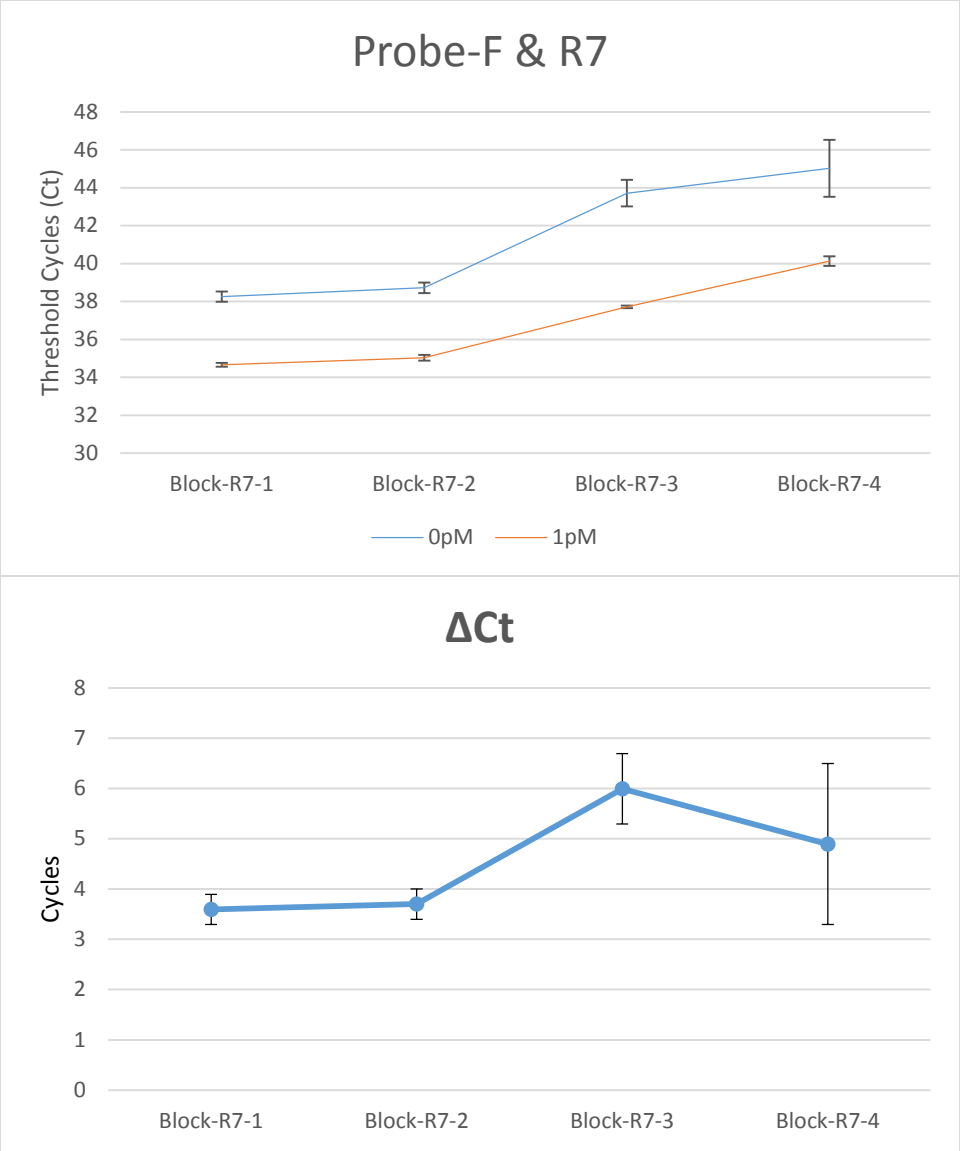

Figure 2.6 Probe-F and Probe-R7 with varying lengths of Block-R (From Block-R7-1 to Block-R7-4: 10 n.t., 11 n.t., 12 n.t., 13 n.t.). The upper graph shows threshold cycles (Ct) of both 1 pM streptavidin and the blank. The lower graph shows subtracted threshold cycles (ΔCt) of 1 pM streptavidin from the blank. Real-time qPCR experiments were carried out in triplicate and values are expressed as mean ± SD.

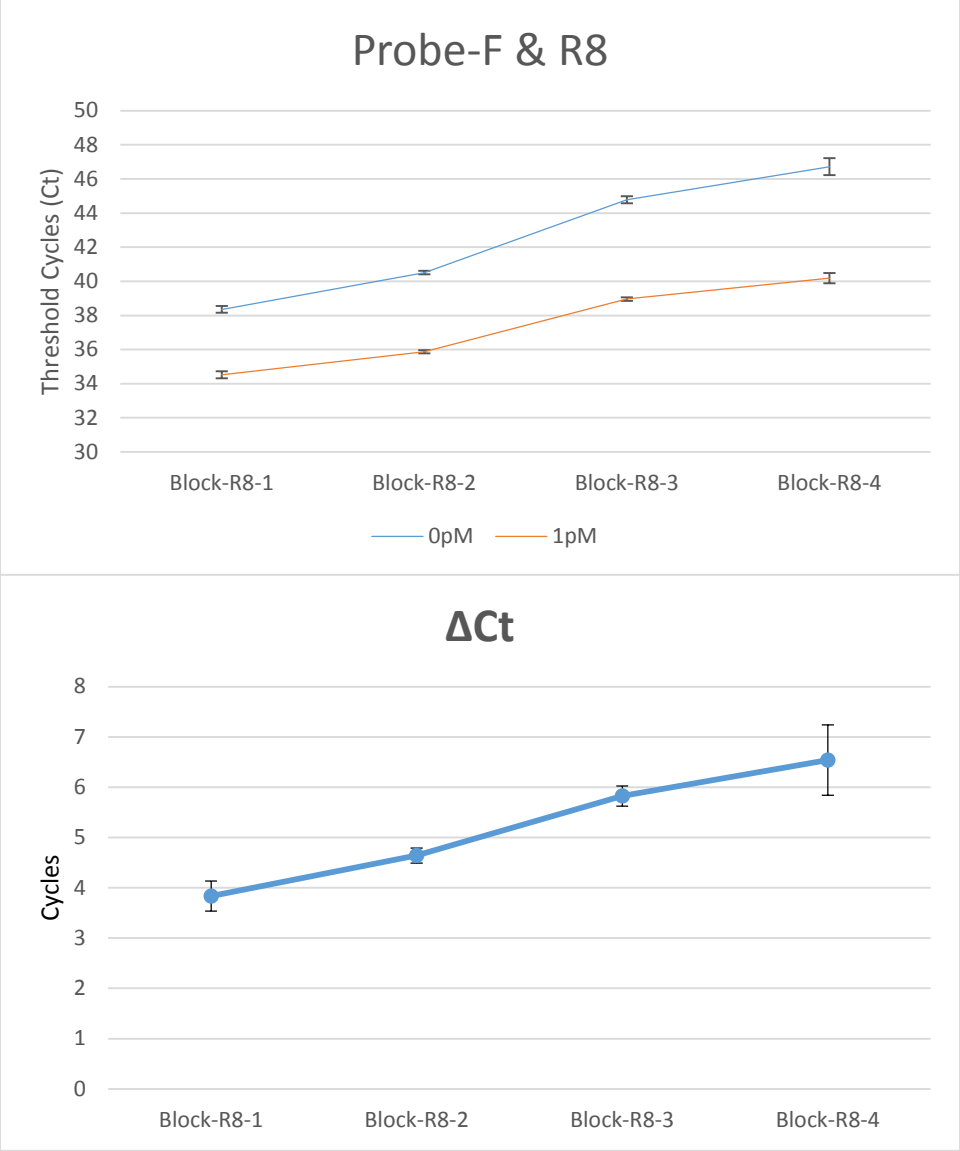

Figure 2.7 Probe-F and Probe-R8 with varying lengths of Block-R (From Block-R8-1 to Block-R8-4: 11 n.t., 12 n.t., 13 n.t., 14 n.t.). The upper graph shows threshold cycles (Ct) of both 1 pM streptavidin and the blank. The lower graph shows subtracted threshold cycles (ΔCt) of 1 pM streptavidin from the blank. Real-time qPCR experiments were carried out in triplicate and values are expressed as mean ± SD.

The best combinations in each length of Probe-R were compared in an assay to minimize the inter-assay variation (Figure 2.8). The results showed that Probe-F & Probe-R6 with Block-R6-3 generated the highest ΔCt.

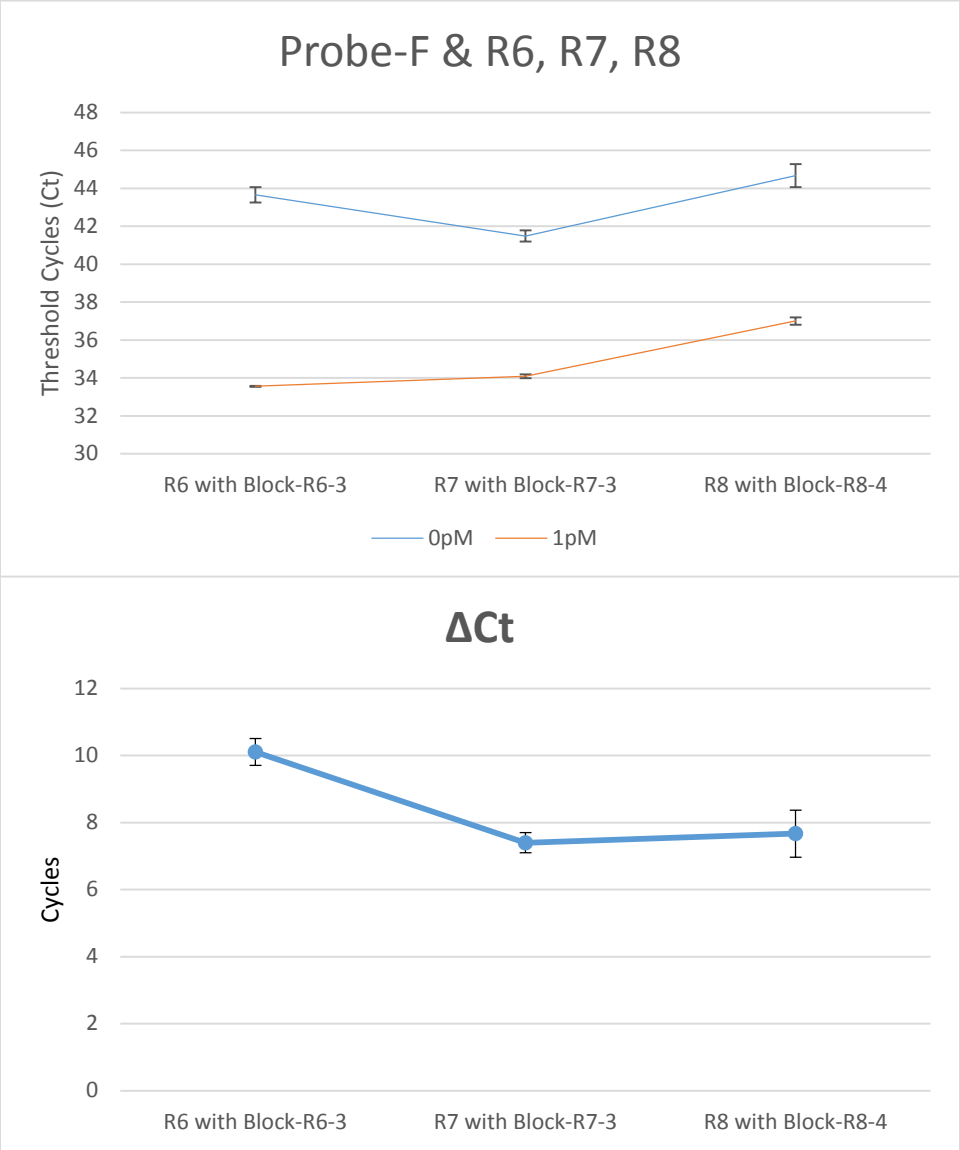

Figure 2.8 Comparison of highest S/N of Probe-R and its corresponding Block-R. The upper graph shows threshold cycles (Ct) of both 1 pM streptavidin and the blank. The lower graph shows subtracted threshold cycles (ΔCt) of 1 pM

streptavidin from the blank. Real-time qPCR experiments were carried out in triplicate and values are expressed as mean ± SD.

In the above optimization steps, Block-F-1 was used to ensure only one variable was present in different testing groups. The effect of the length of Block-F was also studied (Figure 2.9). Streptavidin (1 pM) was used as the target and the blank group contained no streptavidin. The optimized combination of Probe-F & Probe-R6 with Block-R6-3 was added to the incubation with varying length of Block-F (from Block-F-1 to Block-F-4). The result showed Block-F-4 had the largest ΔCt. However, the standard deviation was significantly higher than the other three Blocks. The reason was also the copy number as we could see that the Ct reached 46 cycles. According to Figure 2.4, the Ct of 6 copies assembled DNA was about 45 cycles. With the template copy number of less than 10, the variation of molecules in the sample transferred from the incubation tube to the PCR plate during the experimental operation could be very large. Therefore, Block-F-3 was chosen and the combination of Probe-F/R6 and Block-F-3/Block-R6-3 was used in all the following experiments.

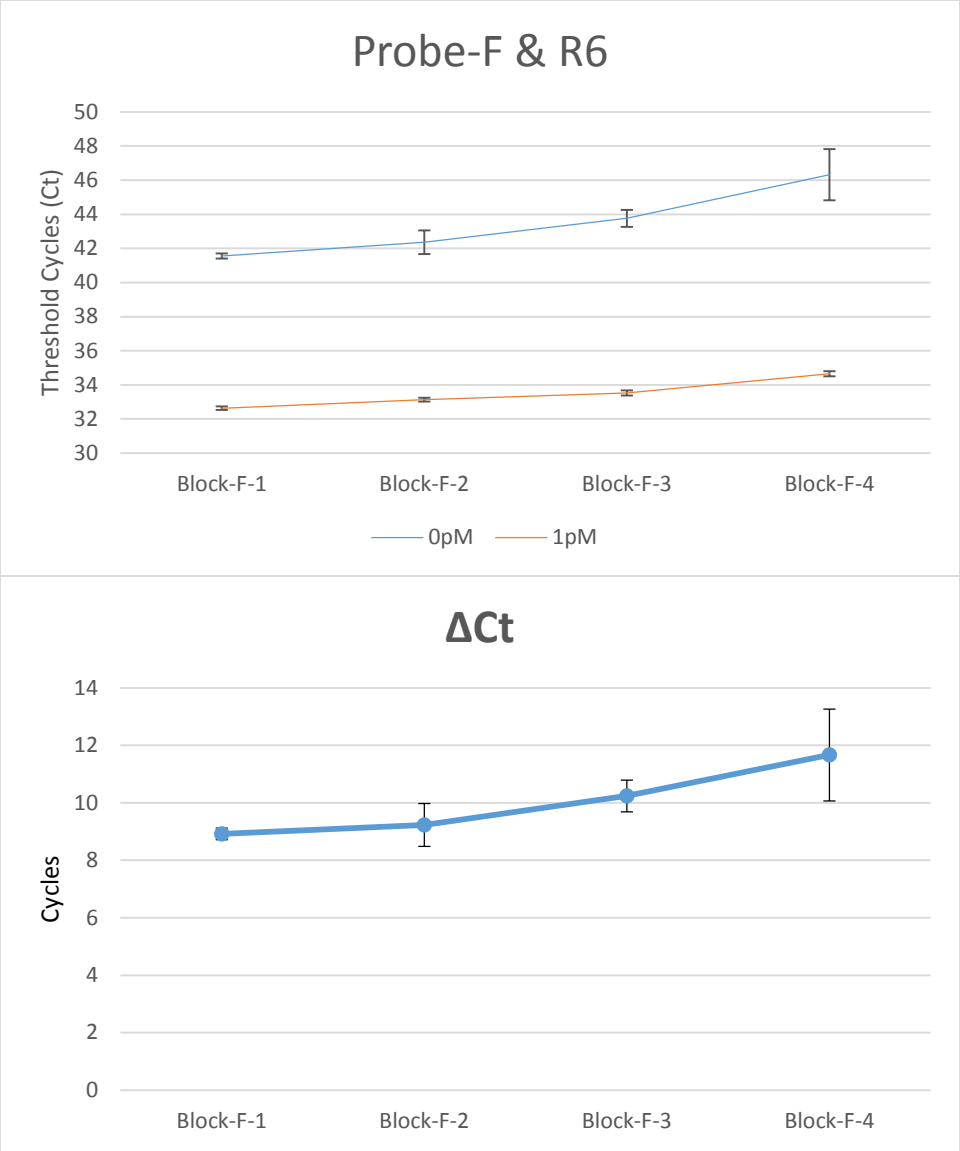

Figure 2.9 Probe-F and Probe-R6 with varying lengths of Block-F (From Block-F-1 to Block-F-4: 9 n.t., 10 n.t., 11 n.t., 12 n.t.). The upper graph shows threshold cycles (Ct) of both 1 pM streptavidin and the blank. The lower graph shows subtracted threshold cycles (ΔCt) of 1 pM streptavidin from the blank. Real-time qPCR experiments were carried out in triplicate and values are expressed as mean ± SD.

After the optimization of the length of stem sequences and blocking sequences, the ratio of the Probes/Blocks in the incubation solution was studied (Figure 2.10). Here the concentration of Probes-F/R6 was fixed at 100 pM and the ratio of Probes:Blocks varied from 1/1000 to 1/10000. With the increase of the concentration of Blocks, the signal from both 1 pM streptavidin and the blank showed a decreasing trend (increase of Ct). In the real-time PCR program, the number of thermal cycles was set to 50. When the Probes:Blocks ratio reached 1/5000, the signal output from the blank decreased to an undetectable level upon completion of the program. However, 1 pM streptavidin showed a Ct of over 43, indicating a very small number of assembled DNA. From the ΔCt chart in Figure 2.10, the ratio of 1/1000 showed the best signal-to-background and therefore was used in the following experiments.

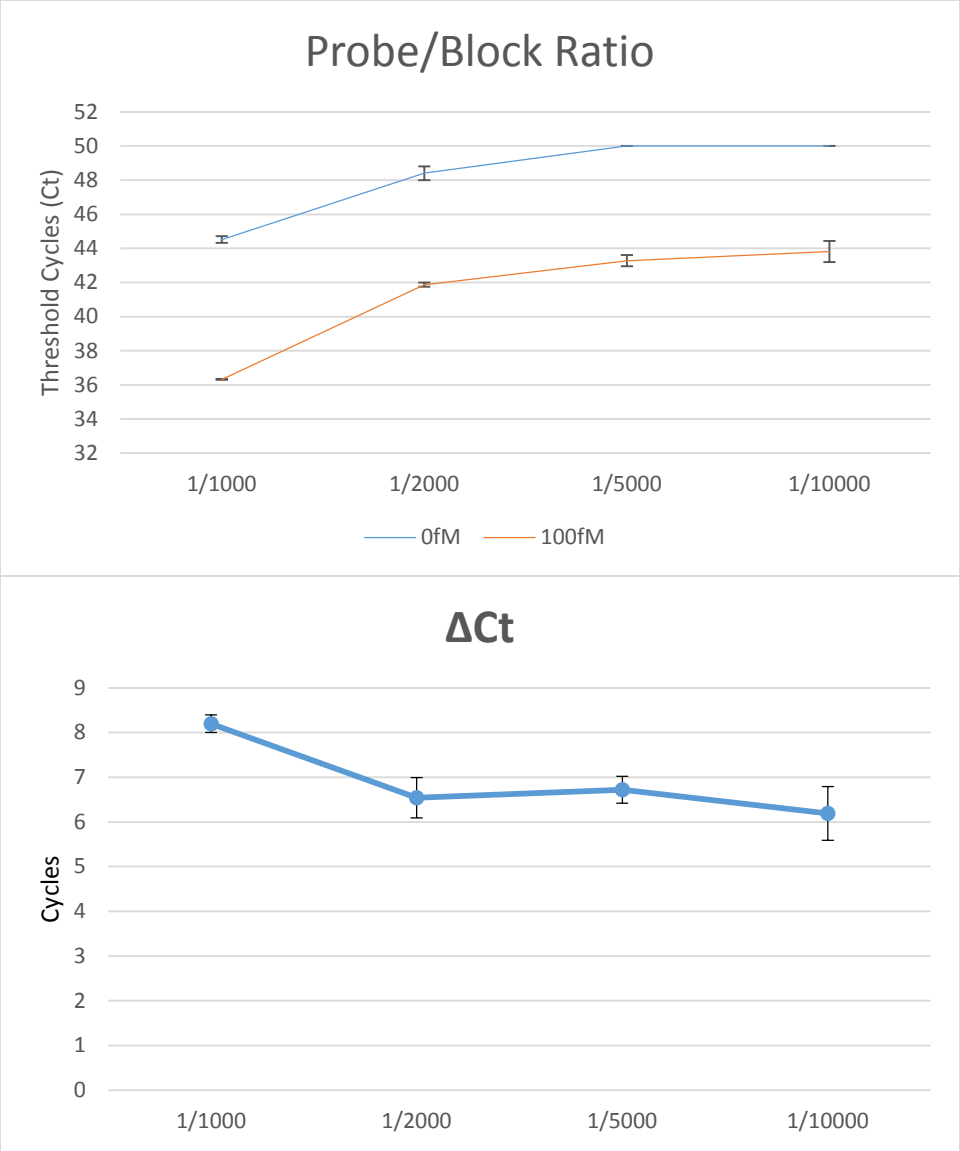

Figure 2.10 Optimization of Probes/Blocks ratio. Ratio of Probes/Blocks was from 1/1000 to 1/10000. Real-time qPCR experiments were carried out in triplicate and values are expressed as mean ± SD.

To test whether the ligation step has some impact on the final signal, one-step combined ligation and PCR was compared to two-step separate ligation and PCR (Figure 2.11). In the one-step method, an incubation solution of Probes/Blocks with streptavidin was transferred to the PCR reaction well containing ligase and

all reagents for real-time PCR. In the two-step method, the incubation solution was first added to the ligation mixture followed by transfer to the PCR reaction well. The one-step method is operationally simple as the PCR tube can be directly applied to Real-Time PCR instrument without any extra steps, but the PCR reaction buffer is not optimal for the ligase, compromising its performance. The two-step method provides the best working environment (pH and salt concentration) for ligase but more labor is needed, especially when dealing with a large quantity of samples.

In the two-step method, the incubation buffer was first added to an equal volume of ligation mixture (ATP, ligation buffer, and ligase) and 2 µL of the ligation product was then added to each PCR reaction. However in the one-step method, 1 µL of the incubation buffer was directly added to the PCR reaction. The time for ligation in both methods was 10 min before the PCR reaction.

The results from Figure 2.11 showed that separate ligation and PCR produced a higher background signal while slightly improving the 1 pM streptavidin signal. This indicates that the ligase activity in the PCR reaction buffer was adequate for ligation of the assembled Probe-F and Probe-R6 on the streptavidin molecule. Optimal ligation conditions and more ligase would not enhance the ligation efficiency for assembled Probe-F and Probe-R6 but would promote the ligation of free Probe-F and Probe-R6 molecules in the solution, increasing the background signal. This is because the Probe-F and Probe-R6 in the ternary complex with the target molecule have much higher local concentration than the Probes-F/R6 in free solution (*7*). Thus the ligation of assembled DNA in

the ternary complex does not require very high efficiency. Based on this result, the one-step combined ligation and PCR method was adopted in all the following experiments.

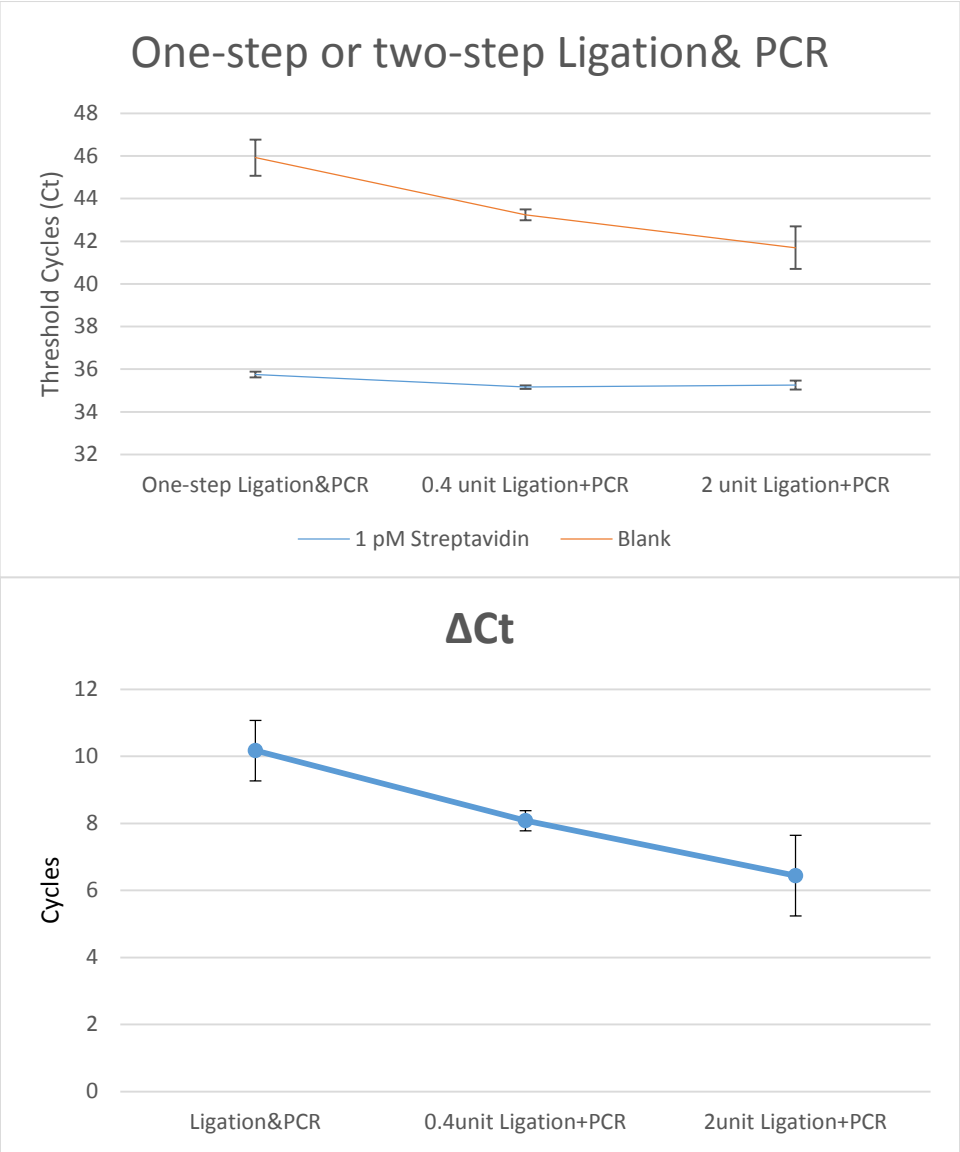

Figure 2.11 Comparison of the one-step combined ligation and PCR and the two-step separate ligation and PCR. Real-time qPCR experiments were carried out in triplicate and values are expressed as mean ± SD.

The ligation time was also optimized (Figure 2.12). Three different ligation times (5 min, 10 min, and 20 min) were compared using 1 pM streptavidin. Increased ligation time could clearly produce more ligated Probe-F/Probe-R6 in free solution (background signal, blue line) but have little influence on the assembled Probe-F/Probe-R6 (target signal, orange line). This result supports the explanation from the comparison of one-strep and two-step ligation and PCR: the assembled Probe-F and Probe-R6 on the streptavidin molecule have a much higher local concentration and therefore are easily ligated. More favorable working conditions for ligase would increase the background signal. A ligation time of 10 min was selected as it generated a smaller standard deviation than the 5 min ligation time and it is easier to minimize the variation of well-to-well ligation time when operating dozens of samples.

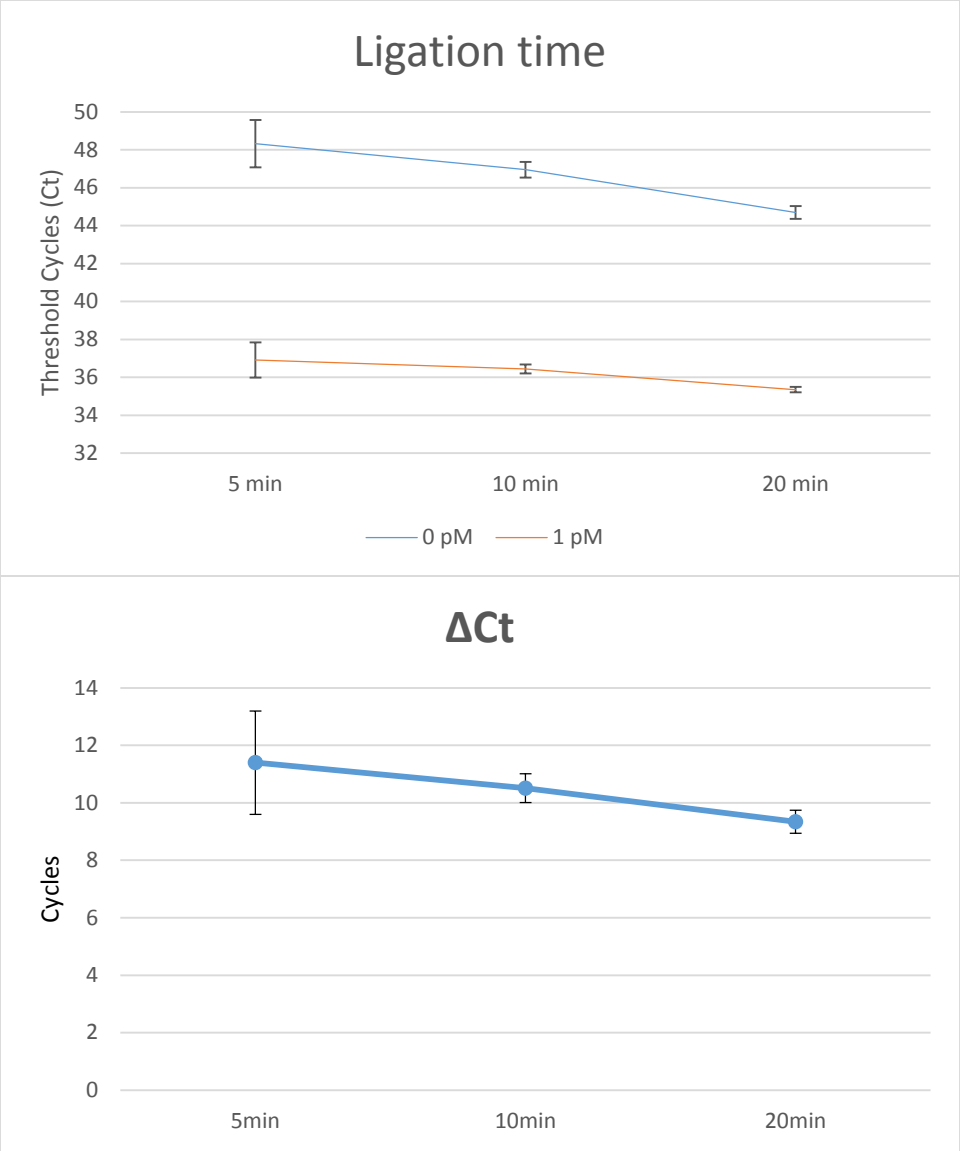

Figure 2.12 Effect of ligation time on the analysis of 1 pM streptavidin. Real-time qPCR experiments were carried out in triplicate and values are expressed as mean ± SD.

2.3.4 Dynamic range of streptavidin analysis

Using all the parameters optimized in the above experiments, a range of streptavidin concentrations were used (Figure 2.13). The assay could produce a

wide dynamic range of over 5 orders of magnitude, from 1 fM to 100 pM. If the detection limit is defined as 3 times the standard deviation plus the background signal, the detection limit of the assay was 1 fM. The streptavidin solutions were diluted by 1×PBS with 0.2% BSA solution (equal to 30 µM in molar concentration) and the excess amount of BSA did not interfere with the streptavidin detection, demonstrating this homogeneous assay is able to achieve sensitive detection of the target in the presence of high concentration of non-targets, providing high quality affinity ligands (e.g. antibodies, aptamers, or other highly specific binding ligands) are available.

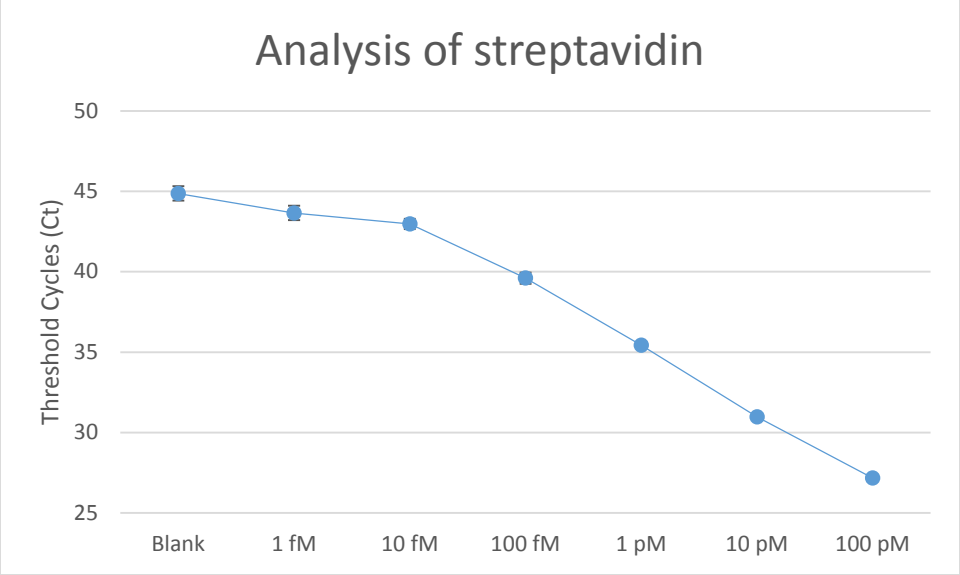

Figure 2.13 Dynamic range of the assay on streptavidin analysis. Real-time qPCR experiments were carried out in triplicate and values are expressed as mean ± SD.

2.4 Conclusions

The results shown here demonstrate a new strategy to construct a DNA

structure for binding-induced DNA assembly assay. The assembled DNA upon binding to the target protein serves as the signal output and therefore converts the protein detection to the detection of assembled DNA. This assay enables the analysis of targets in homogeneous solution. Use of real-time PCR to quantify the output DNA enables comparable high sensitivity for the non-DNA target. In the detection of streptavidin as a model target protein, the sensitivity of the method described in this chapter is comparable to that of the BINDA assay with SYBR Green detection (*5*). Development of the BINDA assay incorporating TaqMan chemistry will enable potential analysis of multiple targets in the same tube when different dyes are labeled on the each TaqMan probe. This method can also enable detection of DNA targets, which broadens the applicability of BINDA assays.

2.5 References

1. T. Sano, C. L. Smith, C. R. Cantor, Immuno-PCR: very sensitive antigen detection by means of specific antibody-DNA conjugates, *Science* **258**, 120–2 (1992).

2. S. Gofflot, M. Deprez, B. Moualij, A. Osman, J.-F. Thonnart, O. Hougrand *et al.*, Immunoquantitative PCR for prion protein detection in sporadic Creutzfeldt-Jakob disease, *Clin. Chem.* **51**, 1605–1611 (2005).

3. J. M. Barletta, D. C. Edelman, W. E. Highsmith, N. T. Constantine, Detection of ultra-low levels of pathologic prion protein in scrapie infected hamster brain homogenates using real-time immuno-PCR, *J. Virol. Methods* **127**, 154–164 (2005).

4. S. Fredriksson, M. Gullberg, J. Jarvius, C. Olsson, K. Pietras, S. M. Gustafsdottir *et al.*, Protein detection using proximity-dependent DNA ligation assays, *Nat. Biotechnol.* **20**, 473–7 (2002).

5. H. Zhang, X.-F. Li, X. C. Le, Binding-induced DNA assembly and its application to yoctomole detection of proteins, *Anal. Chem.* **84**, 877–84 (2012).

6. J. DeChancie, K. N. Houk, The origins of femtomolar protein-ligand binding: hydrogen-bond cooperativity and desolvation energetics in the biotin-(strept)avidin binding site, *J. Am. Chem. Soc.* **129**, 5419–5429 (2007).

7. H. Zhang, F. Li, B. Dever, C. Wang, X.-F. Li, X. C. Le, Assembling DNA through Affinity Binding to Achieve Ultrasensitive Protein Detection, *Angew. Chem. Int. Ed. Engl.* , 10698–10705 (2013).

Chapter Three

Homogeneous BINDA Assay for BPDE-*p53*-exon7 adducts

3.1 Introduction

Sensitive and reliable assays for BPDE-DNA adducts are required to monitor exposure to BP and to evaluate the potential cancer risk arising from exposure to this carcinogen. Although several quantitative methods, such as ^{32}P-postlabeling (*1–3*), enzyme-linked immunosorbent assay (ELISA) (*4*, *5*), capillary electrophoresis-laser induced fluorescence immunoassay (*6–8*), dissociation-enhanced lanthanide fluoroimmunoassay (*9*, *10*), chemiluminescence immunoassay (*11*), and comet assay (*12*), can achieve very low detection limits, none of them could provide information on which sequence or specific gene contains the BPDE adducts.

This chapter describes a homogeneous assay to quantify the BPDE adducts formed on specific target sequences. The assay is built on the technique described in Chapter 2 (Figure 3.1): TaqMan based binding-induced DNA assembly (BINDA) assay. Two probes (Probe-1 and Probe-2) were constructed based on the DNA oligonucleotides selected in Chapter 2. Probe-1 was constructed by conjugating the Probe-F to a BPDE antibody, and Probe-2 was constructed by conjugating Probe-R to a target-hybridization sequence (complementary to part of the target sequence containing the DNA-adduct). Streptavidin-biotin interaction was used for both conjugation steps. The BPDE antibody and target-hybridization

sequence serve as the affinity ligands in the BINDA assay. Target single-stranded BPDE-DNA adducts on *p53*-exon7 were incubated with Probe-1 and Probe-2. After the binding of Probe-1 to the BPDE molecule and Probe-2 to the target DNA, a dramatically increased local concentration of the DNA motifs promoted the formation of a new DNA assembly (Figure 3.1 C). Subsequent addition of DNA ligase helped to join the assembled DNA motifs (Figure 3.1 D). The newly formed longer piece of DNA can be detected using real-time qPCR. Thus, the detection of BPDE-DNA adducts is converted to the detection of the newly formed DNA assembly by real-time qPCR.

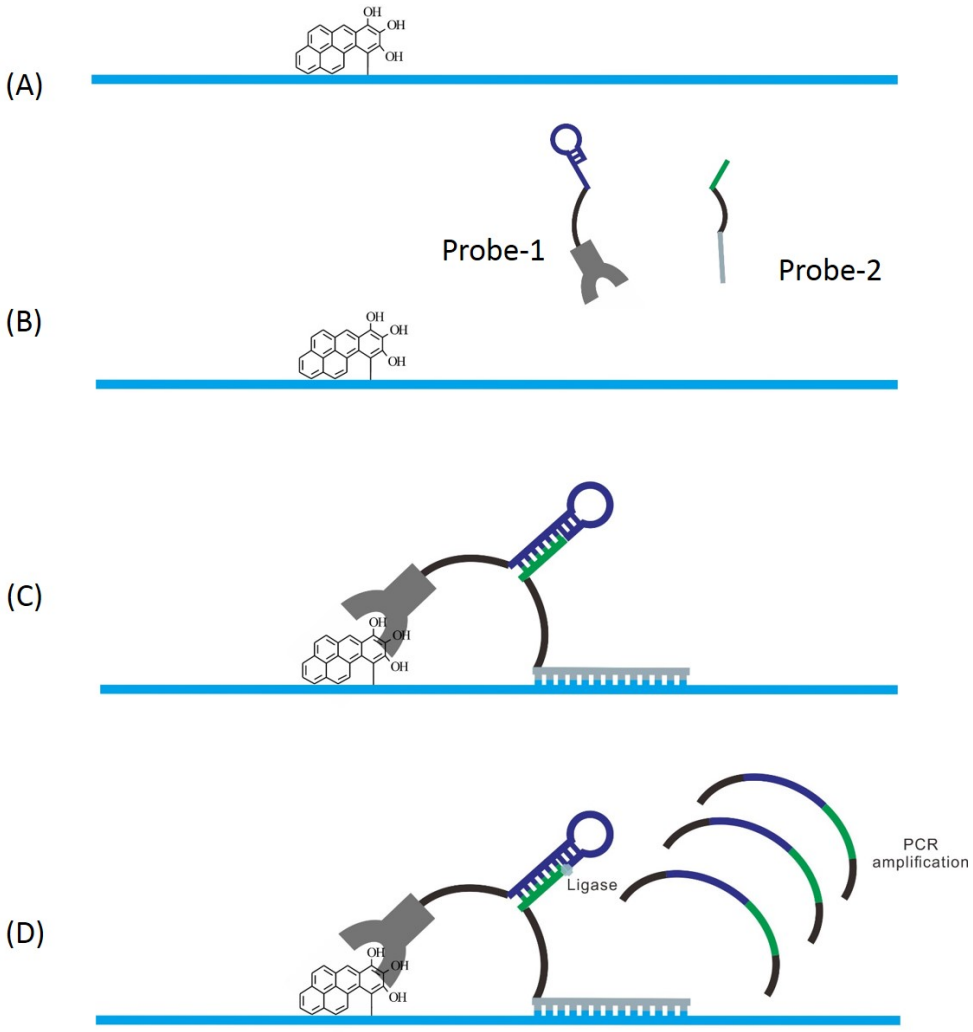

Figure 3.1 Schematic showing the binding induced DNA assembly assay for the detection of BPDE adducts formed on a specific target sequence. (A) BPDE-DNA adduct on the target *p53*-exon7. (B) Incubation of two probes with BPDE-DNA targets. Probe-1 is prepared by conjugating Probe-F with BPDE-antibody; Probe-2 is prepared by conjugation of Probe-R with a target-hybridization sequence. (C) Two binding events trigger the formation of the assembly between Probe-F and Probe-R. (D) The nick between Probe-F and Probe-R is ligated by ligase and the new DNA strand is then amplified and quantified by real-time qPCR.

To demonstrate the proof of principle, I first synthesized BPDE-*p53*-exon7 adducts as a model target. Exon 7 of the *p53* gene contains the frequently mutated codon 248 in all reported cancer cases that have *p53* missense mutations. This piece of single-stranded DNA has 92 nucleotides. A single BPDE is covalently bound at the CpG site of codon 248. Based on the optimization results in Chapter 2, the use of Probe-F and Probe-R6 containing a 6 n.t. stem sequence showed the highest signal-to-background ratio in the BINDA assay for streptavidin. Thus, I chose this probe pair for the development of the homogeneous BINDA assay for BPDE-*p53*-exon7 adducts.

3.2 Experimental

3.2.1 Reagents and instruments

(±)-*anti*- Benzo[a]pyrene diol epoxide (BPDE) (MRI No. 477) was supplied by the National Cancer Institute Chemical Carcinogen Reference Standard Repository (Midwest Research Institute, Kansas City, MO). Anhydrous tetrahydrofuran (THF, Cat. No. 401757, ≥99.9%), triethylamine (TEA, Cat. No. 471283, ≥99.5%) and bovine serum albumin (Cat. NO. A7906) were obtained from Sigma-Aldrich (ON, Canada). Trizma-hydrochloride buffer (Cat. No. T2663, 1M) was purchased from Fisher Scientific (Pittsburgh, PA). Monoclonal anti-BPDE antibody clone 8E11 (Cat. No. 4360-MC-100) was purchased from Trevigen (Gaithersburg, MD). Biotin-XX microscale protein labeling kit (Cat. No. B30010), Platinum® qPCR SuperMix UDG (Cat. No. 11730), T4 DNA Ligase (Cat. No. 15224), and T4 Polynucleotide Kinase (Cat. No. 18004) was purchased

from Invitrogen (Carlsbad, CA). QIAEX II Gel Extraction Kit was obtained from Qiagen (Valencia, CA). HPLC grade methanol and phosphate buffered saline (1×PBS) (137 mM NaCl, 10 mM phosphate, 2.7 mM KCl, pH 7.4), which was diluted with deionized water from 10×PBS buffer (Fisher Scientific, Nepean, ON). All other reagents were of analytical grade.

The oligonucleotides (listed in Section 3.2.2, except the TaqMan probe) were custom synthesized, labeled, and purified by Integrated DNA Technologies (IDT, Coralville, IA).

A Luna C18(2) column (250 mm×10 mm, 5 μm particle size; Phenomenex, Torrance, CA) and Agilent 1100 series LC system with a diode array spectrophotometric detector (DAD) was used to separate BPDE-adducted oligonucleotides from unreacted oligonucleotides.

The synthesized single-stranded BPDE-*p53*-exon7 was characterized using affinity capillary electrophoresis. A laboratory-built CE-LIF system is shown in Figure 3.2. The system includes a CE power supply (model CZE 1000R; Spellman, Plainview, NY), electrodes, a silica capillary, source and destination vials, a sample vial, a 488 nm argon ion laser (model 2014-65ML; Uniphase, San Jose, CA), a 515 nm band-pass filter, a photomultiplier tube (PMT, R1477; Hamamatsu Photonics, Japan) for signal detection, and a computer installed with data collection software.

A 7500 Fast Real-Time PCR system from Applied Biosystems (Foster City, CA) was used to run all PCR experiments. A 96-well MicroAmp Fast Optical Plate (Cat. No. 4346906) with barcode, and MicroAmp Optical Adhesive Cover

(Cat. No. 4360954) from Applied Biosystems compatible with this Real-Time PCR system were used in this study. The PCR program consisted of 50˚C for 2 min, 95˚C for 2 min, followed by 50 cycles of 95˚C for 15 s, and 60˚C for 30 s. All real-time qPCR experiments were carried out in triplicate.

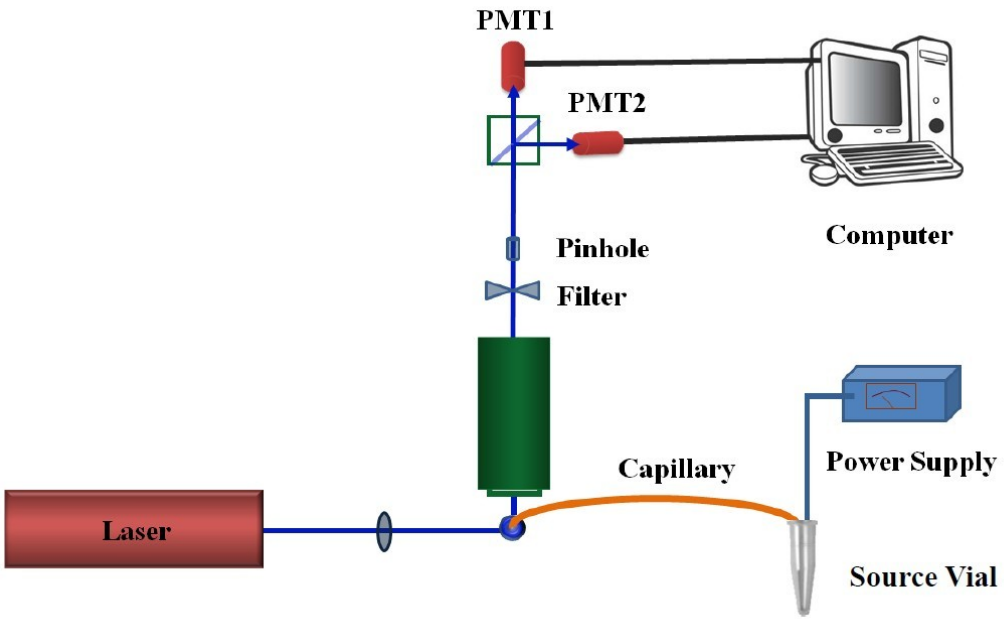

Figure 3.2 Schematic of the laboratory-built capillary electrophoresis with laser-induced fluorescence detection.

3.2.2 Synthesis of single-stranded BPDE-*p53*-exon7 adducts

The sequence of *p53*-exon7 was obtained from GeneBank (NCBI Reference Sequence: NG_017013.2). This sequence was selected because it contains one of the most frequently mutated codons, codon 248, according to *p53* mutations in the cancer database. BPDE-*p53*-exon7 adducts were synthesized by procedures similar to previous work (*13*) with slight modifications (Figure 3.3). Four pieces

of oligonucleotides were used to synthesize the BPDE-*p53*-exon7.

Oligo1: 5'-FAM-GTA CCA CCA TCC ACT ACA ACT ACA TGT GTA ACA GTT CCT GCA TGG GCG G-3'

Oligo2: 5'-CAT GAA CCG* GA-3'

Oligo3: 5'-Phos/GGC CCA TCC TCA CCA TCA TCA CAC TGG AAG AC-3'

Oligo4: 5'-GAT GGG CCT CCG GTT CAT GCC GCC CA-3'

*Starred guanine is the frequently mutated nucleotide in codon 248.

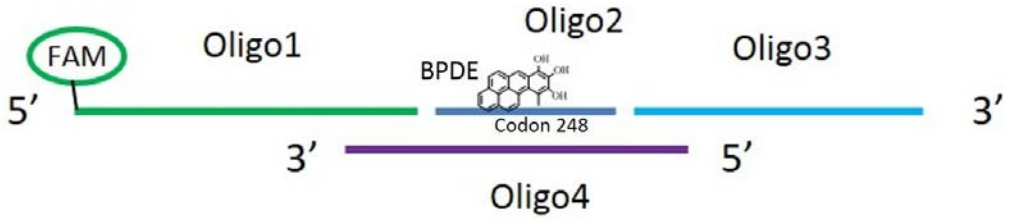

Figure 3.3 Schematic showing the synthesis of BPDE-*p53*-exon7 adducts.

Oligo2 was first reacted with racemic (±) anti-BPDE in 20 mM phosphate buffer containing 1% triethylamine (pH 11.0) at room temperature for 36 hours in the dark. BPDE-adducted oligo2 was separated from unreacted oligos and BPDE based on previous report. Briefly, the separation was achieved via a HPLC separation with a diode array spectrophotometric detector (DAD). An isocratic mobile phase of 20% methanol, 10 mM acetate buffer, and 0.14% triethylamine (pH 6.9) was used. The flow rate was 4 ml per min. Collected BPDE-oligo2 was

lyophilized and reconstituted in 10 mM Tris-HCl, pH 8.0.

The BPDE-oligo2 was phosphorylated at 37˚C for 2 hours in 1×kinase buffer by T4 polynucleotide kinase. After deactivation of the T4 polynucleotide kinase by heating up to 70˚C for 10 min, oligos 1, 3, and 4, ATP, and T4 DNA ligase were added to the solution. The ligation process was conducted overnight at 16˚C. Undamaged *p53*-exon7 was synthesized using the same procedures except that the BPDE-oligo2 was replaced by intact oligo2. Undamaged *p53*-exon7 was used as a negative control to test the specificity of the assay in method development.

The ligated single-stranded BPDE-*p53*-exon7 was then purified using 8% denaturing PAGE containing 7 M urea and the electrophoresis was carried out in 1×TBE buffer (90 mM Tris-Borate, 2 mM EDTA, pH 8.3). The gel was visualized on a Syngene GVM20 transilluminator (Synoptics, UK). Bands of the adducted DNA, BPDE-*p53*-exon7, and the undamaged DNA, *p53*-exon7, were cut from the gel and the DNA was recovered by the QIAEX II Gel Extraction Kit according to the manufacturer's instructions.

3.2.3 Characterization of synthesized BPDE-*p53*-exon7 adducts by CE-LIF

The synthesized single-stranded BPDE-*p53*-exon7 was characterized by affinity capillary electrophoresis. Different concentrations (10 nM, 20 nM, and 40 nM) of BPDE-*p53*-exon7 were incubated with high concentration of BPDE antibody 8E11 (200 nM) in 1×PBS buffer containing 0.2% BSA. The total volume was 20 μL. After 30 min incubation at room temperature, the mixture was subjected to CE-LIF analysis.

In the CE-LIF analysis, uncoated fused-silica capillaries (50 μm inner

diameter, 365 μm outer diameter, 40 cm length; Polymicro Technologies, Phoenix, AZ) were used for separation. Samples were electrokinetically injected into the capillary at a voltage of 10 kV for 5 s. A running voltage of 20 kV (500 V/cm) was used to drive the separation. The running buffer was 1×Tris-Glycine with pH 8.3. The capillary was first conditioned by injecting methanol using syringe for 1 h and then treated with 0.02 M NaOH for another hour followed by running buffer for 2 h. During the CE-LIF experiments, the capillary was washed periodically by 0.05 NaOH for 5 min, ddH_2O for 5 min, and running buffer for 5 min. BPDE-*p53*-exon7 can be separated from *p53*-exon7 without a BPDE adduct because BPDE-*p53*-exon7 binds to the 8E11 antibody which alters its migration rate in the capillary electrophoresis.

3.2.4. Preparation of Probe-1 and Probe-2

BPDE antibody 8E11 was first biotinylated by the Biotin-XX microscale protein labeling kit according to the manufacturer's instructions. Concentrations of biotinylated antibody was quantified using the NanoVue instrument (GE, Fairfield, CT) based on UV absorbance at 280 nm and internal protein-specific standard curve.

The Probes-F/R was prepared as follows: firstly 100 μL of 200 nM Probe-F (or Probe-R) and 100 μL of 200 nM streptavidin were mixed and incubated for 1 hour at room temperature. One hundred microliters of the Probe-F/streptavidin mixture was then mixed with 100 μL of 100 nM biotinylated 8E11 (or target-hybridization sequence for Probe-R/streptavidin mixture) and incubated for another hour at room temperature. All the incubation tubes were placed on a

rotating mixer to allow continuous mixing. At last, equal volume of 1 mM biotin dissolved in 1× PBS buffer was added to the Probe-1 and Probe-2 and the final concentration of the stock solutions were 25 nM.

3.2.5. Analysis of BPDE-*p53*-exon7 by homogeneous BINDA

The experimental procedures are shown in Figure 3.4. The target BPDE-*p53*-exon7 or undamaged *p53*-exon7 was incubated with Probe-1/Probe-2 and Blocks-F/R in 100 μL of 1×PBS with 0.2% BSA and $MgCl_2$ for 30 min at 37˚C followed by 10min at 25˚C. Then 2 μL of the incubation solution was transferred to 18 μL real-time PCR reaction containing 1× PCR buffer, 3 mM $MgCl_2$, dNTPs, 0.1 μM forward and reverse primers, DNA polymerase, 0.25 μM Rox reference dye, 0.1 μM TaqMan probe, and 0.4 unit T4 DNA ligase. The mixture was kept in the dark at room temperature for 10 min and then the PCR plate was applied to real-time qPCR quantification. All real-time qPCR experiments were carried out in triplicate.

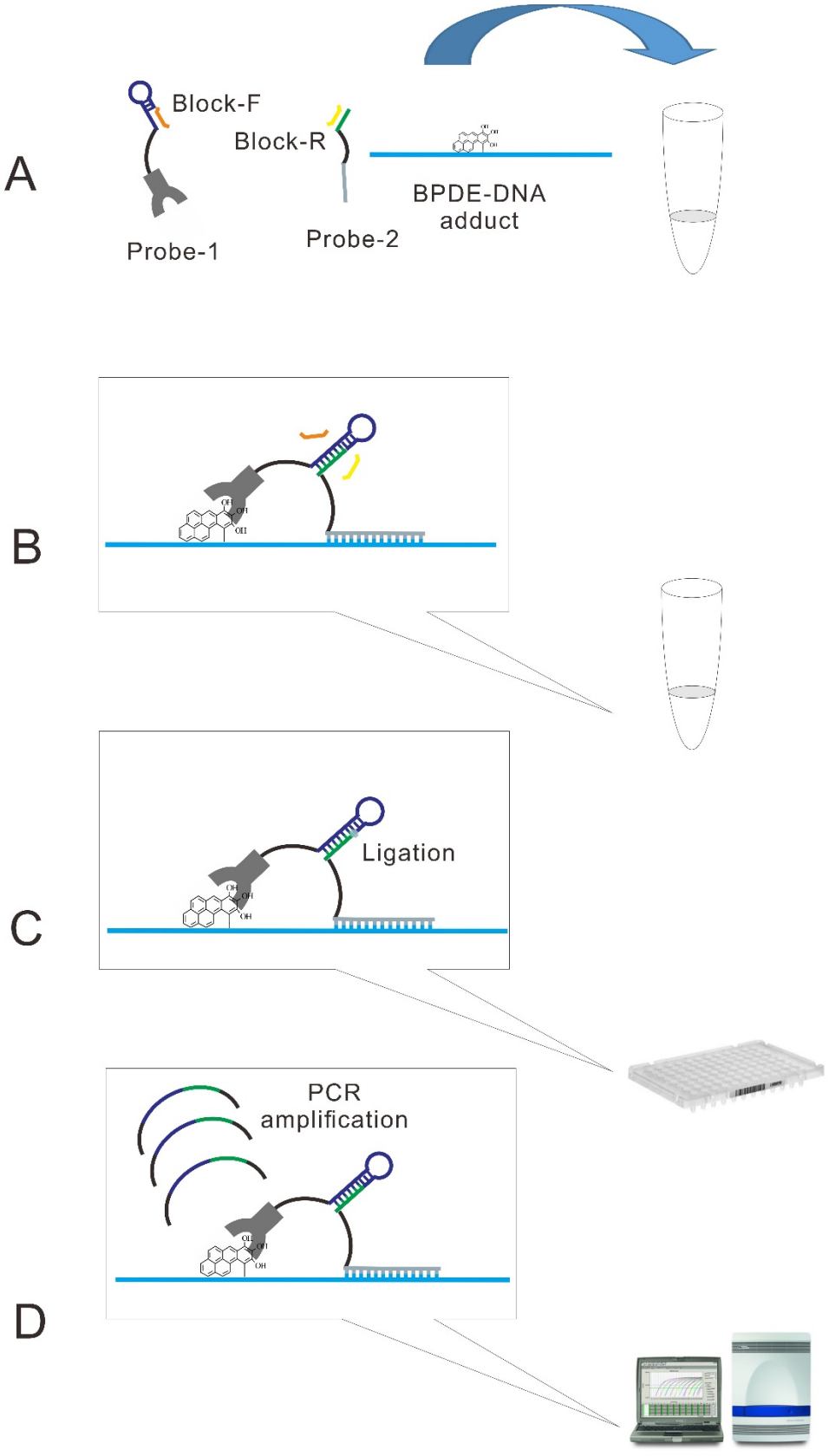
A
Block-F
Block-R
Probe-1
Probe-2
BPDE-DNA
adduct
B
C
Ligation
D
PCR
amplification

Figure 3.4 Analysis of BPDE-*p53*-exon7 by homogeneous BINDA. (A) Probe-1/Probe-2, Block-F/Block-R and BPDE-*p53*-exon7 were added to the incubation buffer. (B) Binding induced DNA assembly occurred after Probe-1 and Probe-2 bound to BPDE-*p53*-exon7. (C) Incubation buffer was transferred to the PCR reaction on a real-time qPCR plate. Probe-1 and Probe-2 were ligated by ligase in the PCR reaction mixture. (D) The extended DNA sequence from the ligated Probe-1 and Probe 2 was amplified and quantified by real-time qPCR.

3.3 Results and Discussion

3.3.1 Synthesis of BPDE-*p53*-exon7 adducts

After the reaction of oligo2 with BPDE, the BPDE-oligo2 was purified through HPLC equipped with a DAD. Figure 3.5 shows chromatograms from the HPLC separation of BPDE-oligo2 from the unreacted oligo2. Elution was monitored using UV absorption at 343 and 254 nm. BPDE has a specific absorption peak at 343 nm while the absorption peak of DNA is at 254 nm. BPDE-oligo2 is more hydrophobic than oligo2 due to the addition of a BPDE group, therefore it has longer retention time on the C18 column. Unreacted oligo2 was eluted very fast (3 min) with only one absorption peak at 254 nm. The BPDE-oligo2 was eluted at 9.5 min with two absorption peaks at both 254 nm and 343 nm (Figure 3.5).

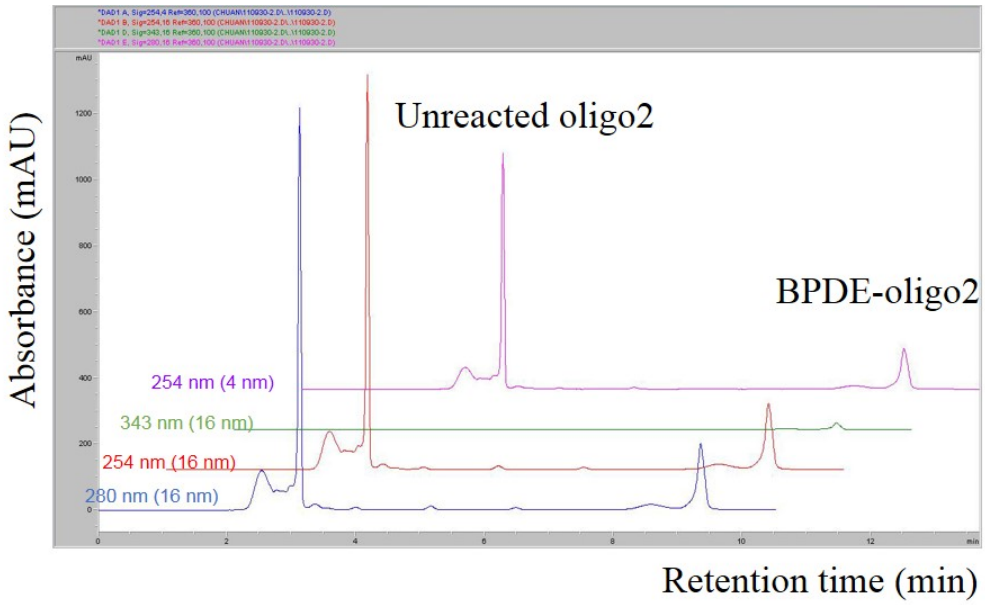

Figure 3.5 Chromatogram from HPLC separation and UV absorption detection of BPDE-oligo2. Y-scale: signal intensity (a. u.), X-scale: retention time (min). From bottom to top: 254 nm (width 4 nm), 254 nm (width 16 nm), 343 nm (width 16 nm), 280 nm (width 16 nm).

The eluent containing BPDE-oligo2 eluted at 9.5 min was collected and lyophilized. The lyophilized BPDE-oligo2 was then reconstituted in 10 mM Tris-HCl (pH 8.0). BPDE-oligo2 was phosphorylated before it was used to synthesize BPDE-*p53*-exon7 through joining other pieces of oligos. Figure 3.6 shows the ligation product separated on a denaturing PAGE gel. Comparing the bands in the ligation products and the molecular DNA standards, ligated BPDE-*p53*-exon7 adducts were confirmed (shown by red circle). The BPDE-*p53*-exon7 adducts and the undamaged *p53*-exon7 with the same migration rate on PAGE gel were extracted and re-dissolved. The purity of the extracted products was examined on

a denaturing PAGE gel (Figure 3.7).

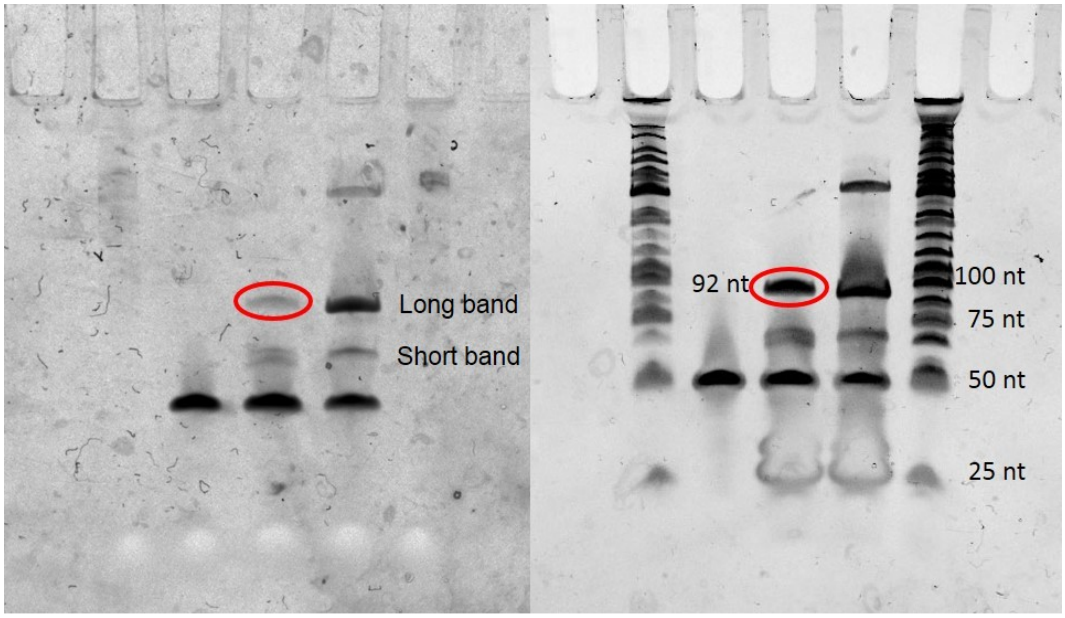

Figure 3.6 Denaturing gel electrophoresis of ligated BPDE-*p53*-exon7 products. The gel was stained by SYBR Gold from Invitrogen. Lanes from left to right: DNA ladder, 5'-FAM-oligo1, BPDE-*p53*-exon7 ligation product, undamaged *p53*-exon7 ligation product, DNA ladder. The red circled bands correspond to the BPDE-*p53*-exon7 adduct. The short band between 5'-FAM-oligo1 and BPDE-*p53*-exon7 ligation products was also cut and recovered.

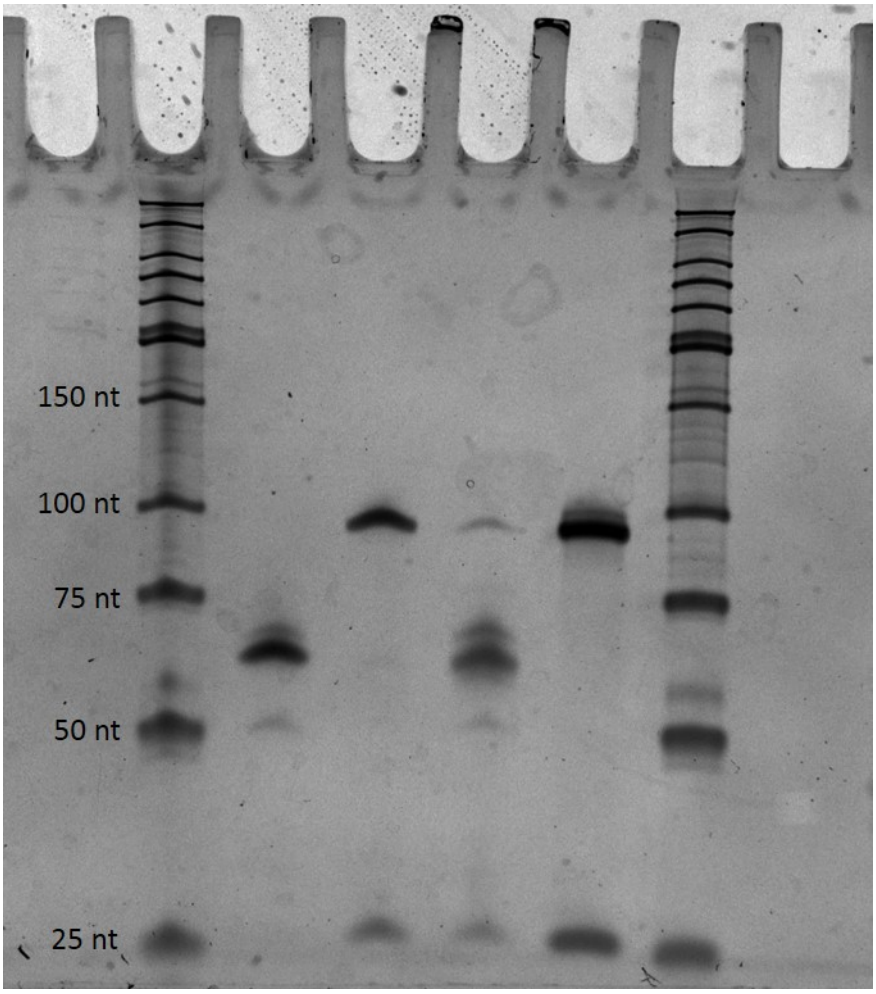

Figure 3.7 Denaturing gel electrophoresis examination of the purity of recovered products from Figure 3.6. Lanes from left to right: DNA ladder, shorter bands from BPDE-*p53*-exon7 ligation products, BPDE-*p53*-exon7, short bands from undamaged *p53*-exon7 ligation products, undamaged *p53*-exon7.

The extracted BPDE-*p53*-exon7 adducts were characterized and quantified by CE-LIF (Figure 3.8). The result showed that approximately 10% of the products contained BPDE adducts. The concentrations of BPDE-*p53*-exon7 and non-adducted *p53*-exon7 were determined based on the peak area in comparison to fluorescently labeled oligo1 which is not shown in Figure 3.8.

The reason that only a small portion of the synthesized product contained BPDE adducts might be due to the hydrolysis of BPDE from the DNA strand during the purification and extraction procedures. It had been reported that BPDE adducts on DNA can be hydrolyzed in acidic condition (*14*).

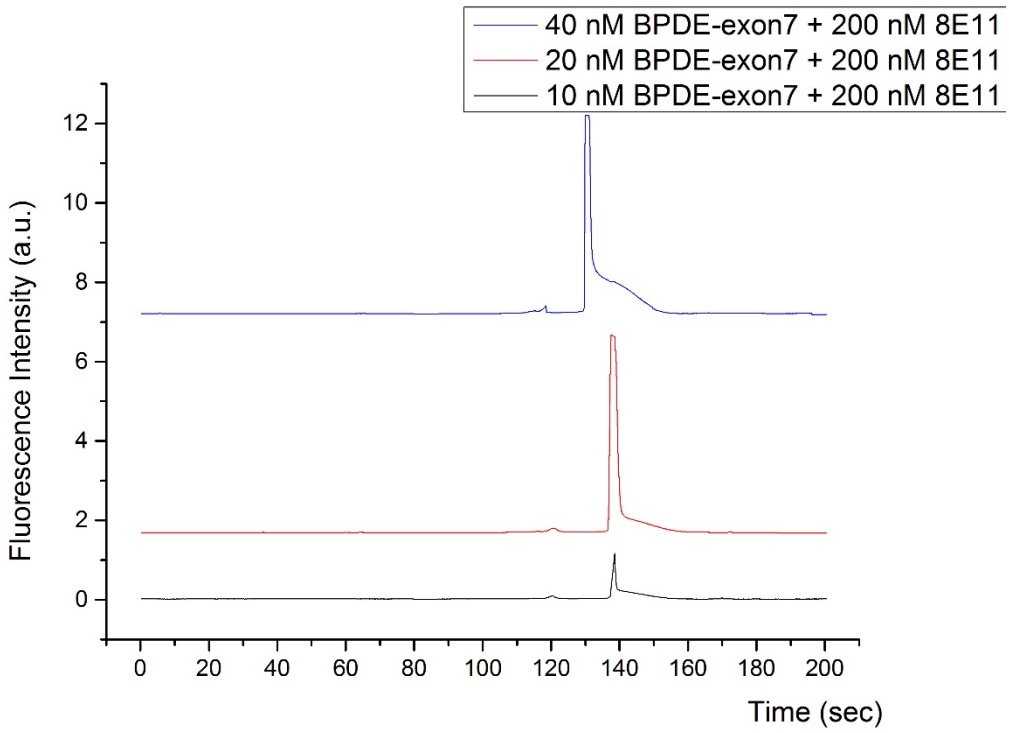

Figure 3.8 CE-LIF characterization of the synthesized BPDE-*p53*-exon7 adducts. Three concentrations (10 nM, 20 nM, and 40 nM) of BPDE-*p53*-exon7 were incubated with a high concentration of BPDE antibody 8E11 (200 nM). The BPDE-DNA adduct-antibody complex was analyzed using CE-LIF.

3.3.2 Analysis of BPDE-*p53*-exon7 by homogeneous BINDA

The longer target-hybridization oligonucleotide in Probe-2 results in higher affinity to the BPDE-*p53*-exon7. It is reasonable to hypothesize that a longer

target-hybridization oligonucleotide could generate a higher signal-to-background ratio in the homogeneous BINDA assay. To test this hypothesis, various lengths of target-hybridization oligonucleotides (Table 3.1) were used to construct Probe-2. The target-hybridization oligonucleotides were biotinylated at the 3' end for conjugation. Considering the size of streptavidin molecule, the target-hybridization oligonucleotides were extended by three thymines (T) to avoid possible steric hindrance. BPDE-*p53*-exon7 adducts at a concentration of 100 pM was used as the target.

Table 3.1 Target-hybridization oligonucleotides.

Length of the target-hybridization oligonucleotides	Sequences (5'-3')	T_m (˚C)
19 nt	CAG GAA CTG TTA CAC ATG TTT T	38.8
23 nt	CAG GAA CTG TTA CAC ATG TAG TTT TT	43.5
27 nt	CAG GAA CTG TTA CAC ATG TAG TTG TAT TTT	47

Hybridization sequences are underlined. The T_m was predicted by IDT-OligoAnalyzer 3.1 at 0.1 nM oligonucleotide concentration, 50 mM Na^+ and no Mg^{2+}.

A previous experiment showed that analysis of BPDE-DNA adducts using Probe-2 with 16 nt target-hybridization sequence could not differentiate between

signals containing BPDE-DNA and blanks (data not shown). Therefore, different target-hybridization sequences with a starting length of 19 n.t. were used to prepare the Probe-2. The T_m of these target-hybridization sequences are listed in Table 3.1.

To compare the impact of the length of target-hybridization oligonucleotides, a 100 pM of BPDE-*p53*-exon7 sample and a blank sample were incubated with Probe-2 containing different target-hybridization sequences (Figure 3.9). Difference between the Ct of 100 pM BPDE-*p53*-exon7 sample and the blank sample (ΔCt) indicated the signal/background ratio of the assay. The result showed that Probe-2 with 27 n.t. hybridization oligonucleotide (Probe-2-27nt) gave rise to the highest signal/background ratio and was chosen for subsequent experiments.

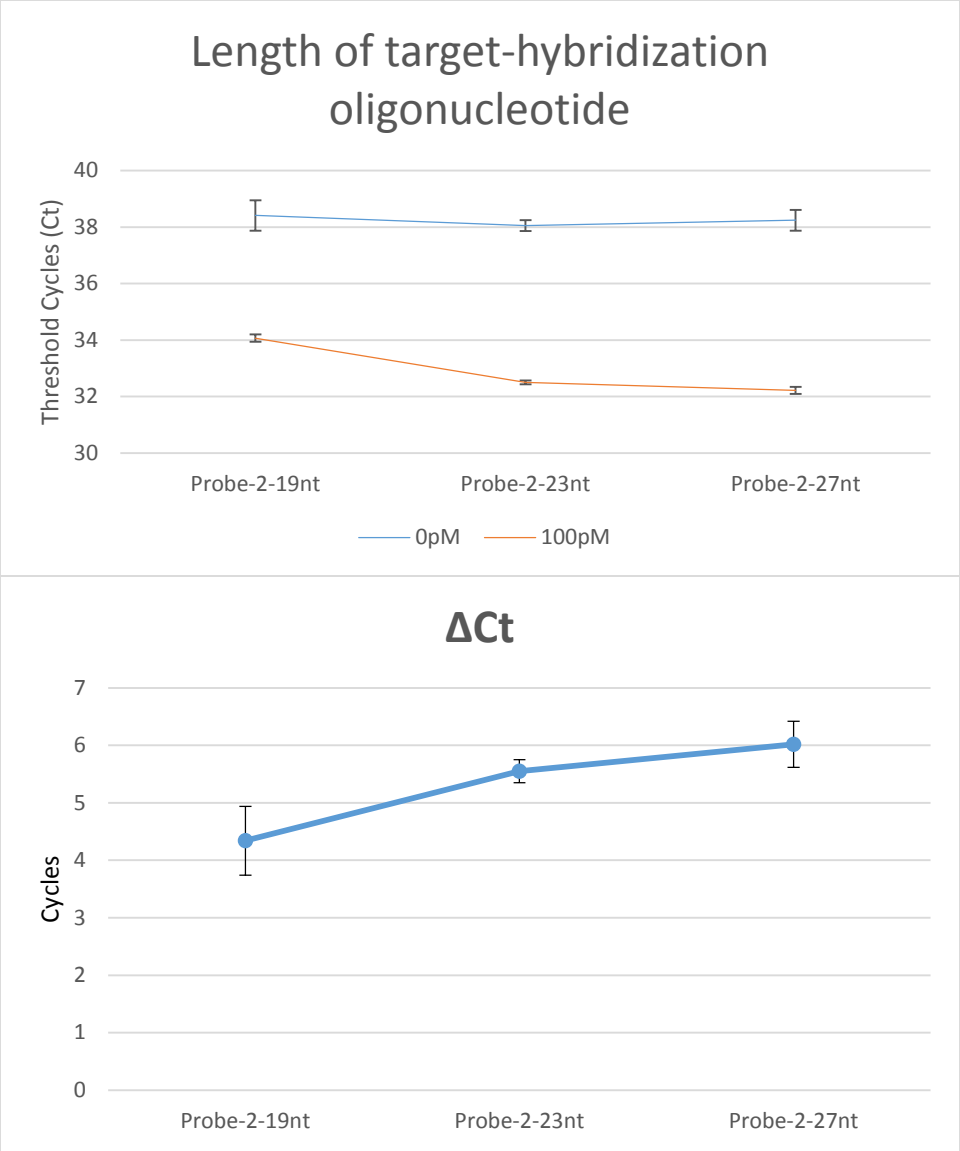

Figure 3.9 Effect of length of target-hybridization oligonucleotides used to construct Probe-2 on the BPDE-*p53*-exon7 analysis. Real-time qPCR experiments were carried out in triplicate and values are expressed as mean ± SD.

Streptavidin has four binding sites for biotin, so Probe-1 could be constructed with up to three biotinylated antibody molecules and one biotinylated Probe-F through streptavidin-biotin interaction. Probe-1 containing 1, 2 or 3

antibody molecules was incubated with two concentrations of BPDE-*p53*-exon7 adducts (Figure 3.10). More antibodies conjugated to the Probe-1 molecule could increase the affinity of Probe-1 to BPDE molecules and thus a higher signal for BPDE-*p53*-exon7 sample could be generated. The results show that Probe-1 with three antibodies (Probe-1-Antibody*3) produced a higher signal in the BPDE-*p53*-exon7 adduct sample than Probe-1 with one or two antibodies. However, the standard deviation in the blank sample was much larger in Probe-1-Antibody*3. Therefore, Probe-1 with two antibodies (Probe-1-Antibody*2) was used in the following experiments.

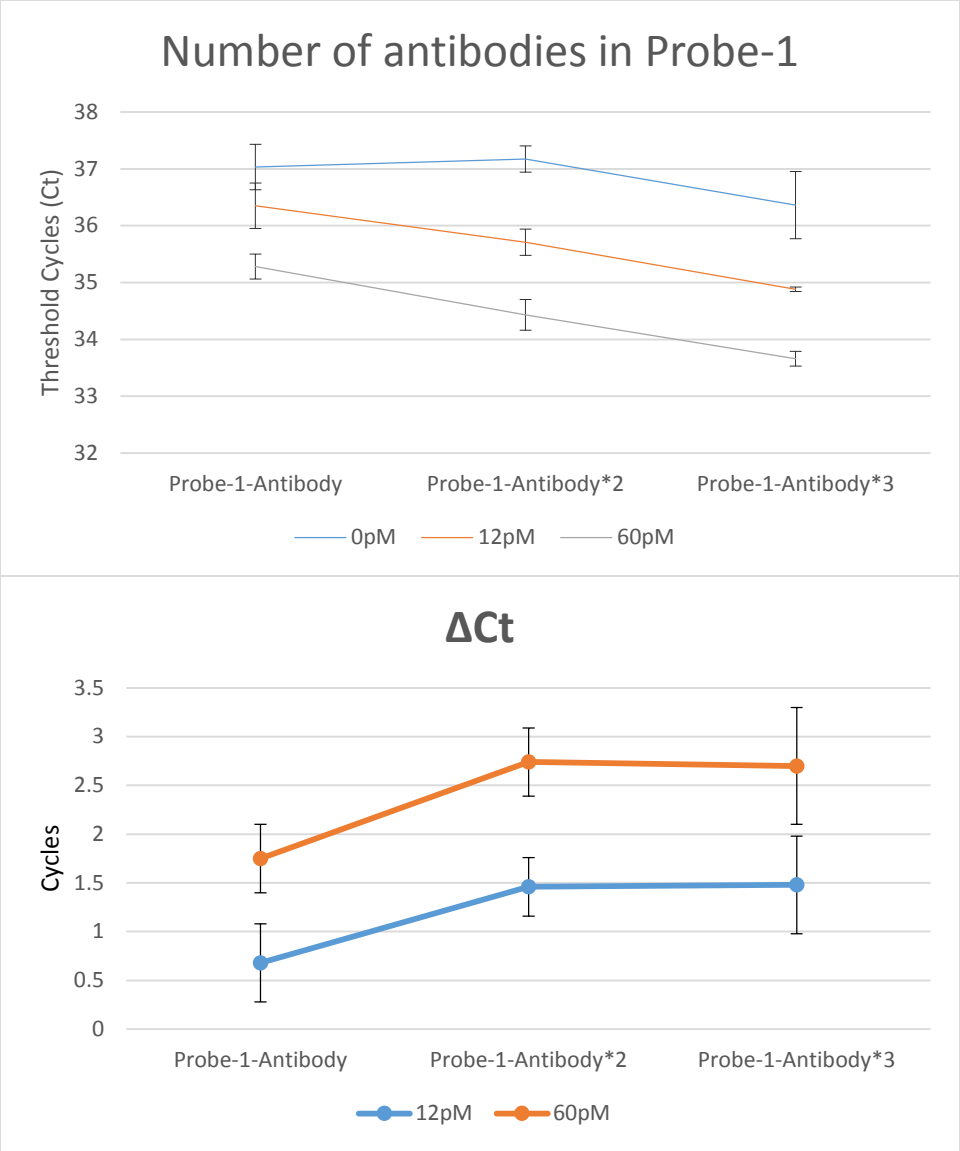

Figure 3.10 Effect of the antibody number conjugated to Probe-1 for the BPDE-*p53*-exon7 analysis. Real-time qPCR experiments were carried out in triplicate and values are expressed as mean ± SD.

To reduce the background from target-independent hybridization between Probes-1 and Probe-2, the effect of Blocks (Block-F and Block-R) that could partially hybridize with the stem sequences of Probe-F or Probe-R were studied.

In this experiment, excess concentration of Blocks (>100 times the concentration of Probe-1/Probe-2) were added into the incubation mixture. Various lengths of Blocks, from 9 n.t. to 12 n.t. (corresponding to Block-F-1/Block-6R-1 to Block-F-4/Block-6R-4) were used to optimize the length of Blocks (Figure 3.11). The result showed longer blocking sequences reduced the signal both from the adducts sample and the blank sample. The block pair with 11 n.t. showed highest ΔCt. As a result, Block-F-3/Block-6R-3 with 11 n.t. was selected.

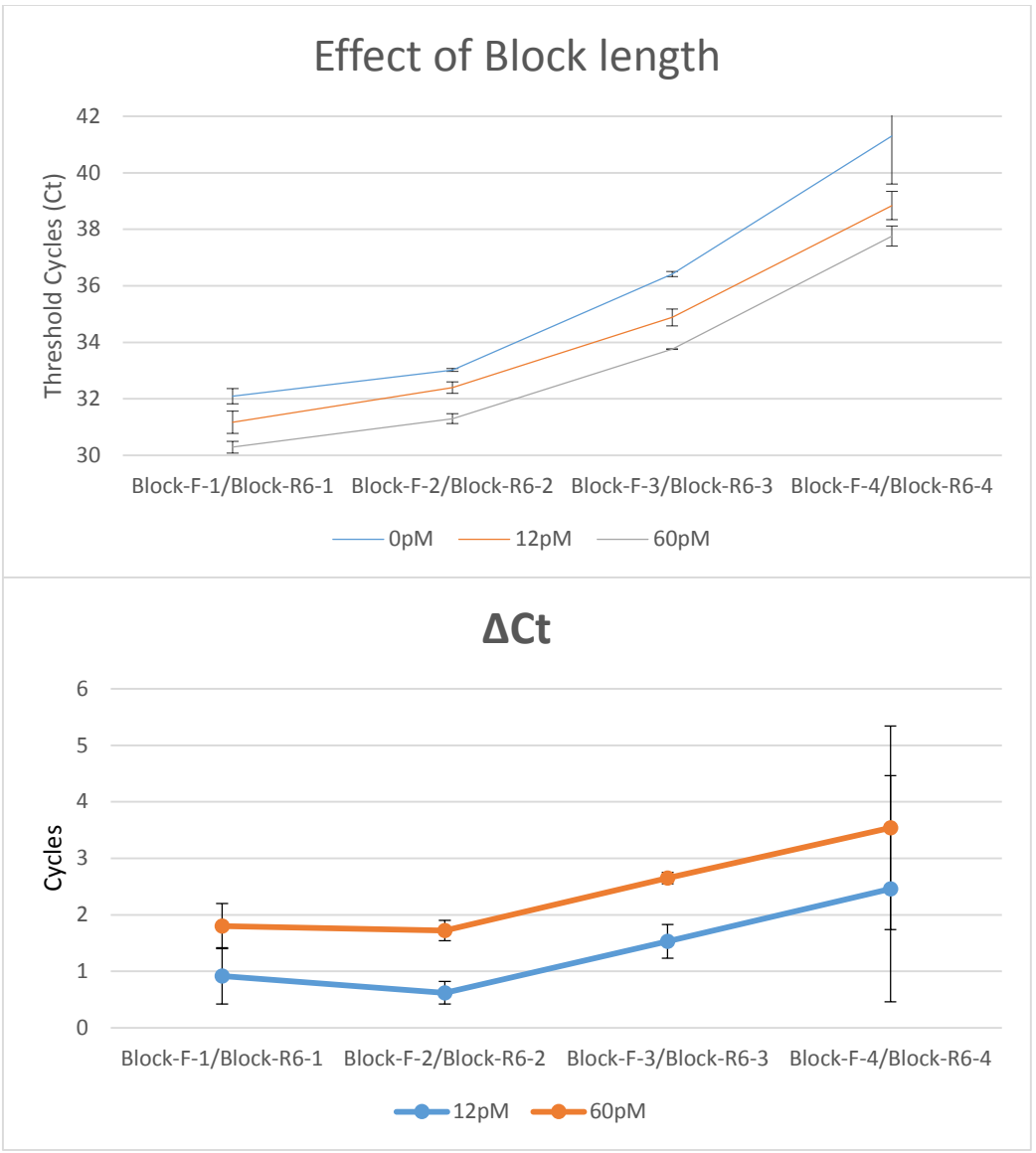

Figure 3.11 Effect of Block length on the BPDE-*p53*-exon7 analysis. Real-time qPCR experiments were carried out in triplicate and values are expressed as mean ± SD.

The influence of the Probes/Blocks ratio in the assay was studied. Ratios from 1/100 to 1/8000 were tested with 60 pM of BPDE-*p53*-exon7 (Figure 3.12). Higher concentration of blocks significantly reduced the background signal;

however, a ratio lower than 1/4000 also suppressed the signal from the 60 pM BPDE-*p53*-exon7 adducts. This is because T_m is concentration dependent: high concentration of Blocks leads to a comparable T_m of Block-Probe pair with the T_m of Probe-1/Probe-2 in the Probe-1/Probe-2/target complex. Under this condition, the efficiency of DNA assembly between Probe-1 and Probe-2 is suppressed even after the formation of the ternary complex. The ratio of 1/800 was chosen in the following experiments as it produced the highest ΔCt with the lowest variability.

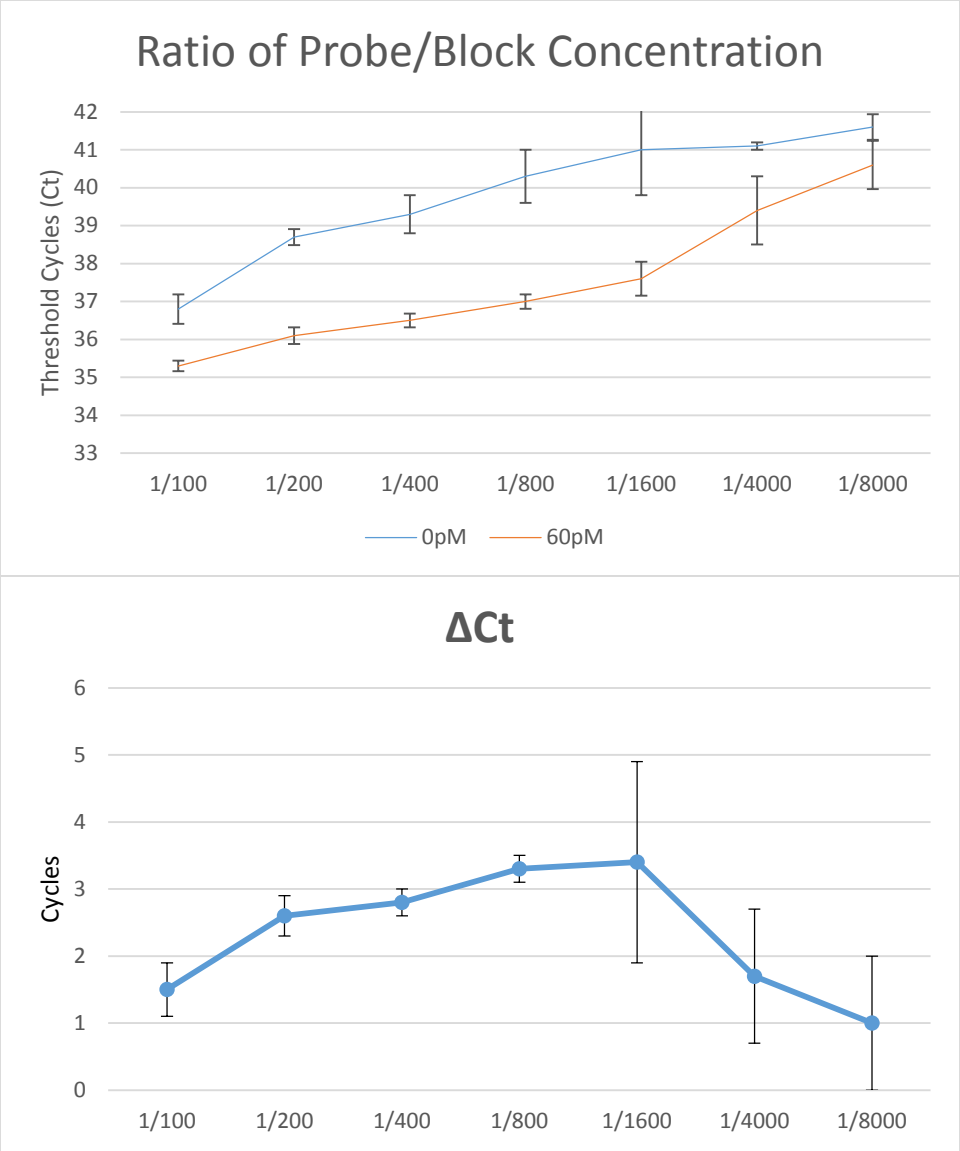

Figure 3.12 Effect of Probe/Block ratio on the BPDE-*p53*-exon7 analysis. Real-time qPCR experiments were carried out in triplicate and values are expressed as mean ± SD.

In the next step, the ratio of Probe/Block was fixed at 1/800 and the concentration of Probes-1/Probe-2 was optimized. A series of Probes-1/Probe-2 concentrations ranging from 62.5 pM to 1 nM was used for incubation with 30

pM BPDE-*p53*-exon7 adducts and the signal output from real-time qPCR is shown in Figure 3.13. As expected, increased concentration of Probe-1/Probe-2 can generate higher signal as they provide more binding opportunities between Probe-1/Probe-2 and target molecules. However, this also generates a higher background signal because the T_m between free Probes-1 and Probe-R in the incubation buffer increased with the concentration. A Probe-1/Probe-2 concentration of 250 pM resulted in the highest ΔCt.

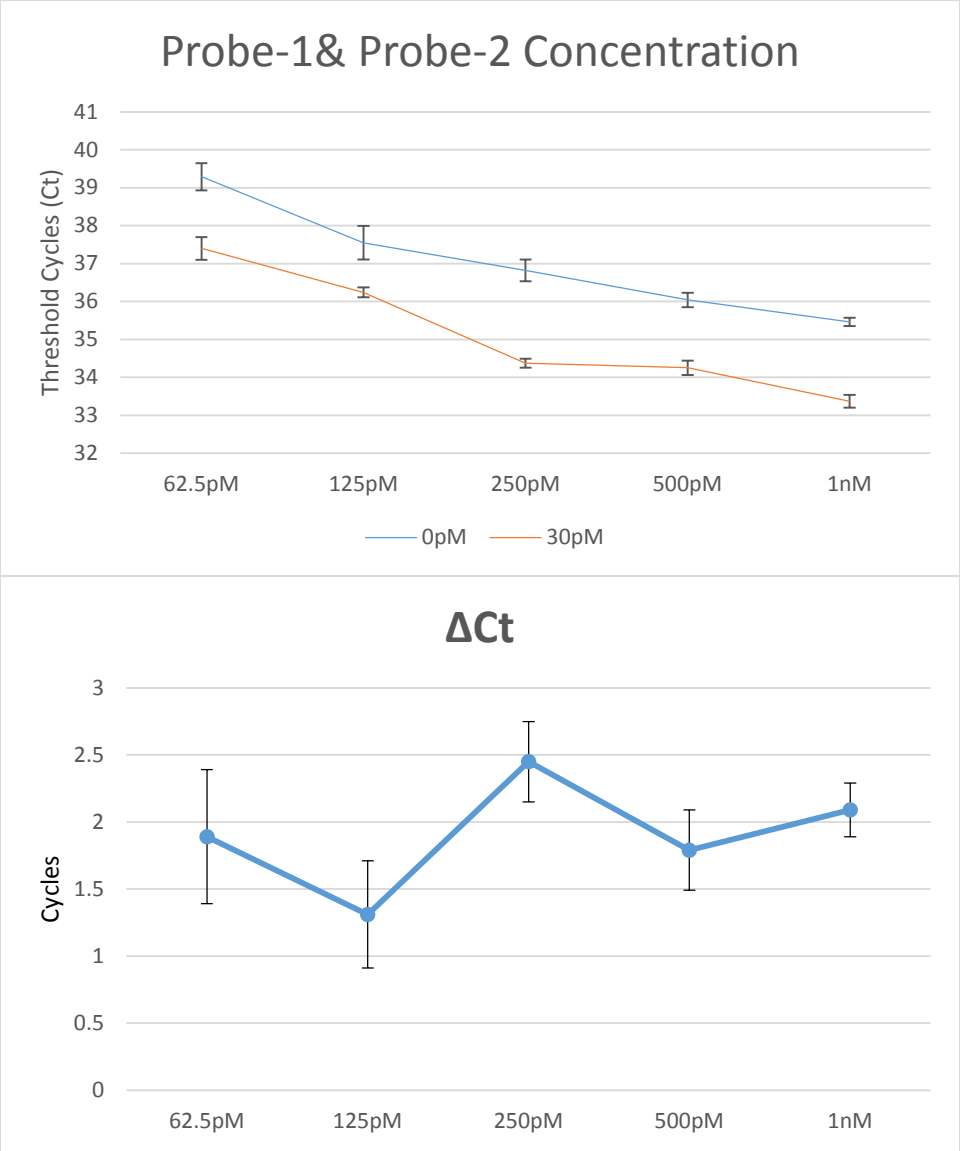

Figure 3.13 Effect of Probes-F/R concentration on the BPDE-*p53*-exon7 analysis. Real-time qPCR experiments were carried out in triplicate and values are expressed as mean ± SD.

The bivalent magnesium cation (Mg^{2+}) can impact the formation and stability of short DNA duplexes (*15*). It can influence the stability of DNA assembly between Probe-1 and Probe-2 after target binding and ternary complex formation.

It could also influence the signal output by enhancing the hybridization between Probe-2 and BPDE-*p53*-exon7 adducts. The effect of magnesium concentration in the incubation buffer was investigated. Mg^{2+} concentrations ranging from 0 mM to 5 mM were used in the incubation buffer and 12 pM or 60 pM BPDE-*p53*-exon7 adducts were incubated with 250 pM Probe-1/Probe-2 and 2 nM Block-F4/Block-6R-4 (Figure 3.14). Higher concentrations of Mg^{2+} increased the signal from both BPDE-*p53*-exon7 adducts and the blank sample because it promoted hybridization between Probe-1 and Probe-2. Mg^{2+} could further increase the signal by enhancing the hybridization between BPDE-*p53*-exon7 adducts and Probe-2. In Figure 3.14, 2 mM Mg^{2+} gave rise to the largest ΔCt.

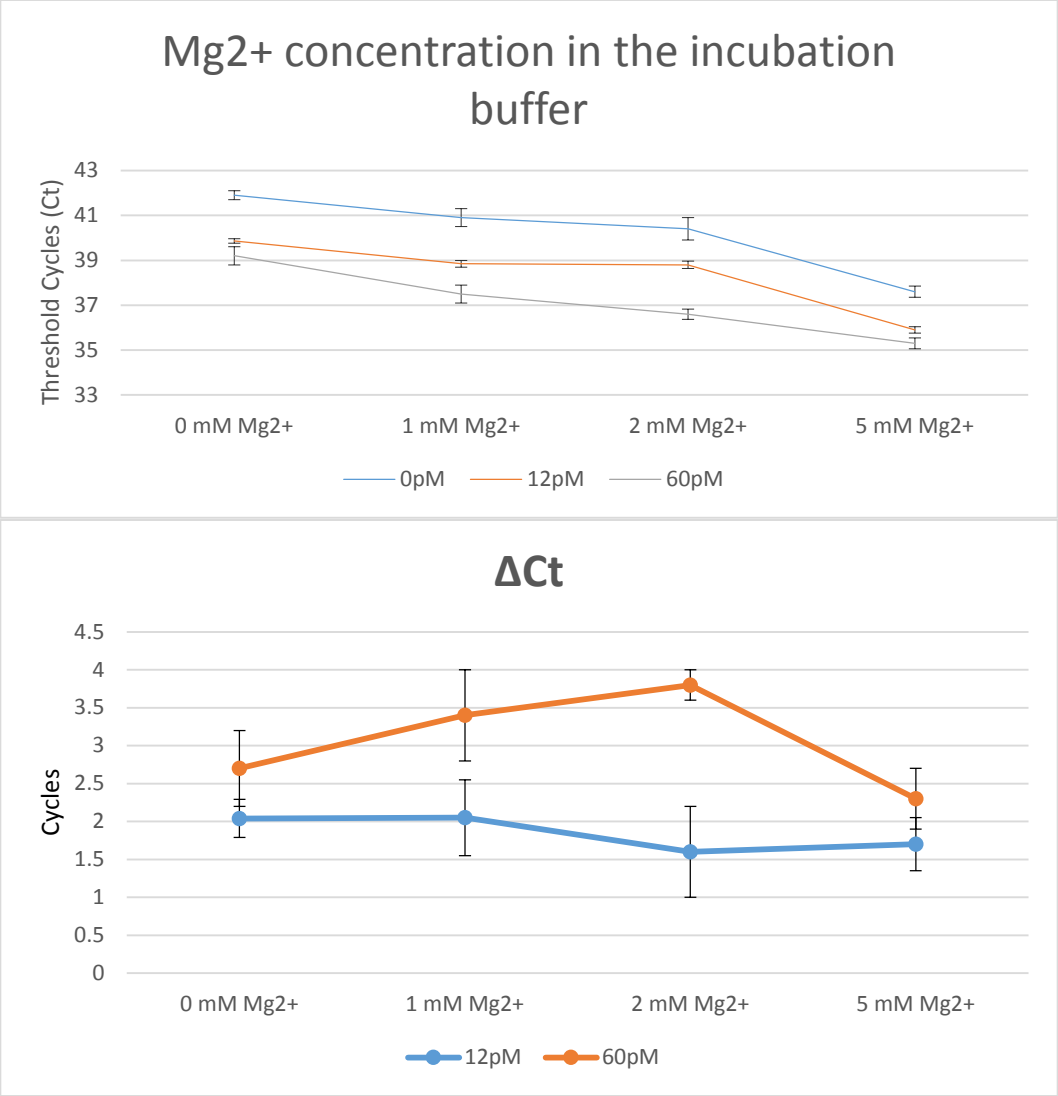

Figure 3.14 Effect of Mg^{2+} concentration on BPDE-*p53*-exon7 analysis. Real-time qPCR experiments were carried out in triplicate and values are expressed as mean ± SD.

With these optimized parameters, the dynamic range, detection limit, and specificity of the assay were tested using BPDE-*p53*-exon7 adducts and undamaged *p53*-exon7 (Figure 3.15). The dynamic range of the assay was found to be 3 pM to 150 pM. The detection limit is defined as the background signal

plus three times of the standard deviation and therefore it was 3 pM in a 2 µL incubation sample, i.e., 6×10^6 BPDE-*p53*-exon7 adduct molecules. The signal began decreasing as adduct concentrations were greater than 150 pM. This is due to the smaller quantity of the Probe-1/Probe-2/adduct ternary complex. When the BPDE-DNA adduct concentration exceeded Probes-1/2, the probability of one Probe-1 and one Probe-2 binding to the same BPDE-*p53*-exon7 adduct molecule decreased. As a result, the highest signal is present when the BPDE-*p53*-exon7 adducts concentration is close to the Probe-1/2 concentration. In Figure 3.15, highest signal was from 150 pM of BPDE-*p53*-exon7 adducts, which is lower than the Probe-1/2 concentration. This is because the target BPDE-*p53*-exon7 adducts contains large amount of *p53*-exon7 without a BPDE adduct (Figure 3.8).

The specificity of the assay was confirmed by testing a high concentration of undamaged *p53*-exon7 (Figure 3.15 inset). The results show that the signal from 750 pM of *p53*-exon7 was comparable to the blank sample and lower than 3 pM of BPDE-*p53*-exon7 adduct.

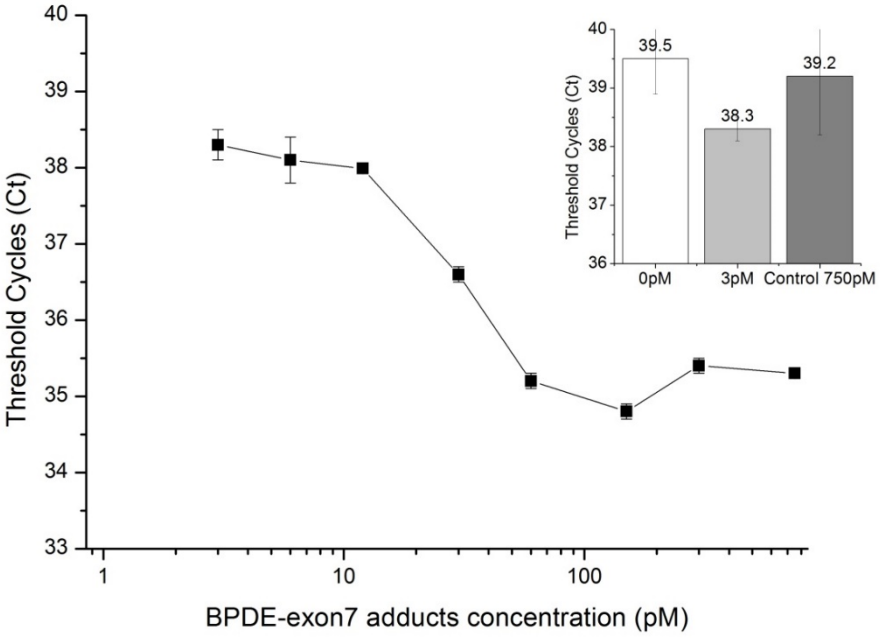

Figure 3.15 Dynamic range and specificity of homogeneous binding induced DNA assembly assay for BPDE-p53-exon7. Real-time qPCR experiments were carried out in triplicate and values are expressed as mean ± SD.

3.4 Conclusions

The non-coding regions of genome consist of more than 98% of the whole human genome sequences (*16*). Therefore, detection of DNA damage in cancer-related genes will be more useful for cancer risk assessment than detection of overall DNA damage on the whole genome. This chapter describes a sensitive method that enables quantitative determination of BPDE-DNA adducts formed on a specific target sequence. This method is based on the binding-induced DNA assembly (BINDA) strategy. The reason that detection of BPDE adducts on a

specific target sequence can be achieved is the use of dual recognition. Only simultaneous binding of both Probe-1 and Probe-2 to the same BPDE-*p53*-exon7 molecule could trigger the DNA assembly between Probe-1 and Probe-2. Successful determination of a BPDE-DNA adduct on *p53*-exon7 demonstrates a detection limit of 3 pM in a 2 μL sample. This method is not limited to *p53* sequences or BPDE-DNA adducts, and it can be broadened to other cancer-related genes and other types of DNA damage. Detection of other types of DNA damage requires affinity ligands for the specific DNA damage.

3.5 References

1. R. C. Gupta, M. V Reddy, K. Randerath, 32P-postlabeling analysis of non-radioactive aromatic carcinogen–DNA adducts, *Carcinogenesis* **3**, 1081–92 (1982).

2. R. C. Gupta, Enhanced Sensitivity of 32P-Postlabeling Analysis of Aromatic Carcinogen: DNA Adducts Enhanced Sensitivity of 32P-Postlabeling Analysis of Aromatic Carcinogen: DNA, *Cancer Res.* **45**, 5656–5662 (1985).

3. M. V Reddy, K. Randerath, Nuclease P1-mediated enhancement of sensitivity of 32P-postlabeling test for structurally diverse DNA adducts, *Carcinogenesis* **7**, 1543–51 (1986).

4. F. P. Perera, M. C. Poirier, S. H. Yuspa, J. Nakayama, A. Jaretzki, M. M. Cumen *et al.*, A pilot project in molecular cancer epidemiology: determination of benzo[a]pyrene–DNA adducts in animal and human tissues by immunoassays, *Carcinogenesis* **3**, 1405–10 (1982).

5. J. Nakayama, S. H. Yuspa, M. C. Poirier, Benzo(a)pyrene-DNA Adduct Formation and Removal in Mouse Epidermis in Vivo and in Vitro : Relationship of DNA Binding to Initiation of Skin Carcinogenesis, *Cancer Res.* **44**, 4087–4095 (1984).

6. H. Wang, M. Lu, N. Mei, J. Lee, M. Weinfeld, X. C. Le, Immunoassays using capillary electrophoresis laser induced fluorescence detection for DNA adducts, *Anal. Chim. Acta* **500**, 13–20 (2003).

7. H. Wang, M. Lu, M. Weinfeld, X. Le Chris, Enhancement of immunocomplex detection and application to assays for DNA adduct of benzo[a]pyrene, *Anal. Chem.* **75**, 247–54 (2003).

8. Z. Wang, M. Lu, X. Wang, R. Yin, Y. Song, X. C. Le *et al.*, Quantum dots enhanced ultrasensitive detection of DNA adducts, *Anal. Chem.* **81**, 10285–9 (2009).

9. B. Schoket, W. A. Doty, I. Vincze, P. T. Strickland, G. M. Ferri, G. Assennato *et al.*, Increased Sensitivity for Determination of Polycyclic Aromatic Adducts in Human DNA Samples by Lanthanide Fluoroimmunoassay (DELFIA), *Cancer Epidemiol. Biomarkers Prev.* **2**, 349–353 (1993).

10. B. Schoket, D. H. Phillips, M. C. Poirier, I. Vincze, DNA adducts in peripheral blood lymphocytes from aluminum production plant workers determined by 32P-postlabeling and enzyme-linked immunosorbent assay, *Environ. Health Perspect.* **99**, 307–309 (1993).

11. R. L. Divi, F. A. Beland, P. P. Fu, L. S. V. Tungeln, B. Schoket, J. E. Camara *et al.*, Highly sensitive chemiluminescence immunoassay for benzo[a]pyrene-DNA adducts: validation by comparison with other methods, and use in human biomonitoring, *Carcinogenesis* **23**, 2043–9 (2002).

12. U. A. Harréus, N. H. Kleinsasser, S. Zieger, B. Wallner, M. Reiter, P. Schuller *et al.*, Sensitivity to DNA-damage induction and chromosomal alterations in mucosa cells from patients with and without cancer of the oropharynx detected by a combination of Comet assay and fluorescence in situ hybridization, *Mutat. Res.* **563**, 131–8 (2004).

13. C. Wang, F. Feng, Z. Wang, T. Li, X. C. Le, H. Wang, Synthesis and characterization of DNA fluorescent probes containing a single site-specific stereoisomer of anti-benzo[a]pyrene diol epoxide-N2-dG, *Chem. Res. Toxicol.* **22**, 676–82 (2009).

14. L. Shugart, J. McCarthy, B. Jimenez, J. Daniels, Analysis of adduct formation in the bluegill sunfish (Lepomis Macrochirus) between benzo[a]pyrene and DNA of the liver and hemoglobin of the erythrocyte, *Aquat. Toxicol.* **9**, 319–325 (1987).

15. R. Owczarzy, B. G. Moreira, Y. You, M. A. Behlke, J. A. Walder, Predicting stability of DNA duplexes in solutions containing magnesium and monovalent cations, *Biochemistry* **47**, 5336–53 (2008).

16. International Human Genome Sequencing Consortium, Finishing the euchromatic sequence of the human genome, *Nature* **431**, 931–945 (2004).

Chapter Four

Magnetic bead-mediated BINDA assay for BPDE-DNA adducts on *p53*-exon7

4.1 Introduction

In Chapter 3, a sensitive homogeneous BINDA assay was developed for BPDE-DNA adducts formed on a specific DNA sequence, using the synthesized BPDE-*p53*-exon7 adducts to demonstrate the proof-of-principle. In this assay, all the Probes, Blocks, and targets were added to the incubation buffer and then the incubation mixture containing the assembled Probes was transferred to the PCR plate for ligation and subsequent real-time qPCR quantification.

This homogeneous BINDA assay is simple, without the need for separation. The assay utilizes the increased local concentration of the two Probes after target binding, which promotes the DNA assembly in the Probes–target ternary complex. Without target binding, the local concentration of the free Probes in the solution does not change. Therefore, background due to non-specific assembly without target is low.

To further improve the sensitivity and specificity of the BINDA assay, we explored a different approach combining magnetic beads with the BINDA assay (Figure 4.1). In this new format, two elements of the Probe-1, Probe-F, and the BPDE antibody, as described in Chapter 3, were immobilized on magnetic beads. The Probe-F and BPDE antibody conjugated magnetic bead served as the new "Probe-1". After one target molecule has bound to the antibody on the magnetic

bead surface, multiple Probe-F molecules surround the target, further increasing the local concentration by the conjugated magnetic bead. This is the advantage of this new “Probe-1”.

In the magnetic bead-mediated BINDA assay, the BPDE-*p53*-exon7 adducts are captured on the bead surface after incubation of the magnetic beads with the adducts, while undamaged *p53*-exon7 remains in the incubation buffer. Probe-2 is added to the incubation buffer, allowing the binding-induced DNA assembly to occur. The magnetic beads carrying the assembled DNA are directly transferred to the PCR plate containing the ligase and all the real-time qPCR reagents. The ligated DNA is then amplified and quantified.

To develop the proposed magnetic bead-mediated BINDA assay for BPDE-*p53*-exon7, streptavidin-coated magnetic beads were used to immobilize biotinylated Probe-F and BPDE antibody. Synthesized BPDE-*p53*-exon7 adducts, described in Chapter 3, were used as the target for method development.

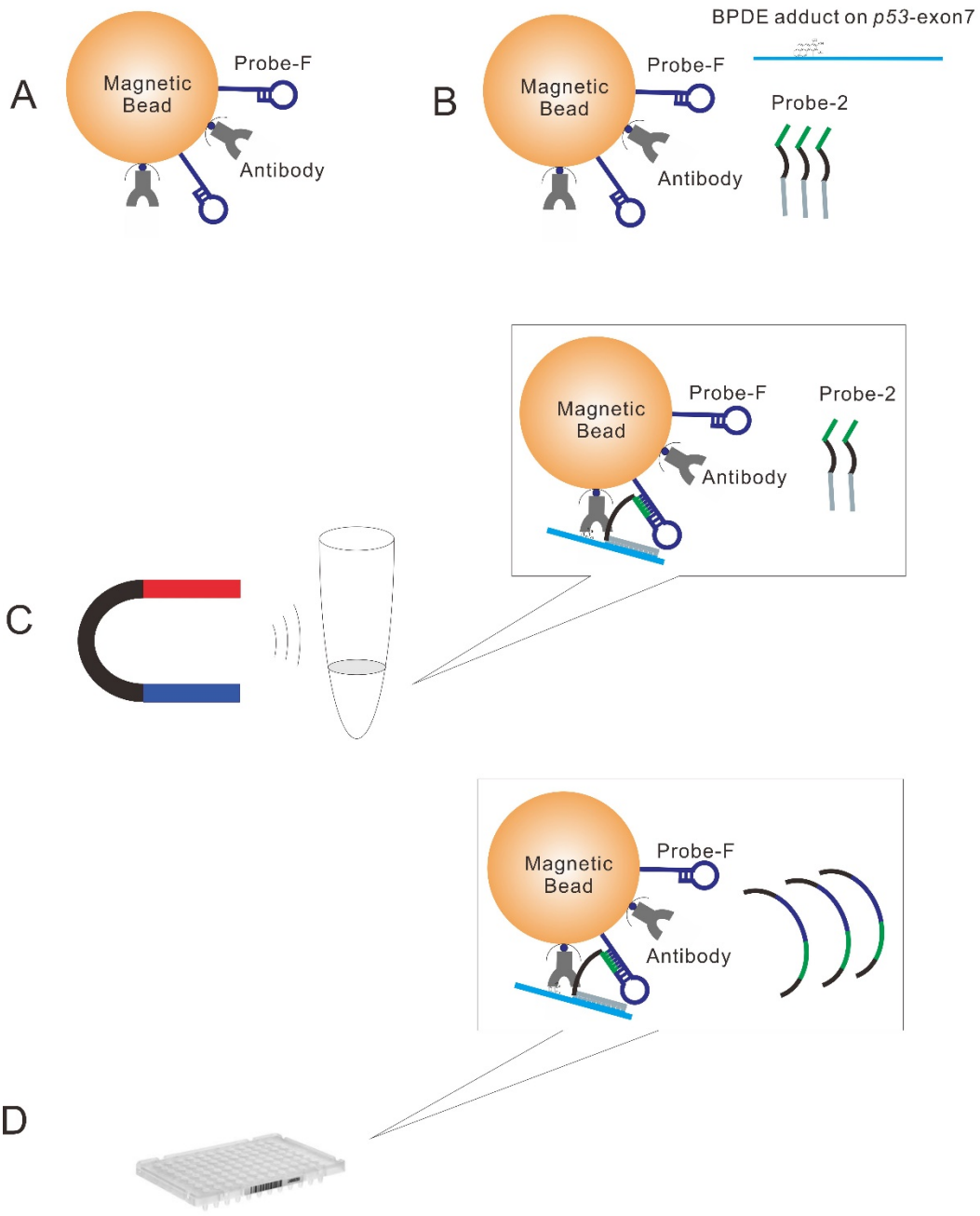

Figure 4.1 Schematic showing magnetic bead-mediated BINDA assay for BPDE-*p53*-exon7. (A) The new "Probe-1": magnetic bead conjugated with the Probe-F and the BPDE antibody. (B) The magnetic beads are incubated with Probe-2 and the BPDE-*p53*-exon7 adducts. (C) The BPDE-*p53*-exon7 is captured on the surface of magnetic beads. Probe-2 is absorbed to the magnetic bead surface upon

hybridization. Probe-F and Probe-2 assemble on the surface of the magnetic bead. The excess Probe-2 is removed with a magnet. (D) Assembled Probe-F and Probe-2 are ligated in the PCR plate that contains the ligase and all the real-time qPCR reagents followed by real-time qPCR quantification.

4.2 Experimental

4.2.1 Reagents and instruments

Bovine serum albumin (Cat. NO. A7906) was purchased from Sigma-Aldrich (Oakville, ON). Anti-BPDE antibody clone 8E11 (Cat. No. 4360-MC-100) was purchased from Trevigen (Gaithersburg, MD). Biotin-XX microscale protein labeling kit (Cat. No. B30010), Platinum® qPCR SuperMix UDG (Cat. No. 11730), T4 DNA Ligase (Cat. No. 15224), and T4 Polynucleotide Kinase (Cat. No. 18004) were purchased from Invitrogen (Carlsbad, CA). NanoOrange Protein Quantification Kit (Cat. No. MP06666) used to quantify low concentration of proteins was purchased from Molecular Probes (Eugene, OR). Phosphate buffered saline (1×PBS) (137 mM NaCl, 10 mM phosphate, 2.7 mM KCl, pH 7.4) was diluted with deionized water from 10×PBS buffer (Fisher Scientific, Nepean, ON). All other reagents were of analytical grade.

The oligonucleotides (except the TaqMan probe) were custom synthesized, labeled, and purified by Integrated DNA Technologies (IDT, Coralville, IA).

Streptavidin-coupled magnetic beads, Dynabeads MyOne C1 (Cat. No. 65001), and the DynaMag-Spin Magnet (Cat. No. 12320D) were purchased from Invitrogen (Carlsbad, CA).

A Beckman Coulter DTX880 Multi-Mode Microplate Reader (Beckman Coulter, Pasadena, CA) was used to quantify the fluorescence signal of the orange dye-intercalated protein in the NanoOrange protein assay.

A 7500 Fast Real-Time PCR system from Applied Biosystems (Foster City, CA) was used to run all PCR experiments. A 96-well MicroAmp Fast Optical Plate (Cat. No. 4346906) with barcode, and MicroAmp Optical Adhesive Cover (Cat. No. 4360954) from Applied Biosystems compatible with this Real-Time PCR system were used in this study. The PCR program was set as 50˚C for 2 min, 95˚C for 2 min, followed by 50 cycles of 95˚C for 15 s, and 60˚C for 30 s. All real-time qPCR experiments were carried out in triplicate.

4.2.2 Preparation of conjugated magnetic beads and Probe-2

BPDE antibody 8E11 was first biotinylated by a Biotin-XX microscale protein labeling kit according to the manufacturer's instruction. To immobilize biotinylated Probe-F and BPDE antibody 8E11 on the streptavidin-coupled Dynabeads MyOne C1 magnetic beads, the beads (1 mg/mL) were first washed with PBS buffer 3 times to remove the original buffer and re-suspended in 1 × PBS buffer containing 0.2% BSA. A certain amount of Probe-F and antibody in stock solution was diluted in another tube with 1× PBS buffer containing 0.2% BSA. Then the two solutions were mixed thoroughly by pipetting up and down. The mixture was put on a mixer and rotated for 30 min to prevent the precipitation of the magnetic beads. The mixture was stored in a 4˚C refrigerator overnight (> 8 h). Excess Probe-F and antibody were removed using a magnet followed by washing 3 times with 1 × PBS buffer. The beads were finally re-suspended in 1 ×

PBS buffer containing 0.2% BSA and were ready for use.

Probe-2 was prepared by first mixing 100 µL of 200 nM Probe-R and 100 µL of 200 nM streptavidin. This mixture was incubated for 1 h at room temperature. Next, 100 µL of this mixture was added to 100 µL of 100 nM target hybridization sequence for Probe-R and incubated for 1 h at room temperature. Finally, an equal volume of 1 mM biotin in 1× PBS was added, resulting in a 25 nM stock solution of BPDE-Probe-R.

4.2.3 Analysis of BPDE-*p53*-exon7 adducts by magnetic bead-mediated BINDA assay

The BPDE-*p53*-exon7 adducts or undamaged *p53*-exon7 were first incubated with conjugated magnetic beads, Probe-2, Blocks-F/R, and $MgCl_2$, in 1× PBS with 0.2% BSA for 1 h at room temperature. After incubation, the solution was removed using a magnet and beads were washed with 50 µL wash buffer (1×PCR buffer with or without blocks-F/R) 3 times. The beads were then re-suspended in 50 µL wash buffer. From this, 2 µL of the beads suspension were transferred to a 18 µL real-time PCR reaction containing 1× PCR buffer, 3 mM $MgCl_2$, dNTPs, 0.1 µM forward and reverse primers, DNA polymerase, Rox reference dye, TaqMan probe, and 0.4 unit T4 DNA ligase. The mixture was kept in the dark for 10 min at room temperature before it was subjected to real-time qPCR.

4.3 Results and Discussion

4.3.1 Inhibition effect of real-time qPCR by magnetic beads

The magnetic beads could inhibit the DNA polymerase or significantly suppress the DNA polymerase activity in the real-time qPCR amplification. To

investigate the possible inhibition effect by magnetic beads, the PCR efficiency in the presence of magnetic beads was studied. The ligated Probe-F and Probe-R described in Chapter 2 was used as the template to examine PCR efficiency (Figure 4.2). Different quantities of streptavidin-coupled Dynabeads MyOne C1 magnetic beads (0 µg, 0.2 µg, 1 µg, 5 µg, 10 µg, and 20 µg) were added to the PCR reaction including the same number of the PCR templates (600 molecules).

In real-time qPCR, the relationship between threshold cycles (Ct) and the PCR efficiency could be represented by the following equation:

$$N = N_0*(E+1)^{Ct} \quad (1)$$

Where N_0 is the initial template copy number and N is template copy number after Ct cycles.

If the initial template copy number is the same for two PCR reactions, and the threshold is set to the same value for paralleled experiments, then the N and N_0 are identical for the two PCR reactions, therefore:

$$(E_1+1)^{Ct1} = (E_2+1)^{Ct2} \quad (2)$$

Assuming the PCR efficiency without magnetic beads was 100%, the relative PCR efficiencies of PCR reaction containing magnetic beads were 102.5%, 102.6%, 93.8%, 83.6% and 75.4% for 0.2 µg, 1 µg, 5 µg, 10 µg, and 20 µg of magnetic beads, respectively. Therefore, less than 5 µg streptavidin-coupled magnetic beads did not compromise the PCR efficiency significantly. In the following experiments, less than 5 µg of magnetic beads conjugated with Probe-F and BPDE antibody were used for real-time qPCR quantification after incubation and DNA assembly.

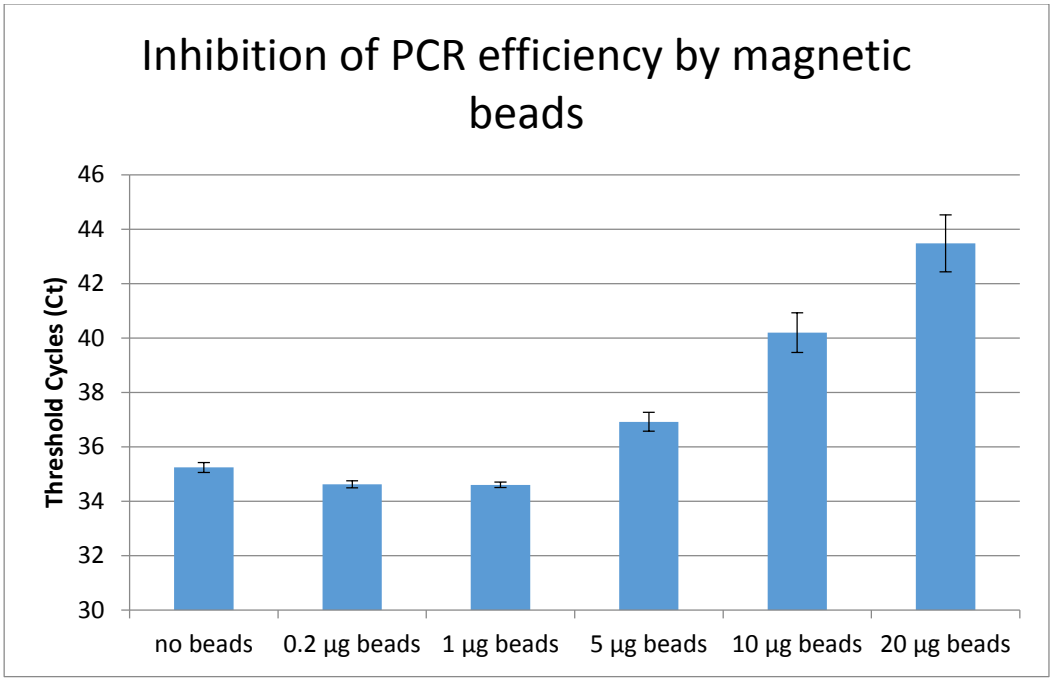

Figure 4.2 Effect of magnetic bead on the real-time qPCR efficiency. Real-time qPCR experiments were carried out in triplicate and values are expressed as mean ± SD.

4.3.2 Effect of antibody and Probe-F density on magnetic bead surface

It is proposed that magnetic beads conjugated with Probe-F and BPDE antibody could further increase the local Probe concentration after target binding in the magnetic bead-mediated BINDA assay. The effect of the antibody and Probe-F density on the magnetic beads surface was first tested.

In this study, the density of antibody and Probe-F is represented by the number of antibody and Probe-F molecules conjugated on one magnetic bead. The number of conjugated molecules was controlled by incubating a certain quantity of biotinylated antibody and Probe-F with the streptavidin-coated magnetic beads.

According to the manufacturer's instruction, 1 mg of streptavidin-coupled

Dynabeads MyOne C1 can bind up to 20 µg of biotinylated antibodies. This is approximately 8×10^4 antibody molecules per bead. An experiment was conducted to study the binding capacity for biotinylated antibodies of the Dynabeads MyOne C1. Biotinylated antibodies were incubated with different amounts of magnetic beads. After incubation, the solution was removed and the protein concentration was quantified by the NanoOrange protein quantification method. Free streptavidin released from the magnetic beads contributing to the protein quantification was subtracted from the control incubation under the same conditions and using magnetic beads only. The result confirmed a binding capacity of more than 3×10^4 antibody molecules per bead. Because the size of Probe-F is much smaller than the antibody, the Probe-F binding capacity will not be considered in this study.

The same quantity of magnetic beads conjugated with different density of antibody and Probe-F were used to analyze 30 pM of BPDE-*p53*-exon7 (Figure 4.3). The result showed an increasing trend of signal from 30 pM of BPDE-*p53*-exon7 with the increasing antibody and Probe-F density on the magnetic beads. This was anticipated as the effective local concentration after target binding is increased with the antibody and Probe-F density. However, magnetic beads conjugated with 10^5 antibodies and Probe-F per bead did not generate higher ΔCt than those with lower antibody and Probe-F densities because the background is much higher. This could be due to the physical absorption of Probe-F on the magnetic bead surface that was released into the incubation buffer after conjugation. To test the feasibility of the assay, a lower concentration of BPDE-

p53-exon7 (6 pM) was included with 10^5 antibody and Probe-F per bead (Figure 4.3). The ΔCt between 30 pM and 6 pM was about 2 cycles, demonstrating a dose-response of the assay.

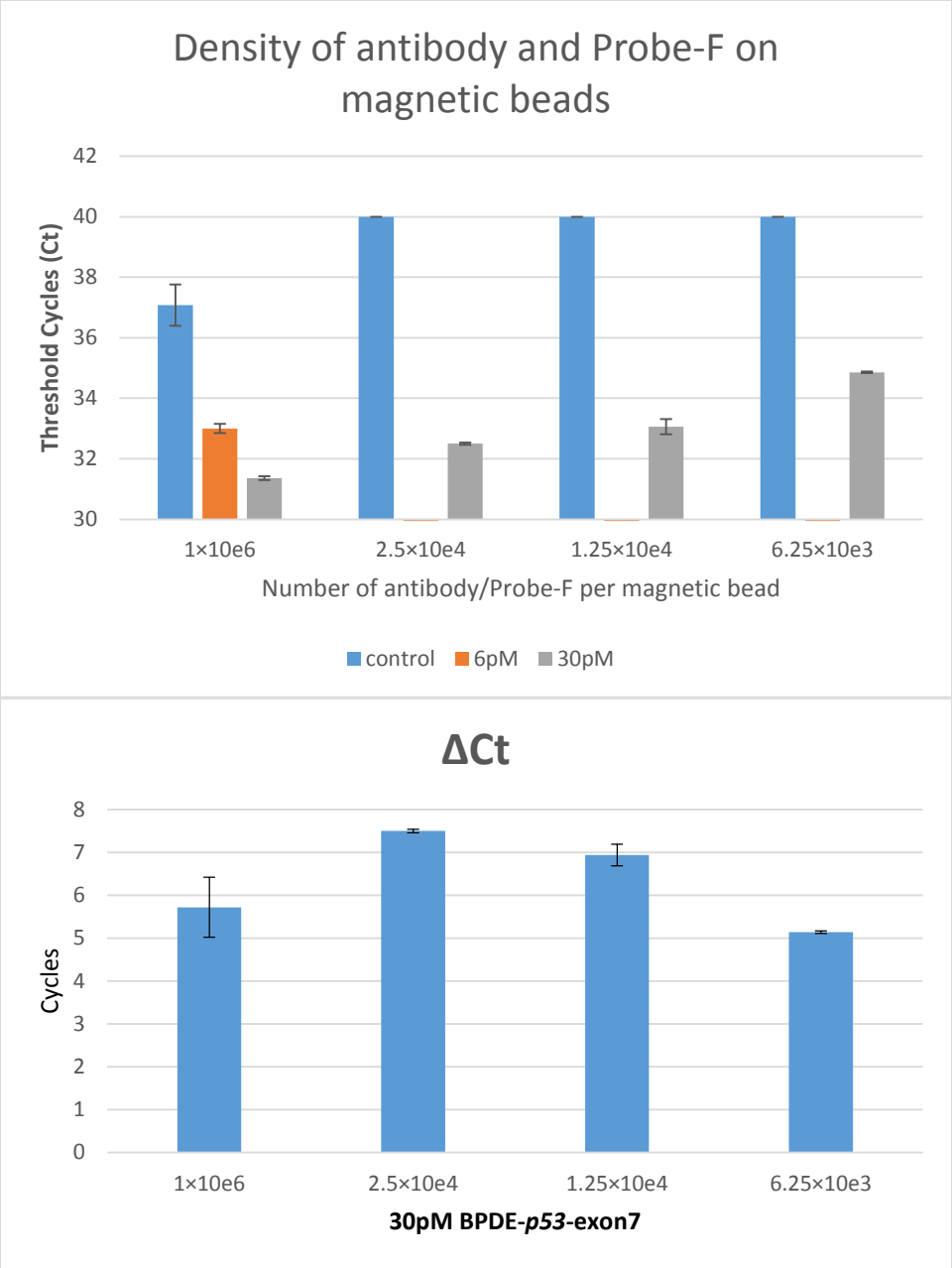

Figure 4.3 Effect of antibody and Probe-F density on the detection of BPDE-*p53*-exon7 adducts. Real-time qPCR experiments were carried out in triplicate and values are expressed as mean ± SD.

Unlike the homogeneous BINDA assay in which both Probe-1 and Probe-2 are free in the solution, antibody molecules are immobilized on the bead surface.

Probe-2 will not be able to reach Probe-F and assemble with it when the distance between the antibody and Probe-F exceeds the total length of Probe-F and Probe-R. In this situation no DNA could assemble even after target binding (Figure 4.4).

Assuming that the same number of antibody and Probe-F molecules are evenly distributed on the magnetic bead surface, the minimum density to allow the DNA assembly would be about 600 antibody and Probe-F molecules per bead. With a density of lower than 600 molecules per bead, there would be no signal from the target because the signal output was proportional to the amount of assembled DNA.

To test this hypothesis, several groups of magnetic beads were prepared with different antibody and Probe-F densities (Figure 4.5). The quantity of each magnetic bead used to incubate with the BPDE-*p53*-exon7 was adjusted so that the total molecules of antibody and Probe-F were equal in each group. Under this circumstance the signal output should only be determined by the efficiency of DNA assembly. In this experiment, 10 pM of BPDE-*p53*-exon7 was used.

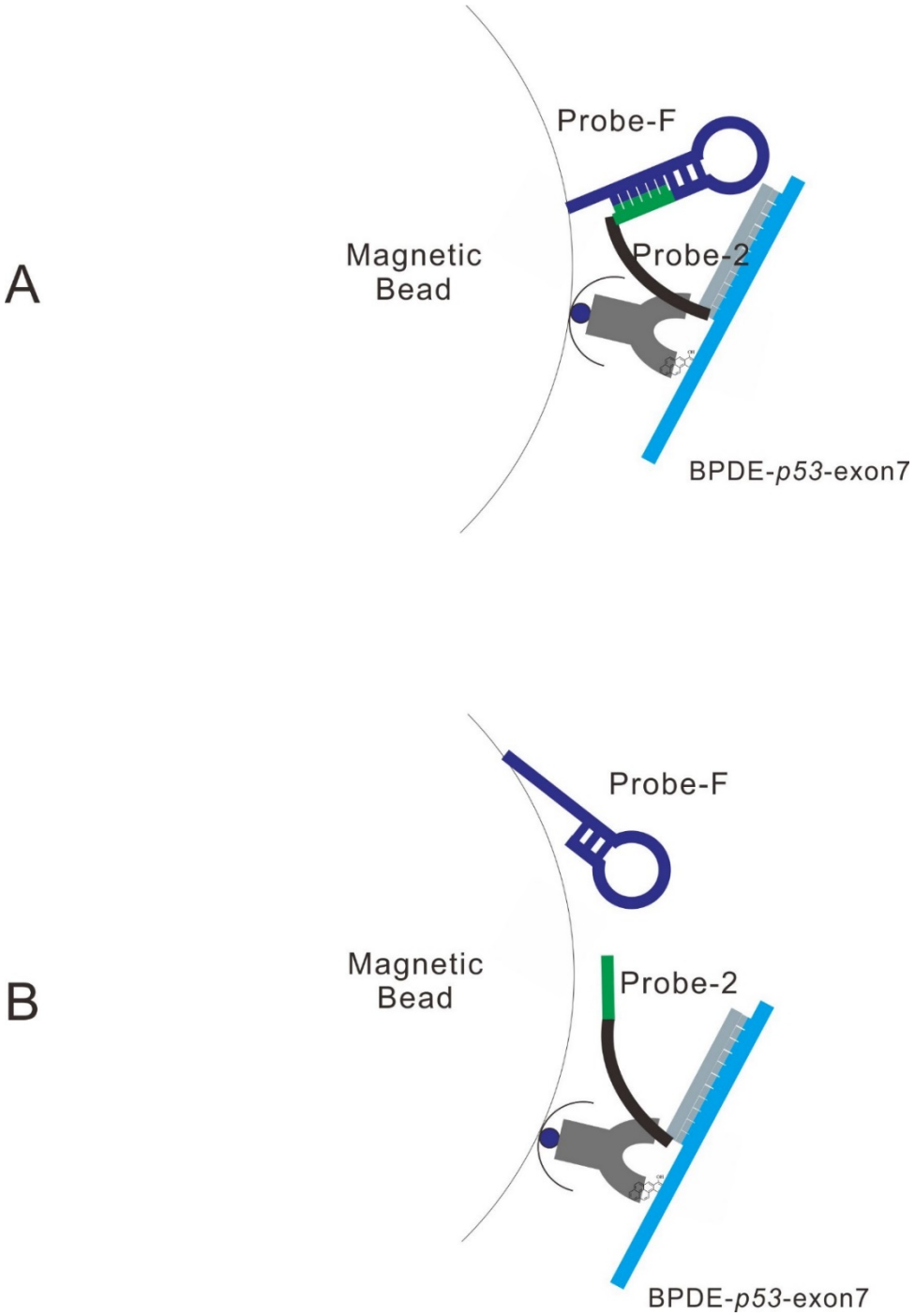

Figure 4.4 Density of antibody and Probe-F could affect the efficiency of DNA assembly upon target binding. (A) Probe-F and Probe-2 assembles in high density of antibody and Probe-F. (B) Probe-F and Probe-2 could not assemble in low density of antibody and Probe-F.

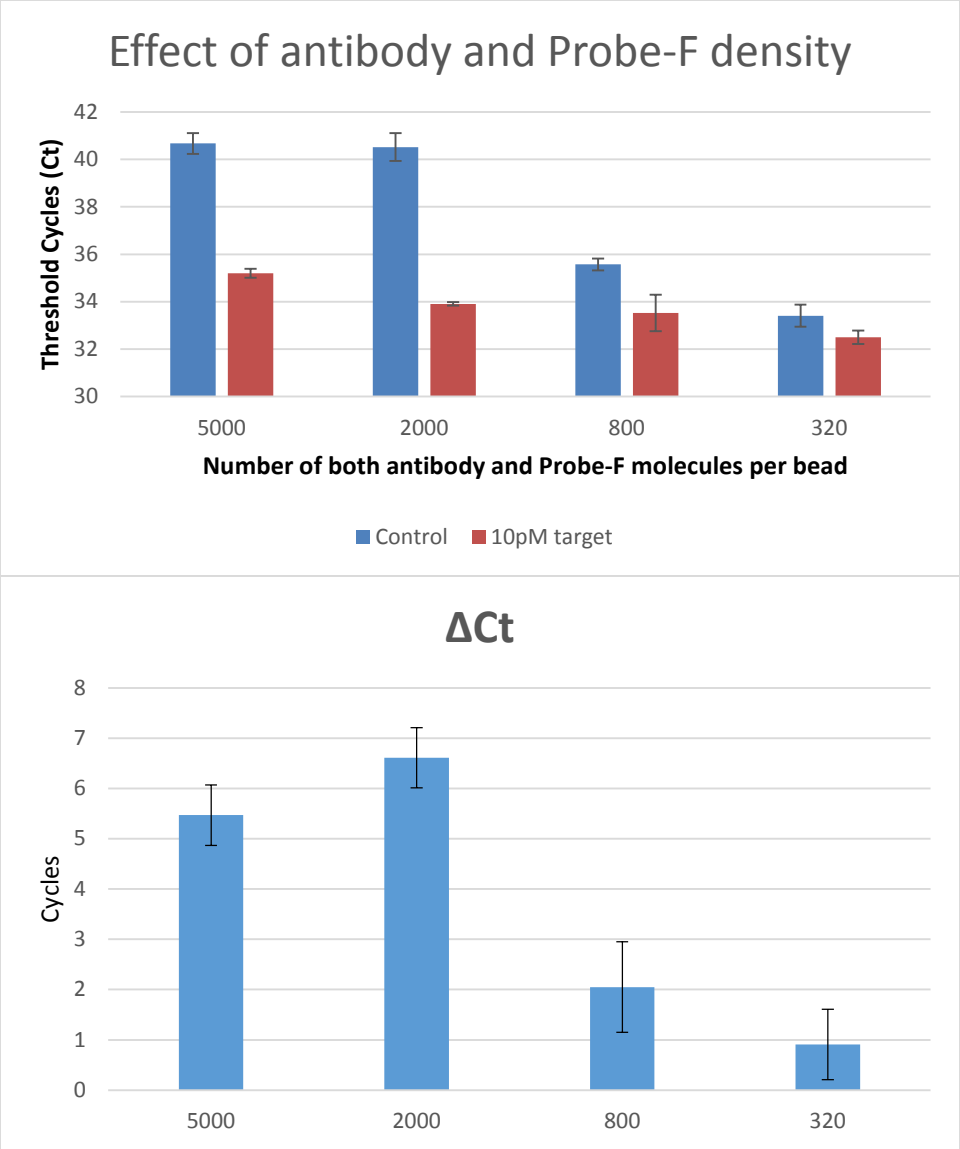

Figure 4.5 Effect of antibody and Probe-F density. Real-time qPCR experiments were carried out in triplicate and values are expressed as mean ± SD.

As expected, the ΔCt decreased significantly when the density dropped to 800 molecules of antibody and Probe-F per bead. At a density of 320 molecules of antibody and Probe-F per bead, the ΔCt was even under 1 cycle.

With such a low density of antibody, if the density of Probe-F increases, the

efficiency of DNA assembly should be recovered. Figure 4.6 shows increasing Probe-F density while fixing the antibody density at 320 molecules per bead. The ΔCt was driven up to above 2.5 cycles when the density of Probe-F reached 5000 molecules per bead. With the considerably increased density of Probe-F, the distance between Probe-F and antibody was reduced. Therefore Probe-2 bound to BPDE-*p53*-exon7 which was captured by the antibody on the magnetic bead surface could reach Probe-F and assemble with it.

However, at low density of Probe-F, an increase of antibody density did not change the efficiency of DNA assembly significantly ($p > 0.05$, Figure 4.7). Although the distance between the antibody and Probe-F was reduced, the local concentration of Probe-F, the key parameter for the binding induced DNA assembly, did not increase. In other words, the increase of antibody density only enhanced the binding affinity of magnetic beads to the BPDE-*p53*-exon7, but could not change the local concentration of Probe-F upon the binding of BPDE-*p53*-exon7.

These experiments confirmed the signal was generated through the DNA assembly on the magnetic bead surface and a minimum density of antibody and Probe-F is required to achieve the BPDE-*p53*-exon7 detection.

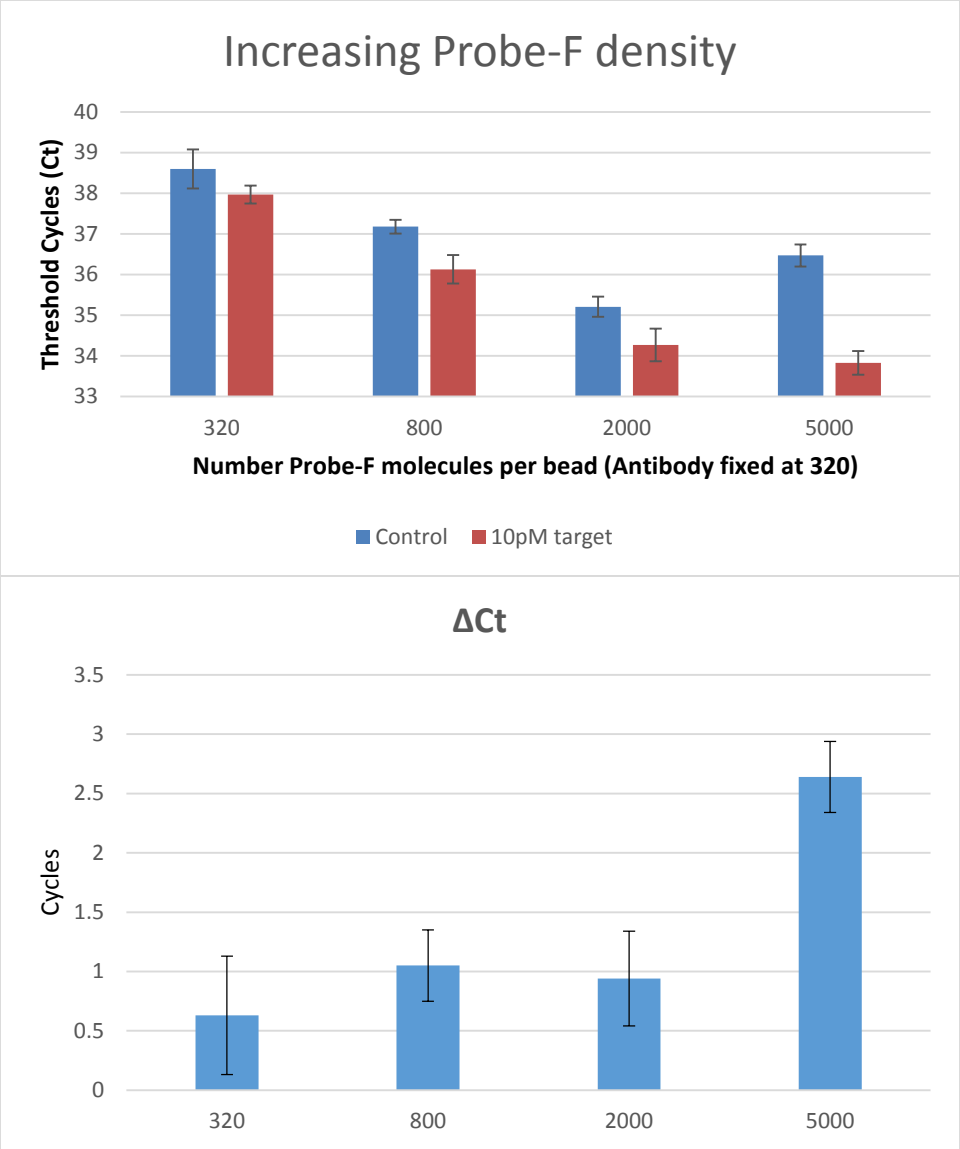

Figure 4.6 Increase in the Probe-F density could recover the efficiency of DNA assembly on the magnetic bead surface. Real-time qPCR experiments were carried out in triplicate and values are expressed as mean ± SD.

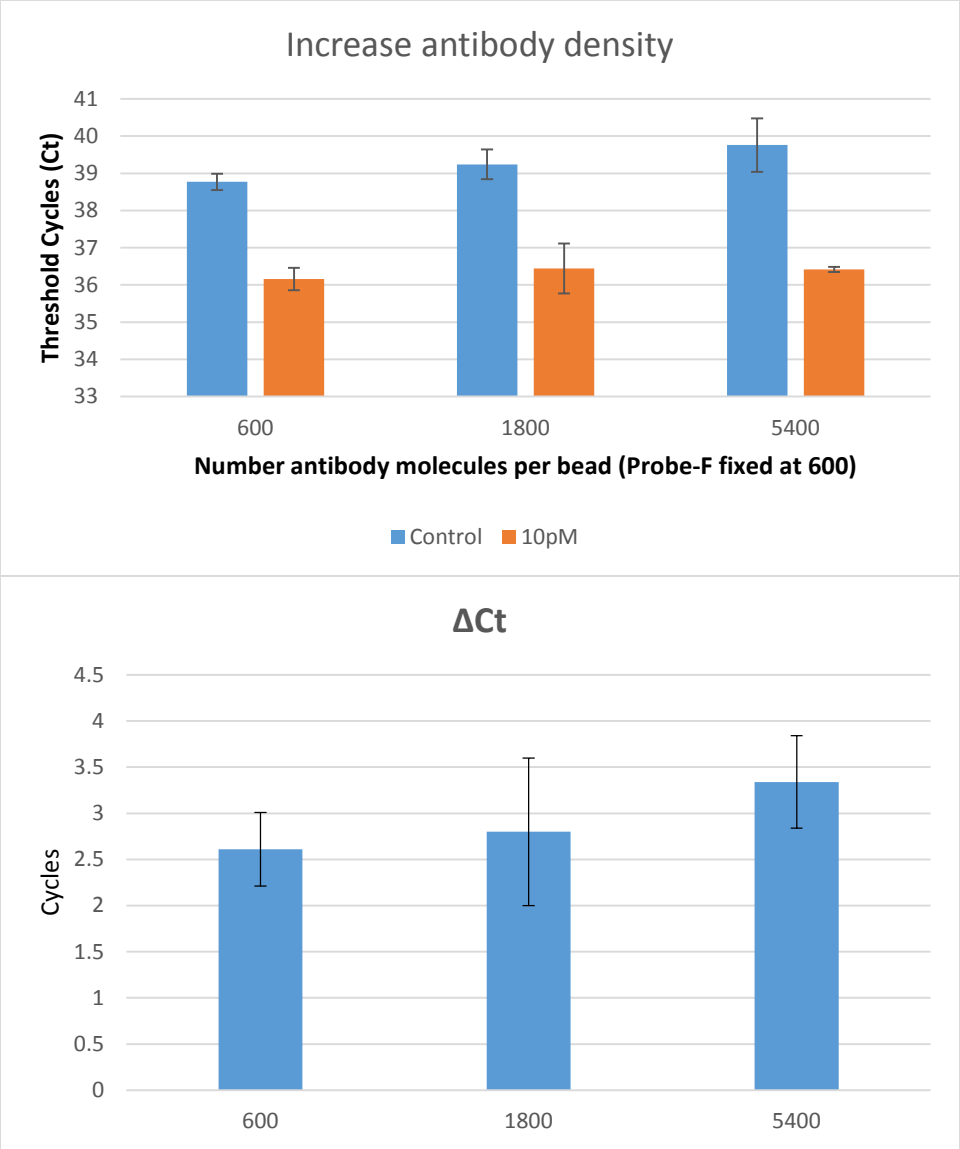

Figure 4.7 Increase in the antibody density did not significantly change the efficiency of DNA assembly on the magnetic bead surface ($p>0.05$). Real-time qPCR experiments were carried out in triplicate and values are expressed as mean ± SD.

To optimize the density of antibody and Probe-F on magnetic beads, the same quantity of magnetic beads with different molecular numbers of antibody

and Probe-F were prepared to analyze 10 pM BPDE-*p53*-exon7 (Figure 4.8). The results showed that with a density of more than 1500 molecules of antibody and Probe-F per bead, the ΔCt is similar. In the following experiments, a density of 2000 molecules of antibody and Probe-F per bead was used.

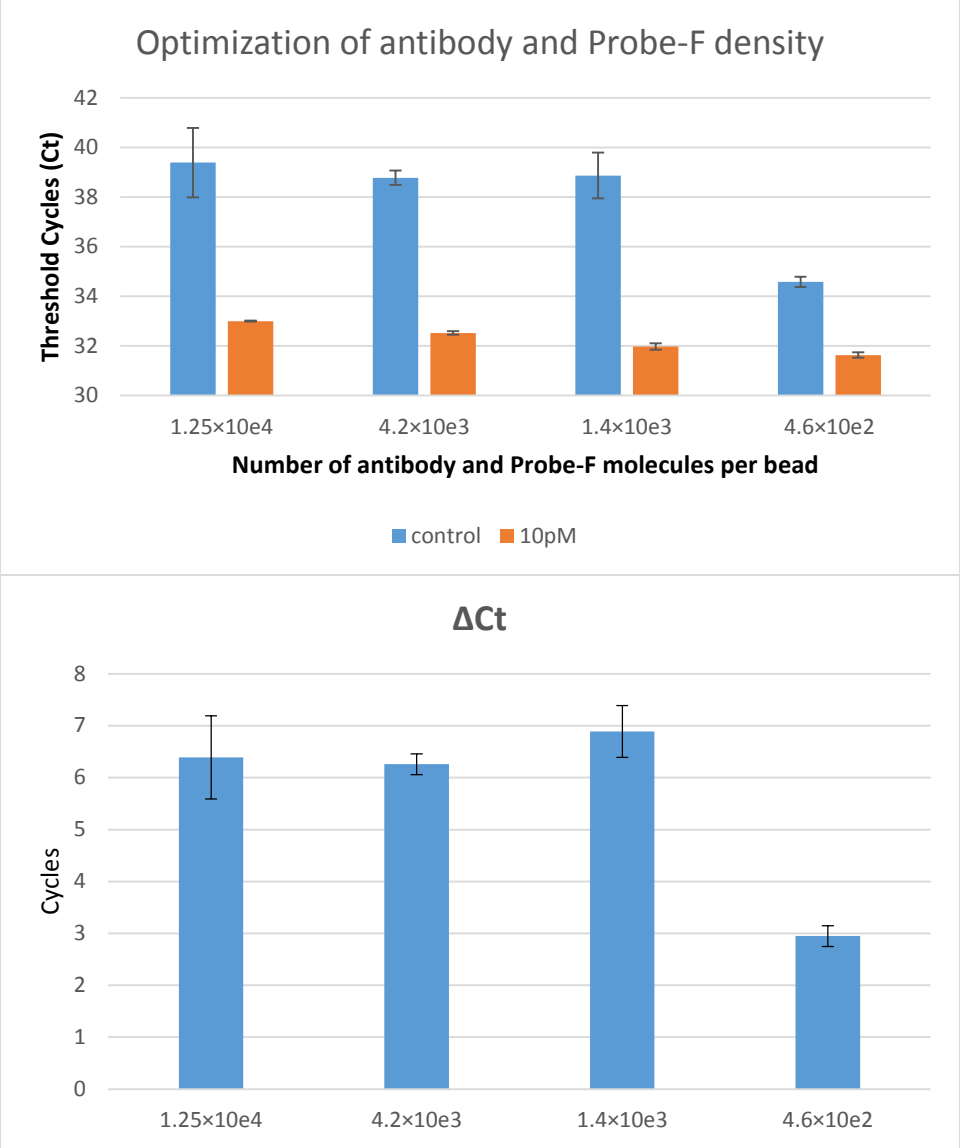

Figure 4.8 Optimization of antibody and Probe-F density for BPDE-*p53*-exon7 analysis. Real-time qPCR experiments were carried out in triplicate and values are

expressed as mean ± SD.

4.3.3 Optimization of incubation and washing steps in the magnetic bead-mediated BINDA assay

The concentration of Probe-2 plays an important role in the BINDA assay. To maximize the ΔCt for BPDE-*p53*-exon7 analysis, the concentration of Probe-2 was optimized. Probe-2 ranging from 0.2 nM to 7.4 nM was used to test 10 pM of BPDE-*p53*-exon7 (Figure 4.9). A low concentration of Probe-2 (0.2 nM) yielded very low ΔCt. Different from homogeneous BINDA, the results using the magnetic bead-mediated BINDA assay showed that ΔCt did not change significantly with different Probe-2 concentrations (1 nM, 2 nM, 4.3 nM, and 7.4 nM). This could be due to the washing step after incubation that removed excess amount of Probe-2 in the solution and target-independent Probe-2 that assembled on the magnetic bead surface. Therefore, a higher concentration of Probe-2 would not increase the background signal resulting from the target-independent DNA assembly. This also reflects the advantage of the extra separation step after incubation of the magnetic bead-mediated BINDA assay. The 2 nM concentration Probe-2 was chosen for the following experiments.

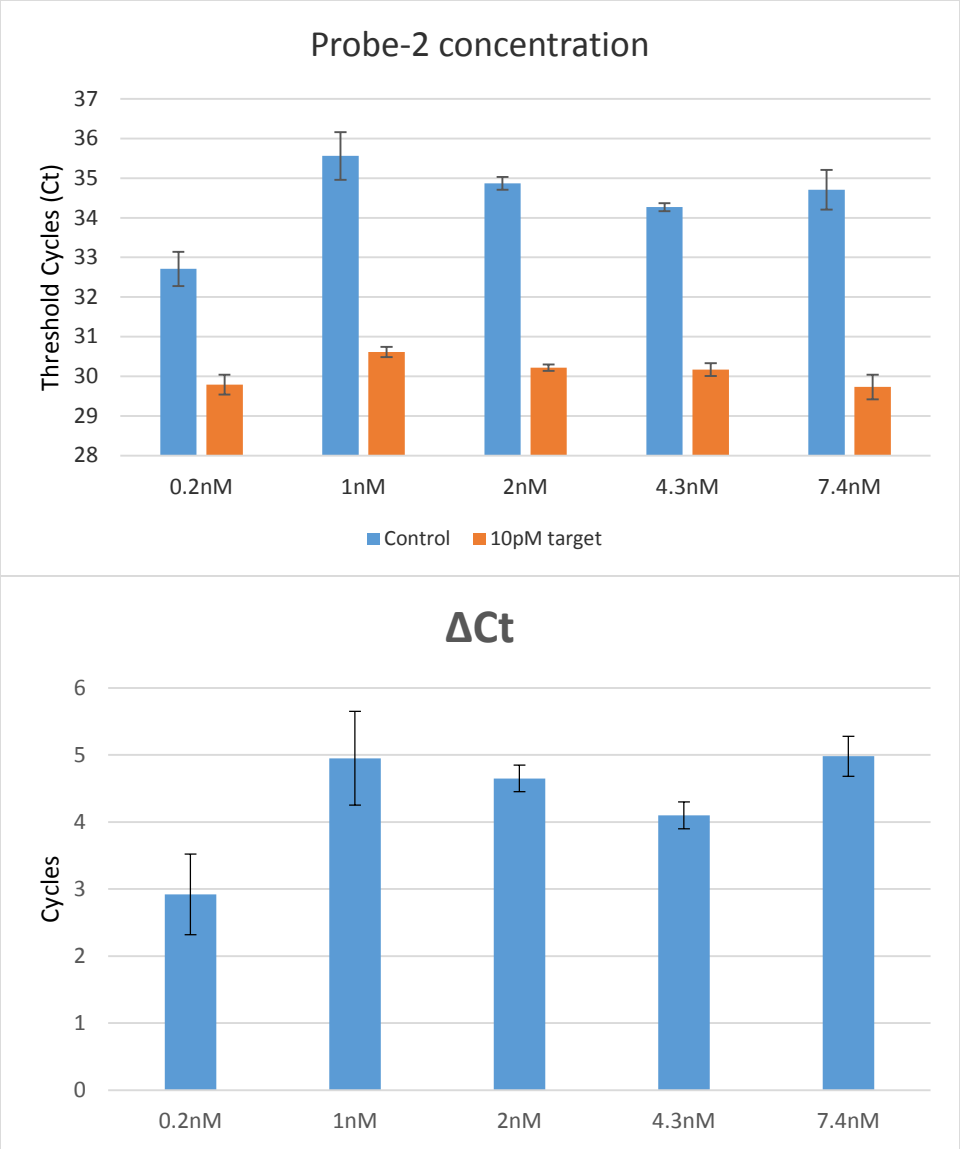

Figure 4.9 Optimization of Probe-2 concentration in the incubation step of magnetic bead-mediated BINDA assay. Real-time qPCR experiments were carried out in triplicate and values are expressed as mean ± SD.

To effectively remove excess Probe-2 and to further minimize the target-independent DNA assembly between Probe-F and Probe-2, Blocks were added to the washing buffer. Block-F and Block-R were used alone, or in combination, in

the wash buffer after the magnetic beads were incubated with 10 pM of BPDE-*p53*-exon7 (Figure 4.10).

Block-F hybridizes with Probe-F on the magnetic bead surface while Block-R hybridizes with Probe-2 in the incubation buffer. Because the concentration of Blocks (>100 nM) is much higher than the concentration of Probes (2 nM), only a small portion of Block-F is on the bead surface while most Block-F will stay in the incubation buffer. The free Block-F in the incubation buffer would not contribute to the removal of excess Probe-2. Block-R binding to Probe-2 in the incubation buffer would be more effective than Block-F in removing the target-independent DNA assembly between Probe-F and Probe-2.

The results in Figure 4.10 show the effectiveness of Blocks in removing the target-independent DNA assembly, compared to the PBS buffer. The background signal was significantly reduced by Block-R or Block-F/R, compared to Block-F. However the signal from DNA adducts was also suppressed by Block-R or Block-F/R. From the ΔCt it could be concluded that 400 nM Block-R in the washing buffer generated the highest signal/background ratio and therefore it was used in the following experiments.

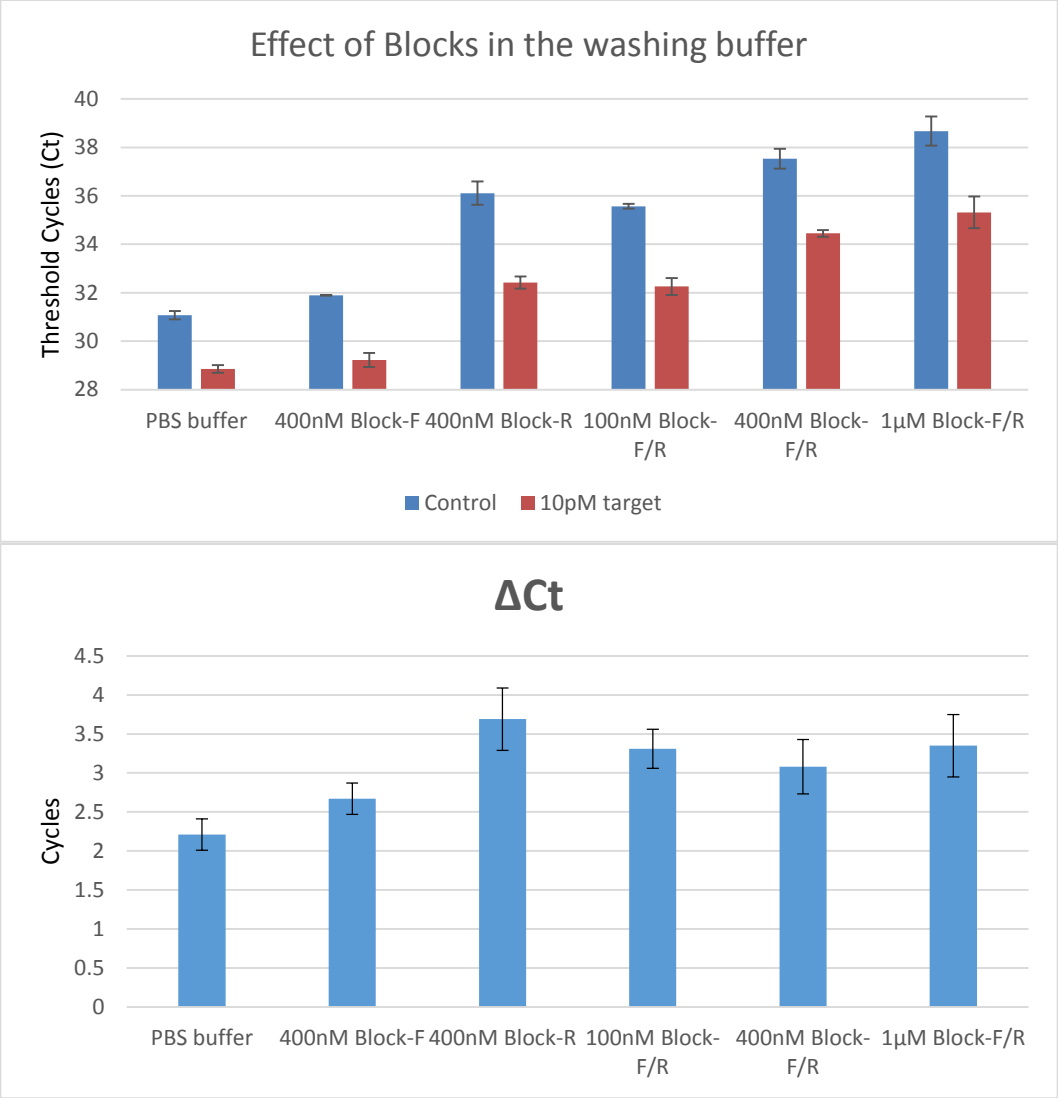

Figure 4.10 Effect of washing buffer with Blocks in removing the target-independent DNA assembly. Real-time qPCR experiments were carried out in triplicate and values are expressed as mean ± SD.

The optimal concentration of Block-R and number of washes in the washing steps were studied (Figure 4.11). Three concentrations of Block-R, 100 nM, 400 nM, 1 μM were used and 3 or 6 times washes were compared using 10pM of BPDE-*p53*-exon7.

Comparing washing 3 times and 6 times in each Block-R concentration, the extra 3 washes did not reduce the background signal significantly while the 10 pM BPDE-*p53*-exon7 signal decreased. The ΔCt of 3 times washes was better than the 6 times in all the three Block-R concentration groups.

Higher concentration of Block-R suppressed both the binding-induced DNA assembly (BPDE-*p53*-exon7) and the target-independent DNA assembly. Washing buffer containing 400 nM of Block-R showed the highest ΔCt among the three concentrations.

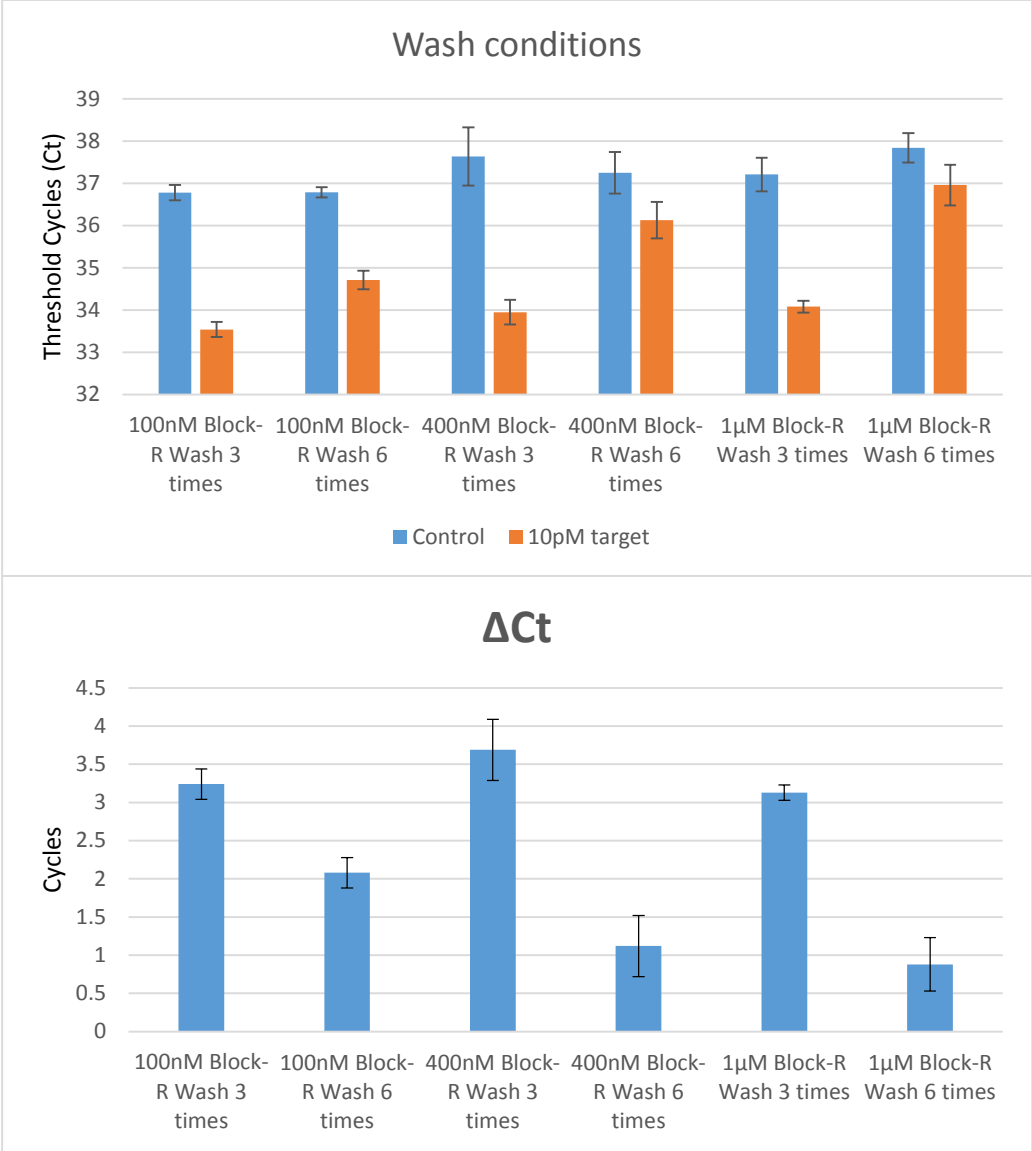

Figure 4.11 Concentration of Blocks in the washing buffer and number of washes after incubation. Real-time qPCR experiments were carried out in triplicate and values are expressed as mean ± SD.

As mentioned in Chapter 3, the bivalent magnesium cation can stabilize the DNA double helix structure (*1*). Use of Mg^{2+} in the washing buffer could stabilize both the Probe-2/BPDE-*p53*-exon7 hybridization and Probe-F/Probe-2 assembly

on the magnetic bead surface, enhancing the target signal. However, the background signal could also be increased because the target-independent DNA assembly on the magnetic bead surface is also stabilized. A series of Mg^{2+} concentrations in the washing buffer was used to test 10 pM of BPDE-*p53*-exon7 (Figure 3.12).

As expected, both binding-induced DNA assembly and target-independent DNA assembly were enhanced by increasing concentration of Mg^{2+}. This is because the Mg^{2+} can stabilize the DNA duplex structure and therefore increase the DNA assembly. The optimal condition was 0 mM for it produced the highest ΔCt.

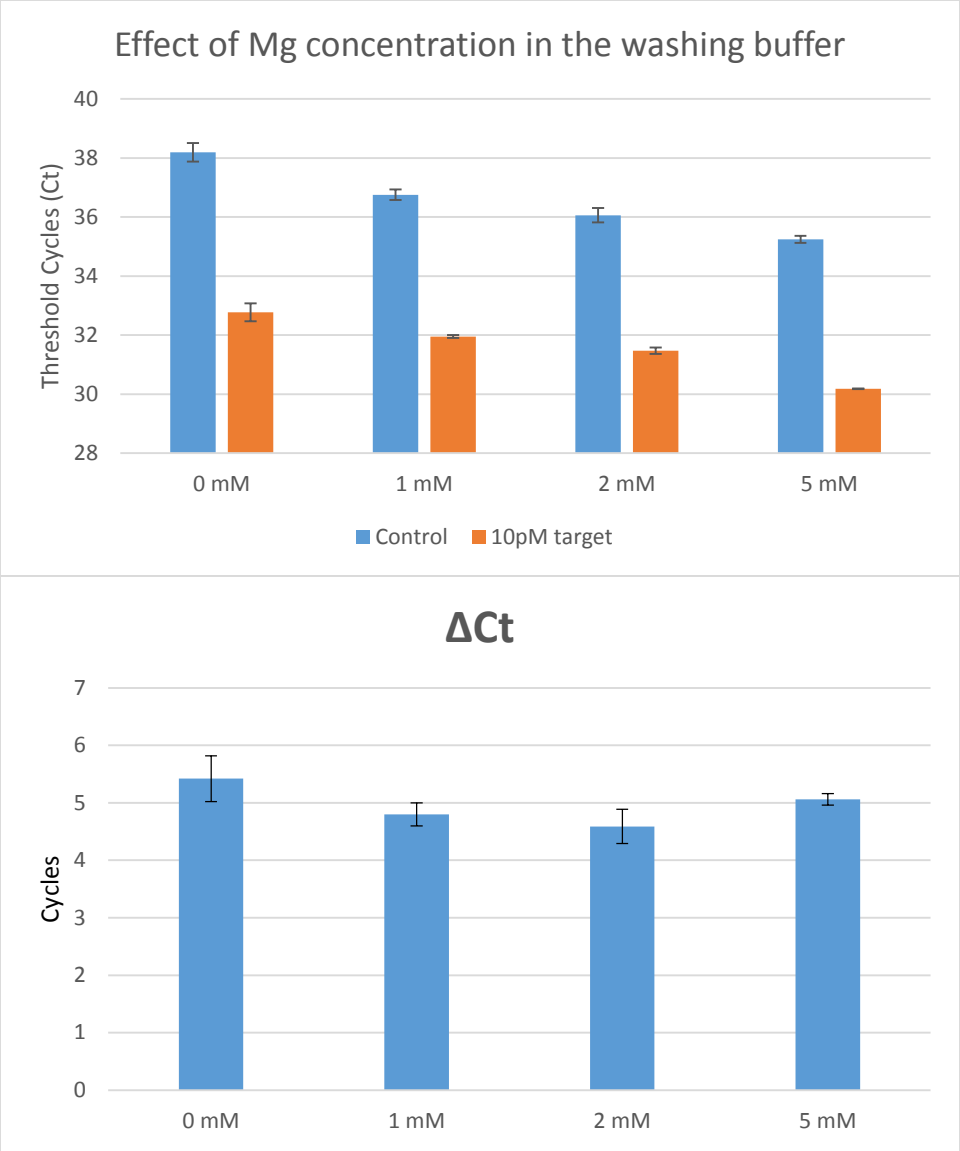

Figure 4.12 Effect of Mg^{2+} concentration in the washing buffer. Real-time qPCR experiments were carried out in triplicate and values are expressed as mean ± SD.

4.3.4 Dynamic range and detection limit of the magnetic bead-mediated BINDA assay for BPDE-*p53*-exon7 adducts analysis

Based on the studied and optimized parameters, a concentration range of BPDE-*p53*-exon7 adducts was used to determine the dynamic range and detection

limit of magnetic bead-mediated BINDA assay (Figure 4.13). A high concentration of undamaged *p53*-exon7 (750 pM) was used as the control to test the specificity of the assay. A dynamic range of 0.5 pM to 150 pM was obtained. A concentration of 750 pM of undamaged *p53*-exon7 produced a similar signal output to the 0.1 pM BPDE-*p53*-exon7. The detection limit, if defined as three times the standard deviation plus the blank signal, was 0.1 pM.

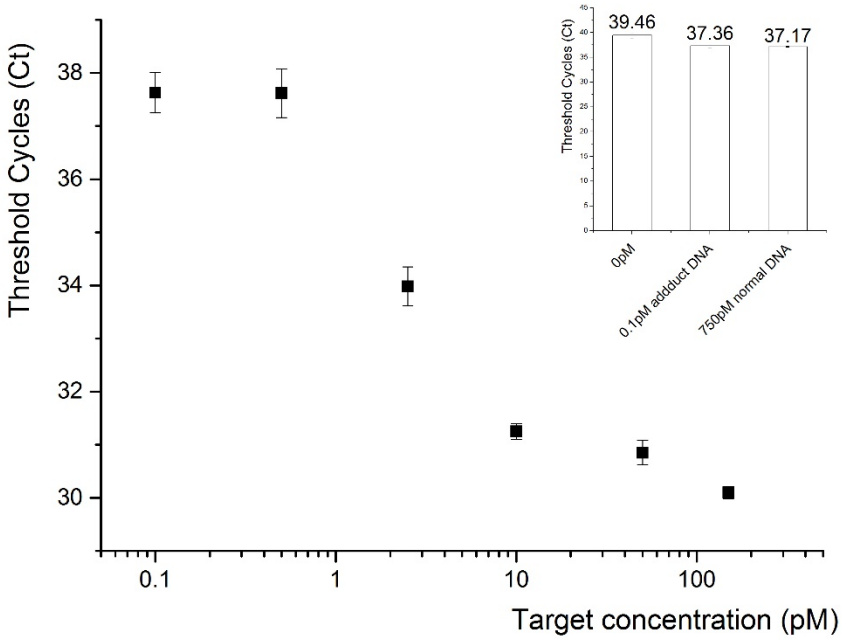

Figure 4.13 Dynamic range and detection limit of the magnetic bead-mediated BINDA assay for BPDE-*p53*-exon7 adducts analysis. Real-time qPCR experiments were carried out in triplicate and values are expressed as mean ± SD.

To test if the concentration detection limit of the assay could be further improved by lowering the concentration of BPDE-*p53*-exon7 in a larger volume

of incubation buffer (250 µL, as compared to 50 µL in the above experiments), the magnetic beads were re-suspended in a smaller volume of washing buffer (10 µL, as compared to 50 µL in the above experiments) before being applied to ligation and real-time qPCR quantification (Figure 4.14).

With this strategy, the assay could now extend the dynamic range down to 25 fM (20 times lower than under standard conditions) and the detection limit could reach 5 fM. However, it should be noted that the absolute detection limit was not improved.

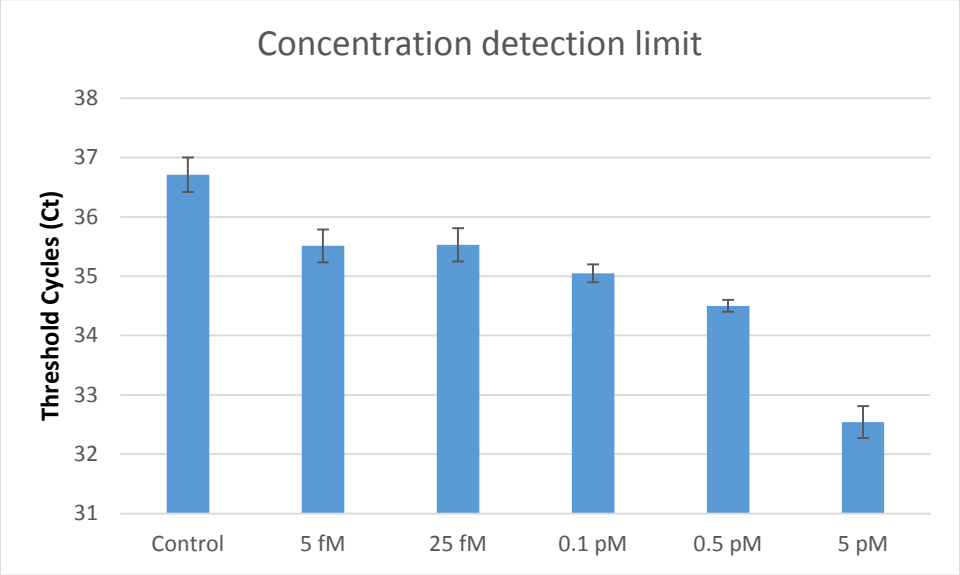

Figure 4.14 Concentration detection limit of the magnetic bead-mediated BINDA assay for BPDE-*p53*-exon7 adducts analysis. Real-time qPCR experiments were carried out in triplicate and values are expressed as mean ± SD.

4.4 Conclusions

The magnetic bead-mediated BINDA assay further enhanced the detection of

BPDE-DNA adducts on *p53*-exon7. As compared to the homogeneous BINDA assay, the new assay immobilized two elements of Probe-1, i.e., Probe-F and BPDE antibody, on the magnetic bead surface. The magnetic bead now serves as a new scaffold and allows the binding-induced DNA assembly to occur on its surface.

The new assay has three advantages over the homogeneous BINDA. Firstly, the local concentration of Probes upon target binding was increased due to multiple Probe-F molecules that could be available for DNA assembly in proximity. Secondly, the magnetic bead as the solid phase support for DNA assembly could be washed to remove the excess amount of Probe-2, which is important in reducing the target-independent DNA assembly. Thirdly, the magnetic bead could concentrate the target in a large volume of incubation buffer. Because of this, the concentration detection limit could be improved compared with the homogeneous BINDA assay. Indeed both the dynamic range and detection limit were improved by the new assay format due to these advantages.

4.5 References

1. R. Owczarzy, B. G. Moreira, Y. You, M. A. Behlke, J. A. Walder, Predicting stability of DNA duplexes in solutions containing magnesium and monovalent cations, *Biochemistry* **47**, 5336–53 (2008).

Chapter Five

Coupling of solid-phase extraction with BINDA assays for BPDE-*p53*-exon7 adducts in genomic DNA

5.1 Introduction

Chapter 3 demonstrates the basic principle of the BINDA assay using target binding to increase local concentration for specific detection of the BPDE-DNA target, while Chapter 4 further improves its sensitivity and specificity using magnetic beads. These two assays were able to detect low concentrations of synthesized BPDE-DNA adduct, containing one BPDE adduct on the 92 nucleotides *p53*-exon7 sequence.

The human genome contains more than 3 billion base pairs, most of them corresponding to non-coding regions (>98%) (*1*). The target, *p53*-exon7, comprises merely 0.000003% of the genomic DNA. In order to apply the proposed assays to the *p53*-exon7 sequence from cellular or tissue DNA samples, the interference from non-target DNA, which is 3×10^7 fold in excess, must be suppressed. The challenge is to reduce the non-specific binding of Probes-F/R to the genomic DNA. This chapter discusses the spiking of the BPDE-*p53*-exon7 adducts into the genomic DNA for assay optimization. It could be expected that the background signal from magnetic bead-mediated BINDA is lower than that of homogeneous BINDA because the extra washing steps reduce the interference from genomic DNA.

To further reduce the interference from genomic DNA, the addition of a solid-phase extraction step prior to the BINDA assays was proposed (Figure 5.1).

A target-hybridization oligonucleotide-conjugated magnetic bead was used for the solid-phase extraction. The extraction step was used to capture the BPDE-DNA adducts on target genes from the genomic DNA. After the captured BPDE-DNA adducts were released from the magnetic beads by alkaline denaturation, the extraction beads were discarded. Both the homogeneous and magnetic bead-mediated BINDA assays were then coupled with solid-phase extraction in order to analyze the released BPDE-*p53*-exon7.

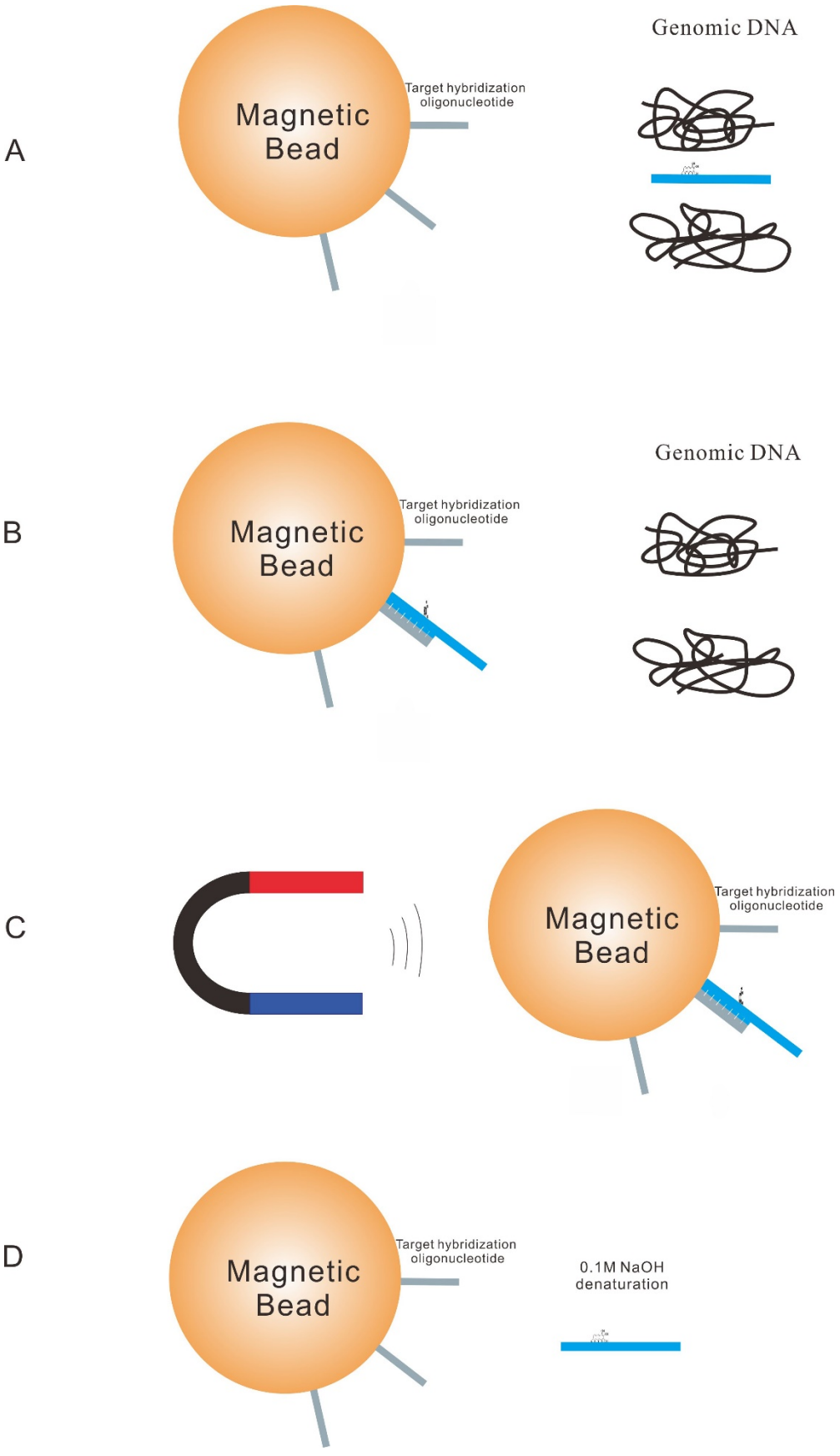
A
Magnetic Bead
Target hybridization oligonucleotide
Genomic DNA
B
Magnetic Bead
Target hybridization oligonucleotide
Genomic DNA
C
Magnetic Bead
Target hybridization oligonucleotide
D
Magnetic Bead
Target hybridization oligonucleotide
0.1M NaOH denaturation

Figure 5.1 Solid-phase extraction of BPDE-DNA adducts from genomic DNA. (A) The target hybridization oligonucleotide-conjugated magnetic bead is incubated with the mixture of BPDE-DNA adduct and genomic DNA. (B) The BPDE-DNA adduct from the target gene binds to the surface of the magnetic beads through interaction with the target hybridization oligonucleotide. (C) The BPDE-DNA adduct is concentrated and genomic DNA is removed through the use of a magnet. (D) The BPDE-DNA adduct is released from the magnetic bead by alkaline (0.1 M NaOH) denaturation.

5.2 Experimental

5.2.1 Reagents and instruments

Bovine serum albumin (Cat. NO. A7906) was obtained from Sigma-Aldrich (Oakville, ON). Anti-BPDE antibody clone 8E11 (Cat. No. 4360-MC-100) was purchased from Trevigen (Gaithersburg, MD). Biotin-XX microscale protein labeling kit (Cat. No. B30010), Platinum® qPCR SuperMix UDG (Cat. No. 11730), T4 DNA Ligase (Cat. No. 15224), and T4 Polynucleotide Kinase (Cat. No. 18004), DNA Ladder, 1 Kb, with sizes ranging from 0.1 kb to 12 kb in 1 µg/µL, and Tris buffer were purchased from Invitrogen (Carlsbad, CA). Phosphate buffered saline (10×PBS) and NaOH stock solution (5N) was purchased from Fisher Scientific (Nepean, ON) and was diluted to 1×PBS (137 mM NaCl, 10 mM phosphate, 2.7 mM KCl, pH 7.4) and 0.1 M NaOH by deionized water, respectively. Tween 20 (Cat. No. BP337500) was obtained from Fisher Scientific. All other reagents were of analytical grade.

Streptavidin-coupled Dynabeads MyOne C1 (Cat. No. 65001) and DynaMag-Spin Magnet (Cat. No. 12320D) were purchased from Invitrogen Dynal AS (Oslo).

The oligonucleotides (except the TaqMan probe) were custom synthesized, labeled, and purified by Integrated DNA Technologies (IDT, Coralville, IA).

The lung carcinoma cell line A549 (biosafety level 1) was used in this study. The cells were cultured in RPMI 1640 with L-glutamine (Cat. No. 11875-093) from Gibco. Cellular DNA was extracted by Qiagen DNeasy Blood & Tissue Kit (Cat. No. 69504). Concentrations of genomic DNA were measured by absorption spectroscopy at 260 nm on a NanoVue instrument from GE (Fairfield, CT).

Endonuclease restriction enzymes Hind III (Cat. No.15207-012) and BamH I (Cat. No. 15201-023) were purchased from Invitrogen. CviQ I (Cat. No. R0639) and Bbs I (Cat. No. R0539) were purchased from New England BioLabs Canada (Whitby, ON). All restriction enzymes are not sensitive to CpG, dam, or dcm methylation.

5.2.2 Preparation of Probes and conjugation of magnetic beads

Probe-1 and Probe-2 were prepared using the procedures described in Chapter 3. Probe-F and BPDE antibody-conjugated magnetic beads were produced by the method discussed in Chapter 4.

Magnetic beads used as the solid phase for BPDE-*p53*-exon7 extraction were prepared as follows: The streptavidin-coupled Dynabeads MyOne C1 magnetic beads were first washed with PBS buffer 3 times to remove the original buffer, then re-suspended in 1×PBS buffer containing 0.2% BSA. The biotinylated target

hybridization oligonucleotide (sequences are listed in Table 3.1) stock solution was diluted with 1×PBS buffer containing 0.2% BSA. The two solutions were mixed thoroughly by pipetting up and down. The mixture was put in a mixer and rotated for 30 min to prevent the precipitation of the magnetic beads. After that, the mixture was stored at 4˚C overnight (>8 h). The excess target hybridization oligonucleotide was then removed using a magnet and 3 times washing with 1×PBS buffer. Finally, following the re-suspension of the beads in 1×PBS buffer containing 0.2% BSA, they were ready for use.

5.2.3 Analysis of BPDE-*p53*-exon7 adducts in genomic DNA by homogeneous BINDA and magnetic bead-mediated BINDA assay

The genomic DNA was extracted from A549 human lung carcinoma cells by the Qiagen DNeasy Blood & Tissue Kit according to the manufacturer's instructions. After quantification of the extracted DNA by A260 on the NanoVue instrument, the DNA was digested by four restriction endonucleases: Hind III, BamH I, CviQ I, and Bbs I. The digestion reaction was carried out at room temperature for 8 h in NEB buffer 2 and 1×BSA. After digestion, the enzymes were deactivated at 65˚C for 20 min. To denature the digested genomic DNA, the tube was placed in the 95˚C water bath for 15 min, then chilled on ice for 30 min.

Assay procedures were similar to those in Chapters 3 and 4, except for the addition of genomic DNA to the sample. In the homogeneous BINDA assay, 50 pM of BPDE-*p53*-exon7 and 2 μg of genomic DNA were incubated with Probe-1/Probe-2 and Blocks-F/R in 100 μL of 1×PBS with 0.2% BSA and $MgCl_2$ for 30 min at 37˚C followed by 10 min at 25˚C . Then 2 μL of the incubated solution was

transferred to a 18 μL of real-time PCR reaction containing 1×PCR buffer, 3 mM $MgCl_2$, dNTPs, 0.1 μM forward and reverse primers, DNA polymerase, 0.25 μM Rox reference dye, 0.1 μM TaqMan probe, and 0.4 unit T4 DNA ligase. The mixture was kept in the dark at room temperature for 10 min prior to the application of the PCR plate to real-time qPCR quantification.

In the magnetic bead-mediated BINDA assay, the BPDE-*p53*-exon7 adducts were first incubated with Probe-F and BPDE antibody conjugated magnetic beads in 1×PBS with 0.2% BSA for 1 h at room temperature. After incubation, the solution was removed using a magnet, and the beads were washed 3 times by 500 μL wash buffer (1×PCR buffer with 0.01% Tween 20). Then the beads were re-suspended in 50 μL 1×PBS buffer with 0.2% BSA containing the Probe-2, Blocks-F/R, and $MgCl_2$. The tube was then incubated at room temperature for another hour. The magnetic beads were washed 3 times by 1×PCR buffer with 400 nM Block-R, then re-suspended in 50 μL wash buffer. Finally 2 μL of the bead suspension was transferred to a 18 μL real-time PCR reaction containing 1×PCR buffer, 3 mM $MgCl_2$, dNTPs, 0.1 μM forward and reverse primers, DNA polymerase, 0.25 μM Rox reference dye, TaqMan probe, and 0.4 unit T4 DNA ligase. The mixture was kept in the dark for 10 minutes at room temperature before being subjected to real-time qPCR.

5.2.4 Solid phase extraction of BPDE-*p53*-exon7 from genomic DNA

The experimental strategy is illustrated in Figure 5.1. At first the BPDE-*p53*-exon7 and genomic DNA were added to 500 μL of 1×PBS buffer containing 0.2% BSA. Then, the target hybridization oligonucleotide-conjugated magnetic beads

were added, and the mixture was put in a mixer and rotated for 30 min to prevent the magnetic beads from precipitating. After the incubation, the solution containing genomic DNA was removed using a magnet. The magnetic beads were washed 3 times by 500 µL of 1×PBS with 0.01% Tween 20. To release the BPDE-*p53*-exon7, 30 µL of freshly diluted 0.1 M NaOH (prepared before the experiment) was added to the magnetic beads. The magnetic beads and the NaOH solution were carefully pipetted, mixing thoroughly. After 10 min, the solution was transferred to a new tube and 30 µL 0.1 M HCl was added to neutralize the alkaline. The BPDE-*p53*-exon7 was now in a solution of 60 µL 0.05 M NaCl and ready for analysis.

5.2.5 Analysis of BPDE-*p53*-exon7 adducts by homogeneous BINDA and magnetic bead-mediated BINDA assay coupled with solid phase extraction

The released BPDE-*p53*-exon7 in 60 µL 0.05 M NaCl solution obtained in 5.2.4 was added to the incubation buffer in either homogeneous or magnetic bead-mediated BINDA assays. The following procedures were the same as those described in Chapters 3 and 4.

5.3 Results and Discussion

5.3.1 Analysis of BPDE-*p53*-exon7 adducts in genomic DNA by homogeneous BINDA assay

In the homogeneous BINDA assay, described in Chapter 3, Probe-F was conjugated with the BPDE antibody, forming Probe-1, and Probe-R was conjugated with the target hybridization oligonucleotide, forming Probe-2 (Figure

3.1). Another conjugation strategy was also used (shown in Figure 5.2). In this strategy, the Probe-R was conjugated to the BPDE antibody, and Probe-F was conjugated to the target hybridization oligonucleotide. Both conjugation strategies were applied for the analysis of BPDE-*p53*-exon7 adducts in genomic DNA.

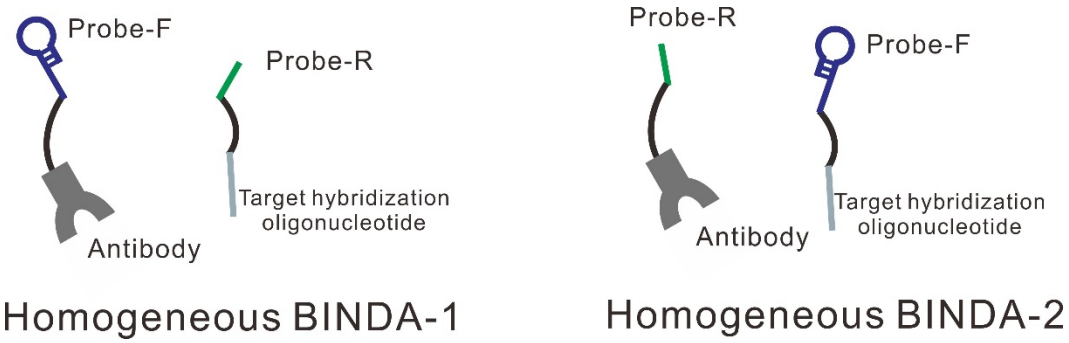

Figure 5.2 Two formats of homogeneous BINDA assay for the detection of BPDE-*p53*-exon7 in A549 DNA. Homogeneous BINDA-1: Probe-F is connected to the BPDE antibody and Probe-R is connected to the target hybridization oligonucleotide. Homogeneous BINDA-2: Probe-R is connected to the BPDE antibody and Probe-F is connected to the target hybridization oligonucleotide.

The genomic DNA used in this study was extracted from A549 human lung carcinoma cells. The genomic DNA was digested by four restriction endonucleases, Hind III, BamH I, CviQ I, and Bbs I. CviQ I and Bbs I were used to specifically cut two ends of the *p53*-exon7 sequence, and Hind III/BamH I were used to digest the extracted genomic DNA into smaller pieces, reducing the viscosity of the DNA solution. The digestion products were examined on agarose

gel (Figure 5.3). A commercially available herring DNA was also included as a reference. The extracted A549 DNA were about 20,000 base pairs. After digestion, most of DNA pieces were below 1000 base pairs. The commercial herring DNA was sonicated, causing the lengths to be about 500 base pairs.

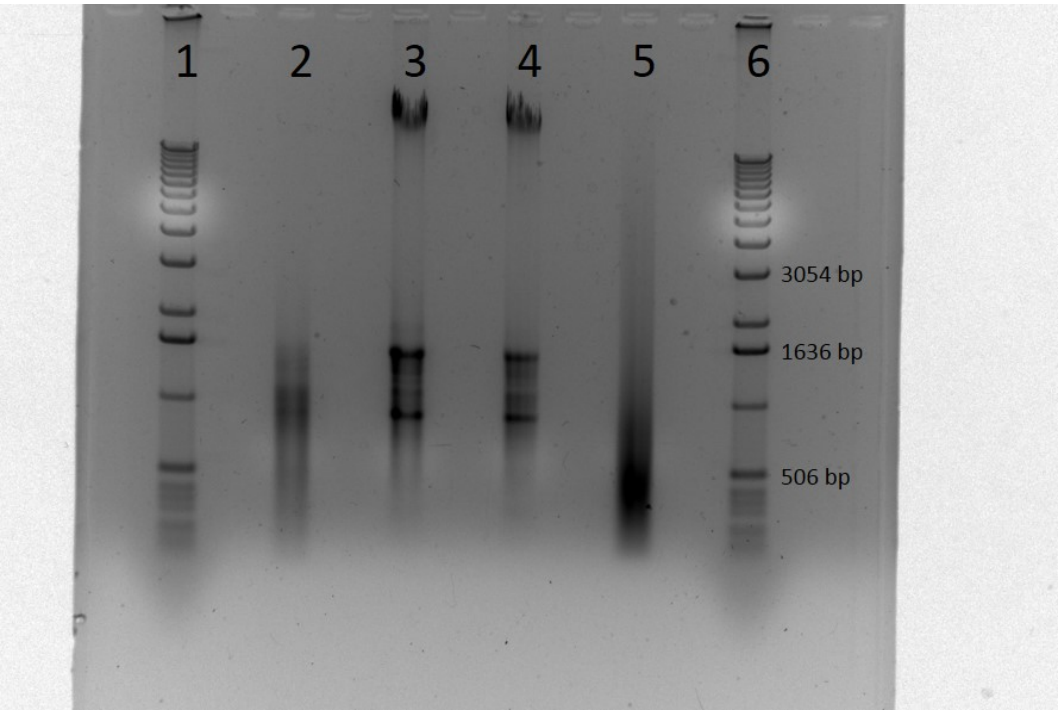

Figure 5.3 Agarose gel electrophoresis for genomic DNA. Samples were run on 0.8% agarose gel. Electrophoresis was conducted at 100 V (10 V/cm) at room temperature. Lanes 1 and 6: high molecular weight DNA ladder; Lane 2: four-enzyme (see experimental part for the enzymes used in this study) digested A549 DNA; Lanes 3 and 4: A549 DNA; Lane 5: herring DNA.

Two micrograms of four-enzyme digested genomic DNA were used as the matrix to spike the target BPDE-*p53*-exon7 adducts. Two micrograms of genomic

DNA equals the amount of DNA extracted from about 2×10^5 cells. BPDE-*p53*-exon7 adducts (50pM) were spiked into the matrix to challenge the assay (Figure 5.4). The result showed Homogeneous-BINDA-2 format could generate slightly higher ΔCt than the Homogeneous-BINDA-1 format without the interference from genomic DNA. However, in the presence of A549 genomic DNA, the background signal significantly increased in both Homogeneous-BINDA formats, from 36 cycles to 29 cycles. The background signal increase indicated 2^7 or a 128-fold of Probe-F and Probe-R were assembled during the incubation, compared to the sample without the A549 genomic DNA. This huge increase resulted from the genomic DNA which contains very complex DNA sequences that cause the assembly of target-independent Probe-F and Probe-R.

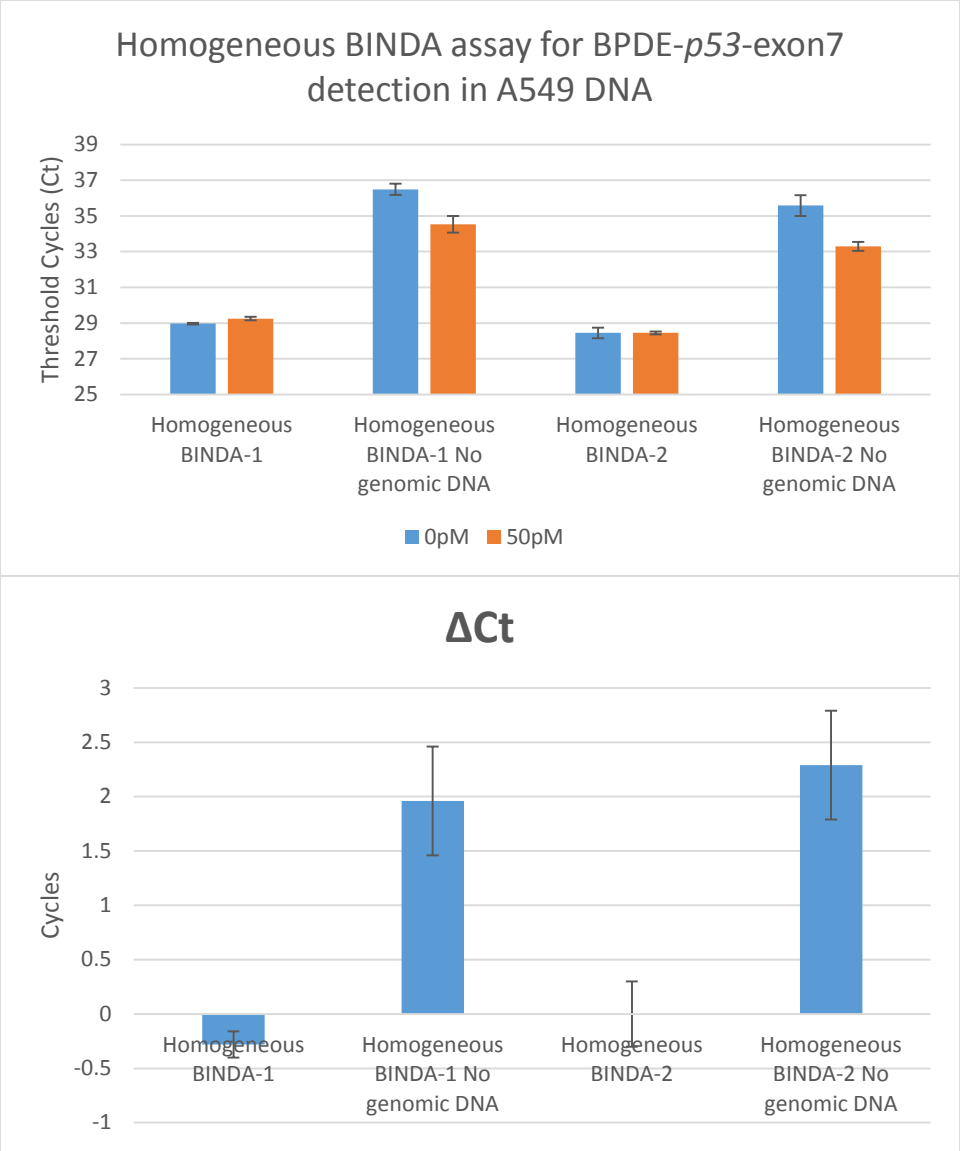

Figure 5.4 Analysis of BPDE-*p53*-exon7 adducts in 2 µg A549 genomic DNA by homogeneous BINDA assay. Real-time qPCR experiments were carried out in triplicate and values are expressed as mean ± SD.

5.3.2 Analysis of BPDE-*p53*-exon7 adducts in genomic DNA by magnetic bead-mediated BINDA assay

The magnetic bead-mediated BINDA assay was challenged by the sample of

5 pM BPDE-*p53*-exon7 adducts spiked into different genomic DNA (Figure 5.5). Herring DNA, undigested A549 DNA, and digested A549 DNA were used in this experiment. As opposed to the Homogeneous BINDA assay, the magnetic beads on which the Probe-F and Probe-R assembled were washed after incubation with the mixture of BPDE-*p53*-exon7 adducts and genomic DNA. The purpose of the washing step was to remove the genomic DNA that could interfere with the Probe-F/R assembly. However, the background signal was still significantly increased by genomic DNA (35 cycles to 30 cycles for herring DNA, 35 cycles to 33 cycles for undigested A549 DNA, and 35 cycles to 33.5 cycles for digested A549 DNA). Due to the wash step, the background increase was lower than the increase in the homogeneous BINDA assay. The background signal increases were about $2^5 = 32$, $2^2 = 4$, and $2^{1.5} = 2.8$ fold, respectively. The high background signal made it difficult to detect the target ($\Delta Ct < 1$ cycle).

The background increase was due to target-independent DNA assembly between Probe-F and Probe-R. In the magnetic bead-mediated BINDA assay, the DNA assembly occurs on the bead's surface. During incubation, the genomic DNA were retained on the bead's surface, but the reason was unclear. The retained genomic DNA induced target-independent DNA assembly between Probe-F and Probe-R, which in turn generated the background signal. The retention of the genomic DNA on the bead's surface could be due to the genomic DNA tangled on the bead or to non-specific absorption from the molecular charge.

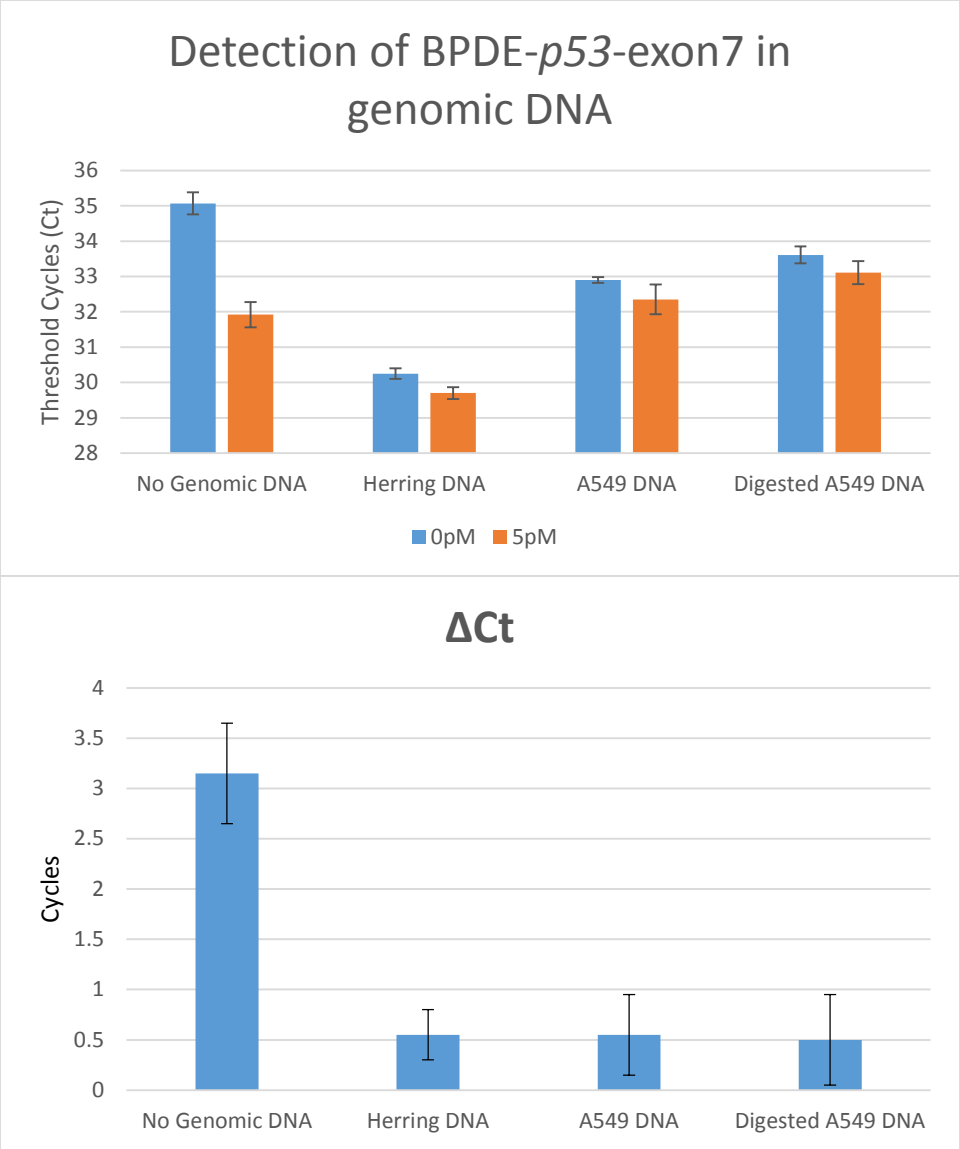

Figure 5.5 Analysis of BPDE-*p53*-exon7 adducts in genomic DNA by magnetic bead-mediated BINDA assay. Two micrograms of Herring DNA, undigested A549 DNA and digested A549 DNA were used. Real-time qPCR experiments were carried out in triplicate and values are expressed as mean ± SD.

To remove the genomic DNA from the magnetic bead surface, the volume of wash buffer (1×PCR buffer with 0.01% Tween 20) was increased from 50 µL to

500 µL (Figure 5.6). This experiment demonstrated that an increase in the volume of wash buffer could effectively remove the attached genomic DNA from the surface of magnetic beads, reducing background signal due to target-independent DNA assembly.

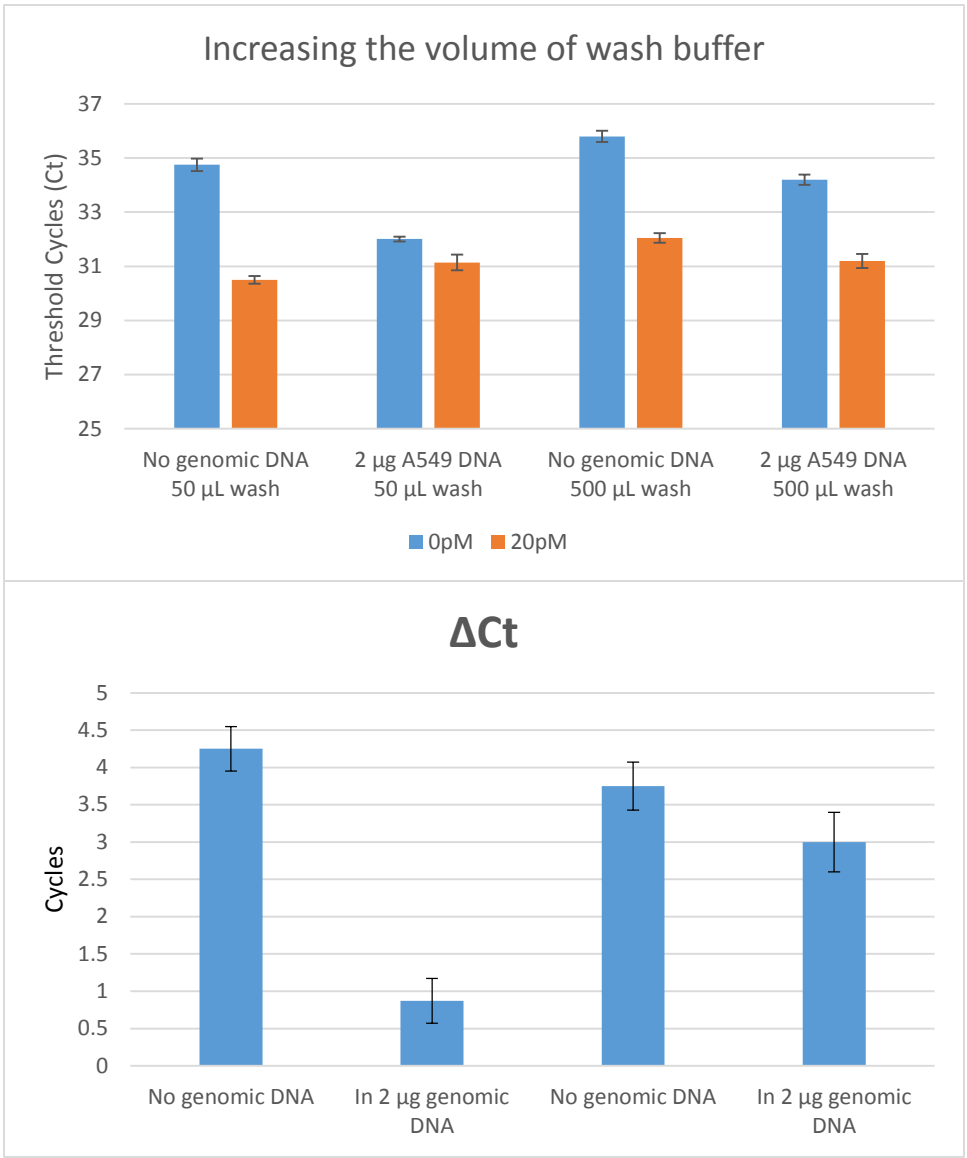

Figure 5.6 Effect of increasing the volume of wash buffer 10-fold. The background signal from the target-independent DNA assembly on the magnetic

bead surface was reduced. Real-time qPCR experiments were carried out in triplicate and values are expressed as mean ± SD.

Compared to the sample without the genomic DNA, it could be concluded that large volumes of wash buffer also reduce the binding-induced DNA assembly (ΔCt was lower than the sample with a small volume of wash buffer). This could also be attributed to the loss of magnetic beads during the operation, during the recovery of a small quantity of magnetic beads from a much larger volume of liquid. Nonetheless, the ΔCt (from 1 cycle to 3 cycles) was improved for the group with genomic DNA showing the positive effect of large volume wash.

The length of the target hybridization oligonucleotide that was used to construct Probe-2 in the magnetic bead-mediated BINDA assay was also studied (Figure 5.7). A different Probe-2 was prepared to test 5 pM of BPDE-*p53*-exon7 in 2 µg of digested A549 DNA. This study was trying to determine if the interference of genomic DNA was related to the length of the target hybridization oligonucleotide. The longer the target hybridization oligonucleotide, the more opportunities there are for the genomic DNA to interact with it due to the base pairing. However, the result showed that using large volumes of wash buffer, with the shorter target hybridization oligonucleotide, did not generate lower background. This result indicated that either the interference of genomic DNA was not quite related to the length of target hybridization oligonucleotide or that the interference was weak so that large volumes of wash buffer could easily dissociate the interaction between the genomic DNA and target hybridization

oligonucleotide.

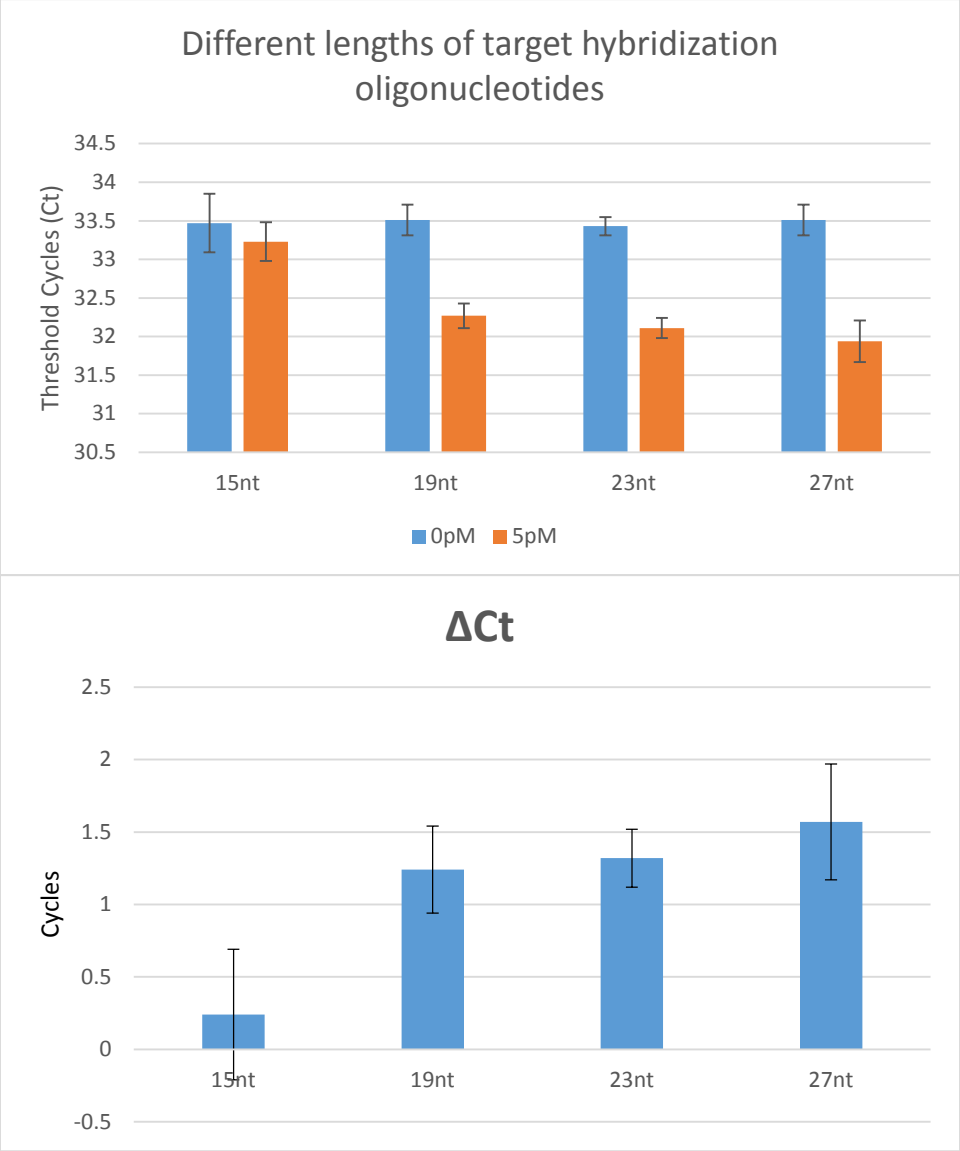

Figure 5.7 Effect of the length of the target hybridization oligonucleotide. Real-time qPCR experiments were carried out in triplicate and values are expressed as mean ± SD.

The dynamic range of the magnetic bead-mediated BINDA assay for BPDE-

p53-exon7 adducts analysis, in 2 µg genomic DNA, was determined using large volumes of wash buffer and Probe-2 with 27 n.t. target hybridization oligonucleotide (Figure 5.8). The assay could detect lower than 5 pM of BPDE-*p53*-exon7 adducts in 2 µg genomic DNA, which was not as good as in the absence of genomic DNA. The dynamic range was from 5 pM to 150 pM.

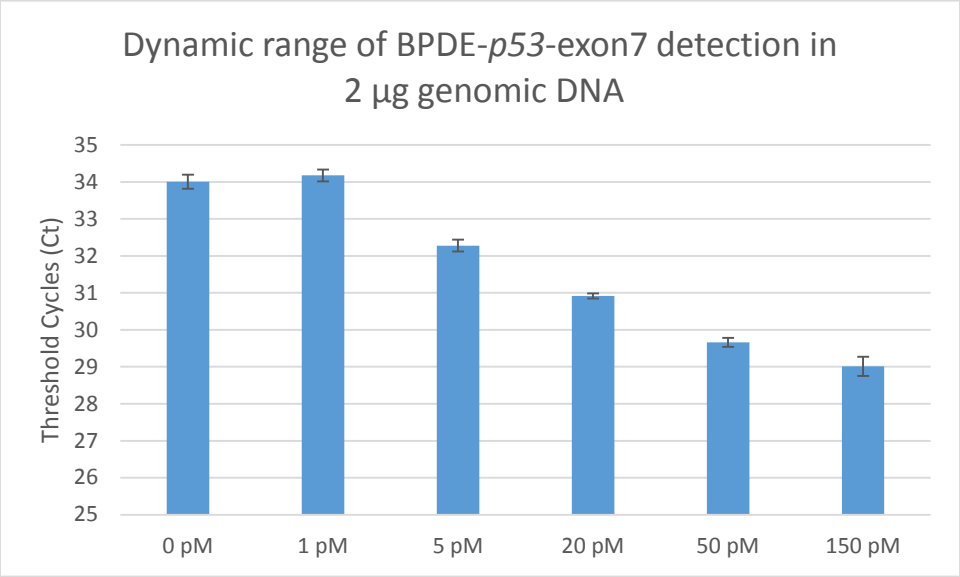

Figure 5.8 Dynamic range of magnetic bead-mediated BINDA for BPDE-*p53*-exon7 adducts in 2 µg A549 DNA. Real-time qPCR experiments were carried out in triplicate and values are expressed as mean ± SD.

To detect the BPDE-*p53*-exon7 adducts from real cell or tissue samples, after the four-enzyme digestion, the genomic DNA must be denatured to generate single-stranded BPDE-*p53*-exon7. Hence, denatured A549 DNA was used in the following experiments as the matrix into which the BPDE-*p53*-exon7 was spiked. These experiments show the ability of the assay to analyze real samples.

BPDE-*p53*-exon7 (20 pM) was mixed with 2 µg or 10 µg denatured A549 DNA, followed by the magnetic bead-mediated BINDA assay, using a large volume of washing buffer. However, the assay was not able to differentiate 20 pM BPDE-*p53*-exon7 from the denatured genomic DNA (Figure 5.9). This result suggested that the single-stranded genomic DNA was much harder to be removed from the magnetic bead surface than the double-stranded genomic DNA. The reason for this was unclear.

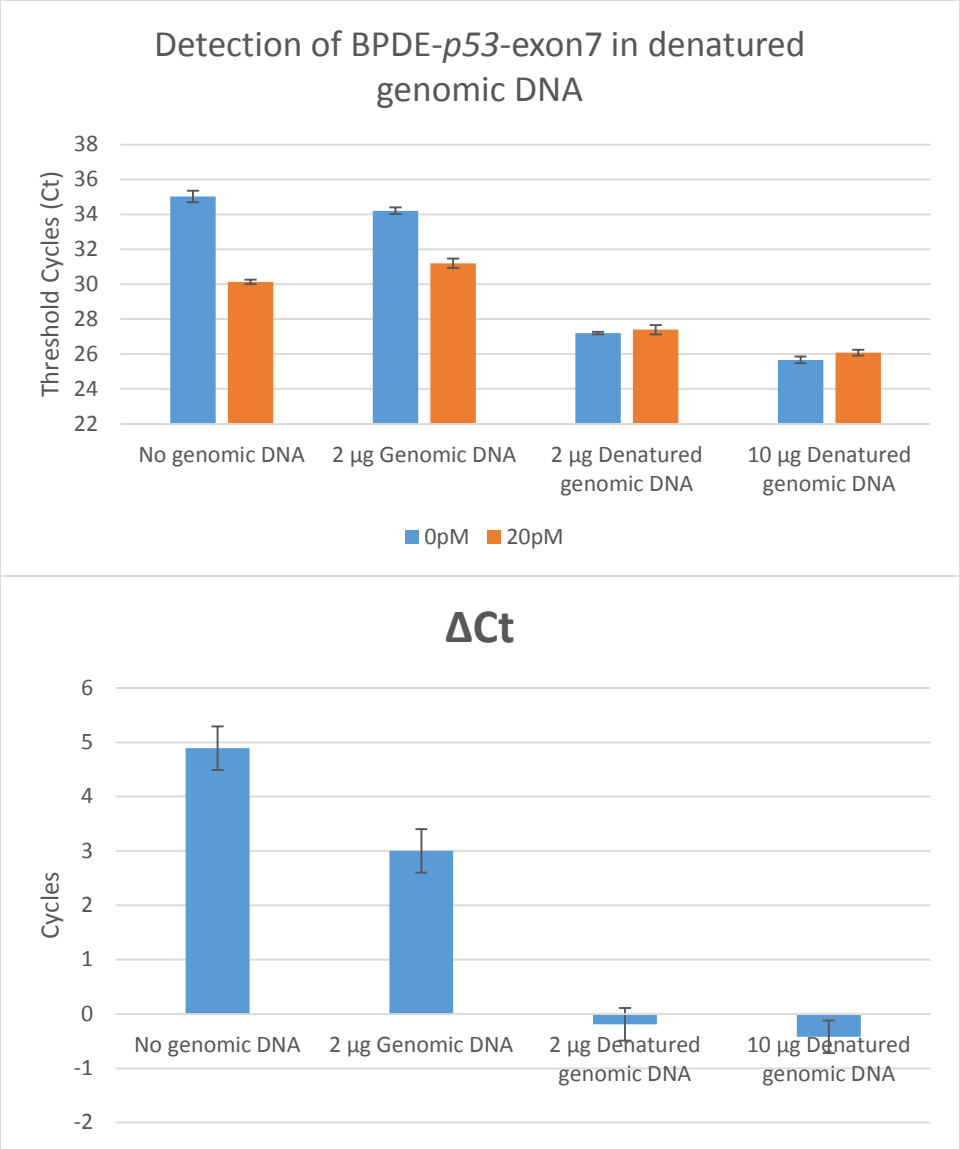

Figure 5.9 Detection of BPDE-*p53*-exon7 in denatured genomic DNA using magnetic bead-mediated BINDA assay. Real-time qPCR experiments were carried out in triplicate and values are expressed as mean ± SD.

Before trying to remove the single-stranded genomic DNA from the bead's surface, another method, which employs short oligonucleotides to protect the bead's surface, was first tested (Figure 5.10). The purpose of using short

oligonucleotides was to occupy the bead's surface to compete with the genomic DNA, and prevent the absorption and retention of the single-stranded genomic DNA on the bead's surface. Three oligonucleotides were involved in this experiment: undamaged *p53*-exon7 (named 92-mer because of its length), 14-mer (5'-CCC ATT CAG ACT GA-3') and 28-mer (5'-TGC AAC TGG CAC GCG GAC TCT GAA AAA A-3'). These short oligonucleotides were incubated with the Probe-F and the antibody-conjugated magnetic beads for 30 min, prior to the addition of 30 pM BPDE-*p53*-exon7 and 2 μg denatured genomic DNA.

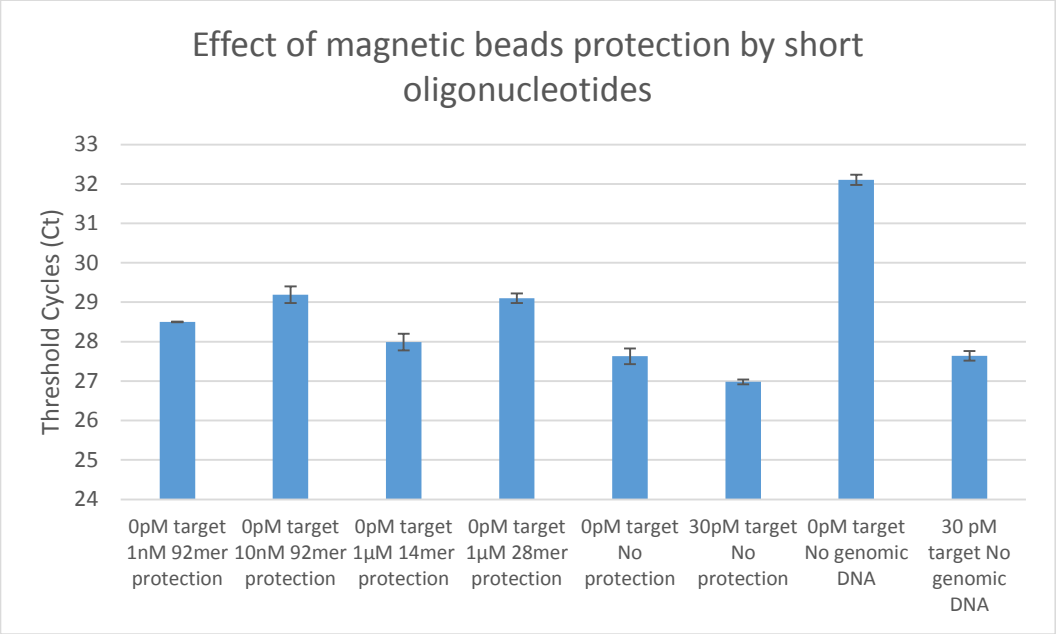

Figure 5.10 Effect of the protection of magnetic beads by short oligonucleotides. Undamaged *p53*-exon7 sequence (92-mer) and two randomly picked oligonucleotides, 14-mer and 28-mer, were tested. The 30 pM BPDE-*p53*-exon7 with or without 2 µg denatured genomic DNA were included for comparison. Real-time qPCR experiments were carried out in triplicate and values are expressed as mean ± SD.

Compared to the background signal produced without short oligonucleotide protection, all three short oligonucleotides used displayed some alleviation of the target-independent DNA assembly (Figure 5.10). A low concentration of undamaged *p53*-exon7 (10 nM) displayed a similar protection effect as 1 µM of the 28-mer. However, the background signal was still too high to produce enough ΔCt for BPDE-*p53*-exon7 detection.

Another set of short oligonucleotides was also included (Figure 5.11).

Varying lengths of poly-thymine, Poly-T10, Poly-T20, and Poly-T30, were added to the test. In this experiment, the concentration of Tween 20 was increased to 0.05%, augmenting the stringency of the washing buffer. The result showed that the use of either poly-thymine to protect the surface of the magnetic bead or the increase of the washing buffer stringency could help reduce the background signal from 2 µg denatured genomic DNA.

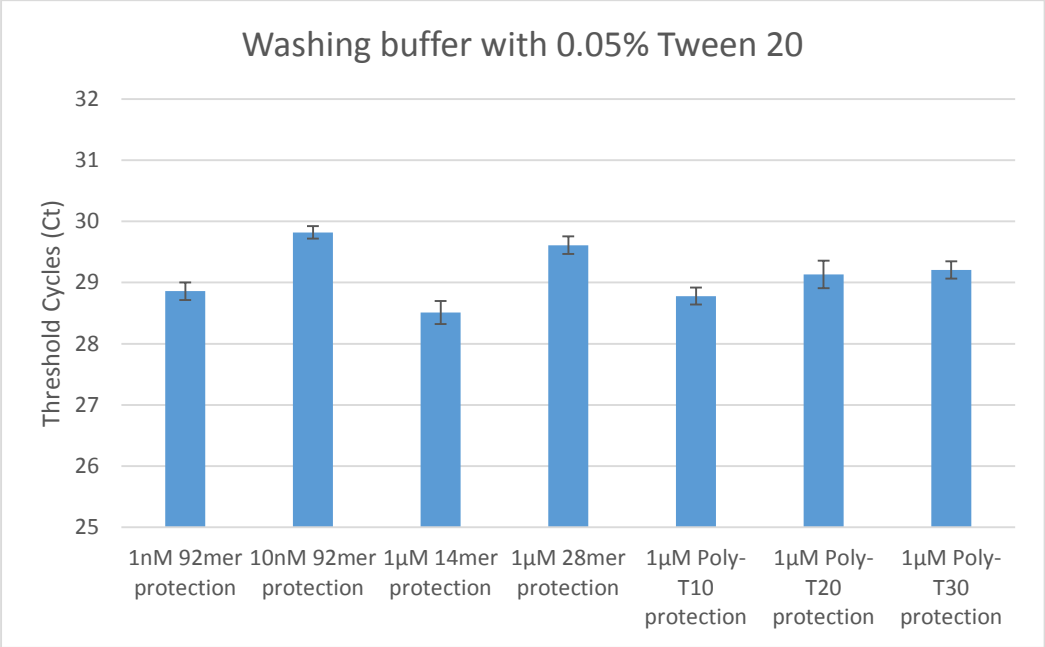

Figure 5.11 Effect of magnetic bead protection by short oligonucleotides and higher Tween 20 concentration in the washing buffer. Undamaged *p53*-exon7 sequence (92-mer) and two randomly picked oligonucleotides, 14-mer and 28-mer, Poly-T10, Poly-T20, and Poly-T30 were tested. The washing buffer contains 0.05% Tween 20. Two micrograms denatured genomic DNA was used in all samples. Real-time qPCR experiments were carried out in triplicate and values are expressed as mean ± SD.

The washing stringency was then further enhanced by increasing the number of washes (Figure 5.12). Washing 5 versus three 3 was compared using 0.05% Tween 20 washing buffer. The undamaged *p53*-exon7 sequence (92-mer) and two randomly picked oligonucleotides, 14-mer and 28-mer were used as the short protection oligonucleotides. A sample of 30 pM BPDE-*p53*-exon7 without protection was included as a reference. The result showed no improvement on the background signal from the additional washes with 1×PBS buffer containing 0.05% Tween 20.

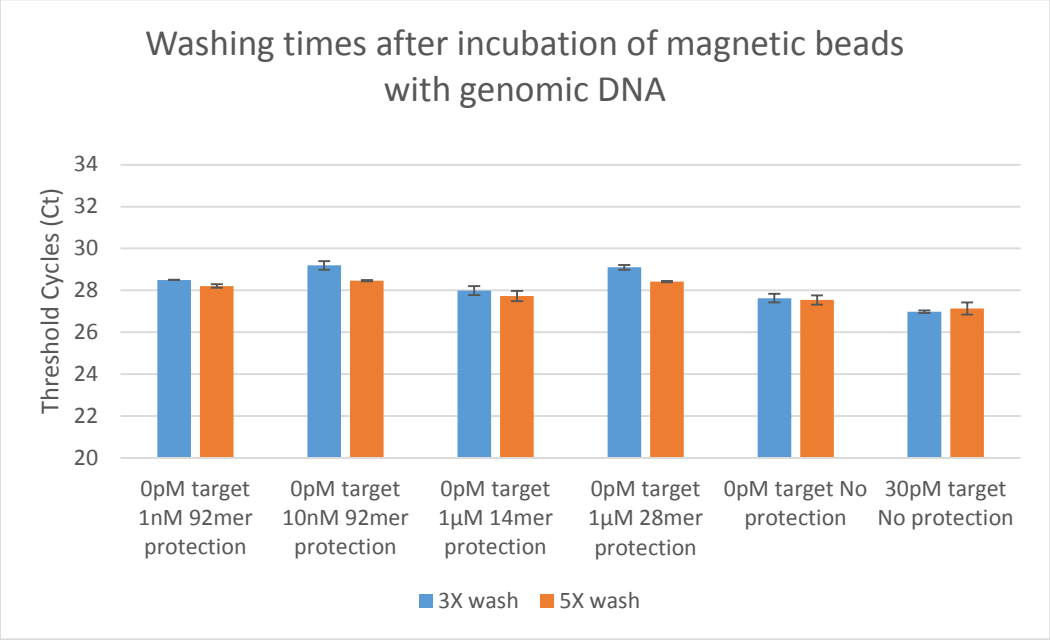

Figure 5.12 Effect of the number of washes with 1×PBS buffer containing 0.05% Tween 20. The undamaged *p53*-exon7 sequence (92-mer) and two random oligonucleotides, 14-mer and 28-mer, were used as the short protection oligonucleotides for the magnetic beads. Real-time qPCR experiments were carried out in triplicate and values are expressed as mean ± SD.

The use of hybridization oligonucleotides is another competitive protection approach that was examined. This method aims to reduce the background signal resulting from the genomic DNA absorbed on the bead surface that promoted target-independent DNA assembly between Probe-F and Probe-R. Based on this strategy, a Partial Block that is able to bind to a partial sequence of the target hybridization oligonucleotide was designed (Figure 5.13).

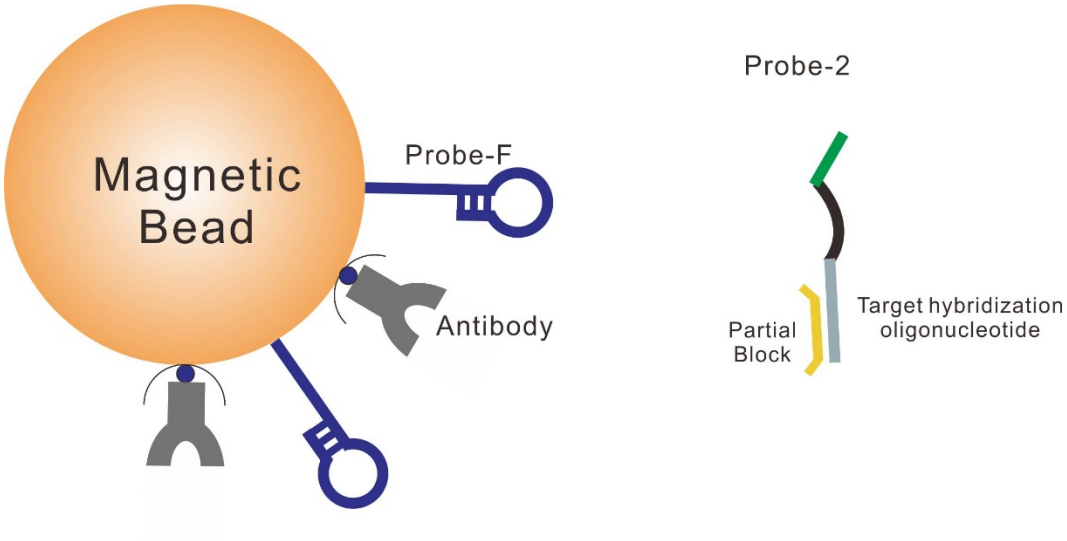

Figure 5.13 Schematic of the competitive protection of the target hybridization oligonucleotide. The partial block was designed to be 7 n.t. shorter than the target hybridization oligonucleotide.

The Partial Block was designed to be 7 n.t. shorter than the target hybridization oligonucleotide. The T_m of a 20 n.t. Partial Block is about 6˚C lower than that of the 27 n.t. target hybridization oligonucleotide. The T_m of a 12 n.t. Partial Block is about 15˚C lower than that of the 19 n.t. target hybridization oligonucleotide. This design principle would minimize the interference of short

complementary sequences with the genomic DNA that causes target independent DNA assembly.

The 30 pM BPDE-*p53*-exon7 was analyzed using the target hybridization oligonucleotide protection strategy, in 2 µg denatured genomic DNA (Figure 5.14). An equal concentration of the Partial Block was used to protect Probe-2 (Probe-R-27nt and Probe-R-19nt). However no change in either the background signal or the signal from BPDE-*p53*-exon7 was observed.

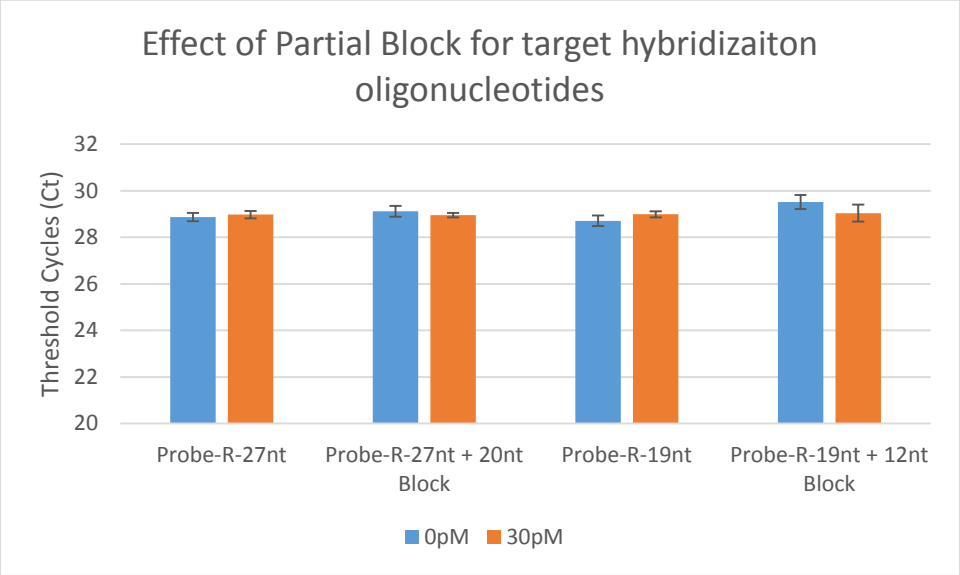

Figure 5.14 Effect of using a Partial Block to competitively protect the target hybridization oligonucleotide. Equal concentrations of Probe-2 (including Probe-R-27nt and Probe-R-19nt) and Partial Block were mixed before addition to the incubation buffer with BPDE-*p53*-exon7 and denatured genomic DNA. Real-time qPCR experiments were carried out in triplicate and values are expressed as mean ± SD.

In the following, the concentration of the Partial Block was increased as follows (Figure 5.15): the ratio of Partial Block to Probe-2 was increased from 2:1 to 50:1. The study of these concentrations showed no effective suppression of the background signal. With the concentration ratio of Partial Block to Probe-2 fixed at 10:1, the effect of increasing the Probe-2 concentration, from 2 nM to 18 nM, was also investigated (Figure 5.16). If the relatively high concentration of Probe-2 could increase the BPDE-*p53*-exon7 signal, while maintaining the background signal (because the ratio of Partial Block:Probe-2 was fixed), the ΔCt would still be enhanced. However, the results showed a trending increase in the background signal, while the concentration of Probe-2 increased and no improvement of ΔCt was obtained.

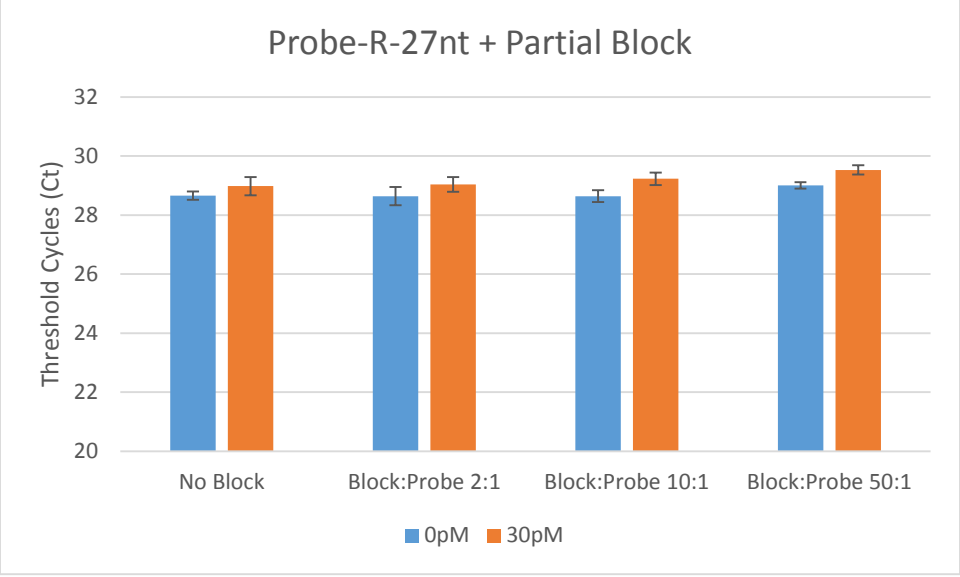

Figure 5.15 Effect of increasing the concentration ratio of the Partial Block to Probe-2. Probe-2 was constructed using Probe-R and a 27 n.t. target hybridization oligonucleotide. Real-time qPCR experiments were carried out in triplicate and

values are expressed as mean ± SD.

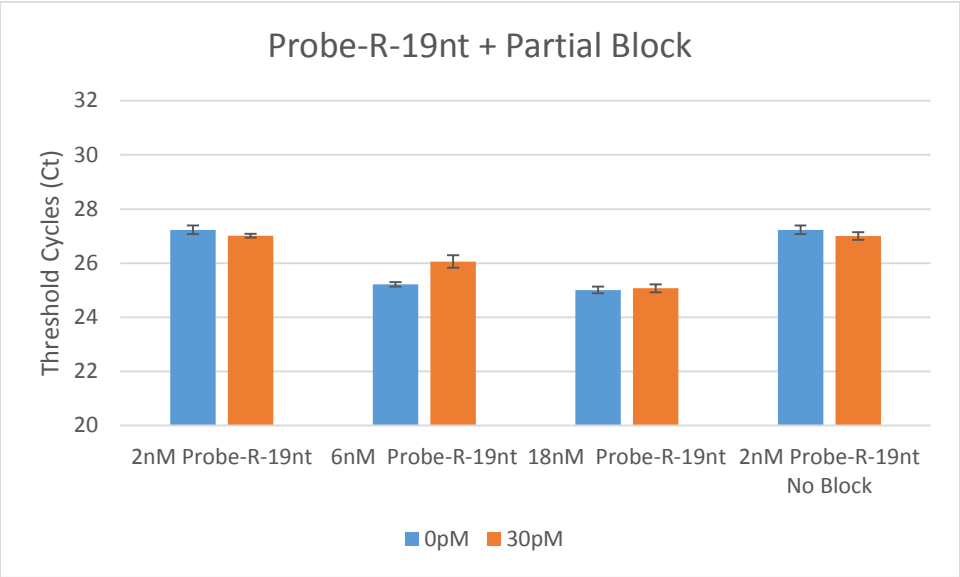

Figure 5.16 Effect of increasing Probe-2 concentration. The concentration ratio of the Partial Block to Probe-2 was fixed at 10:1. Probe-2 was constructed using Probe-R and 19 n.t. target hybridization oligonucleotide. The 30 pM BPDE-*p53*-exon7 adduct was mixed with 2 µg denatured genomic DNA and incubated with magnetic beads. Real-time qPCR experiments were carried out in triplicate and values are expressed as mean ± SD.

Combined with the Partial Block, the washing stringency was further increased by shaking the incubation tube of magnetic beads and genomic DNA at 600 rpm (Figure 5.17). An additional large volume of wash buffer were used after incubation of magnetic beads with Probe-2 (Figure 5.18). None of these procedures could increase the ΔCt of BPDE-*p53*-exon7 adducts.

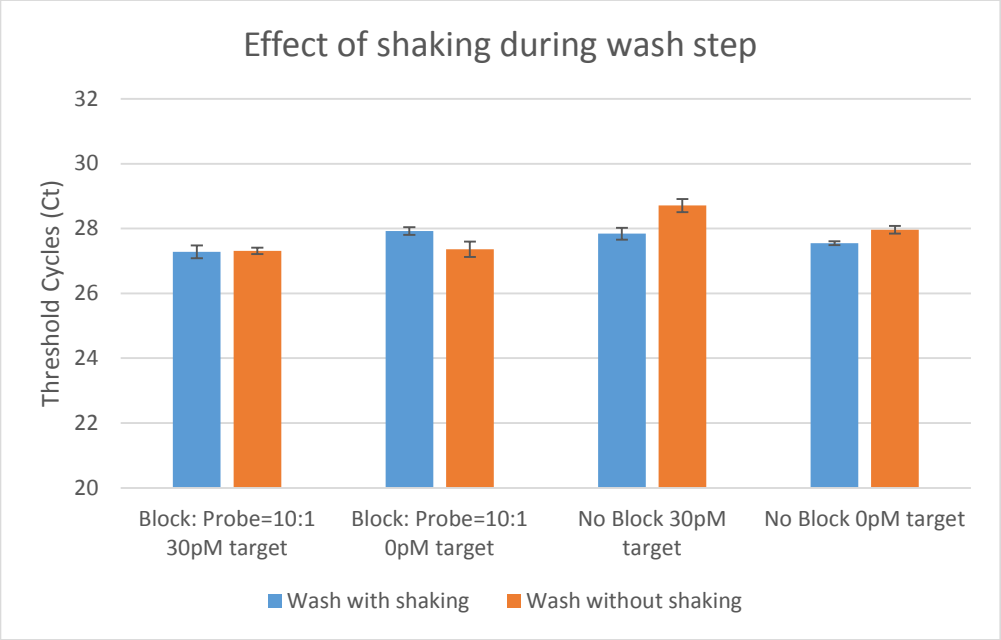

Figure 5.17 Effect of shaking the tube for 10 min after the magnetic beads were suspended in washing buffer. Probe-2 was constructed with Probe-R and 19 n.t. target hybridization oligonucleotide. The 30 pM BPDE-*p53*-exon7 was mixed with 2 µg of denatured genomic DNA and magnetic beads followed by incubation. Real-time qPCR experiments were carried out in triplicate and values are expressed as mean ± SD.

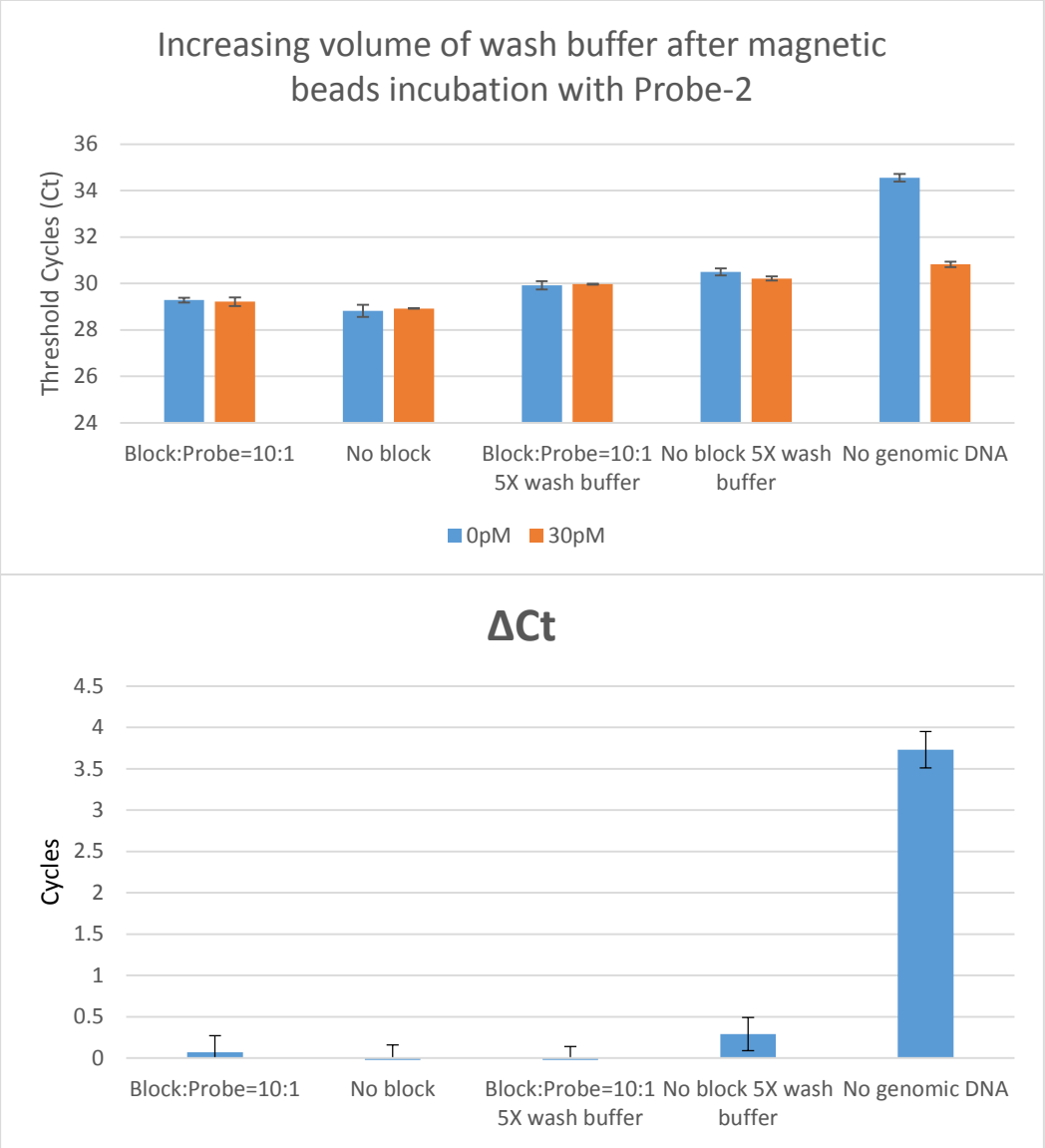

Figure 5.18 Effect of a large volume of washing buffer after incubation of Probe 2 with magnetic beads. Probe-2 was constructed with Probe-R and 19 n.t. target hybridization oligonucleotide. The 30 pM BPDE-*p53*-exon7 was mixed with 2 µg of denatured genomic DNA and magnetic beads followed by incubation. Real-time qPCR experiments were carried out in triplicate and values are expressed as mean ± SD.

5.3.3 Development of a solid-phase extraction step to remove genomic DNA

The homogeneous BINDA assay was not able to reduce interference from genomic DNA. A partially optimized magnetic bead-mediated BINDA assay was able to detect BPDE-*p53*-exon7 in double-stranded genomic DNA but was not able to achieve its detection in denatured genomic DNA (single-stranded). Therefore, an extra step of the BPDE-*p53*-exon7 extraction from genomic DNA was required to achieve detection in denatured genomic DNA (Figure 5.1).

Initially, both the 19 n.t. and the 27 n.t. target hybridization oligonucleotides were conjugated on the magnetic beads to test the extraction efficiency (Figure 5.19). The extracted BPDE-*p53*-exon7 was analyzed by the magnetic bead-mediated BINDA assay. The magnetic beads used to extract the BPDE-*p53*-exon7 were discarded after the BPDE-*p53*-exon7 was released from the beads; however, the genomic DNA may also be released from the beads, increasing the background signal. A control group using the same extraction beads without genomic DNA was used to investigate the possible interference of released genomic DNA from the beads.

The results from four samples showed similar ΔCt confirming that there was no interference from genomic DNA released from the extraction magnetic beads during the extraction. The result also demonstrated that the 19 n.t. and 27 n.t. target hybridization oligonucleotides had similar binding efficiency for BPDE-*p53*-exon7, which was consistent with the results from optimizing the length of target hybridization oligonucleotide. In the following experiments, 19 n.t. target hybridization oligonucleotides were conjugated to the extraction magnetic beads.

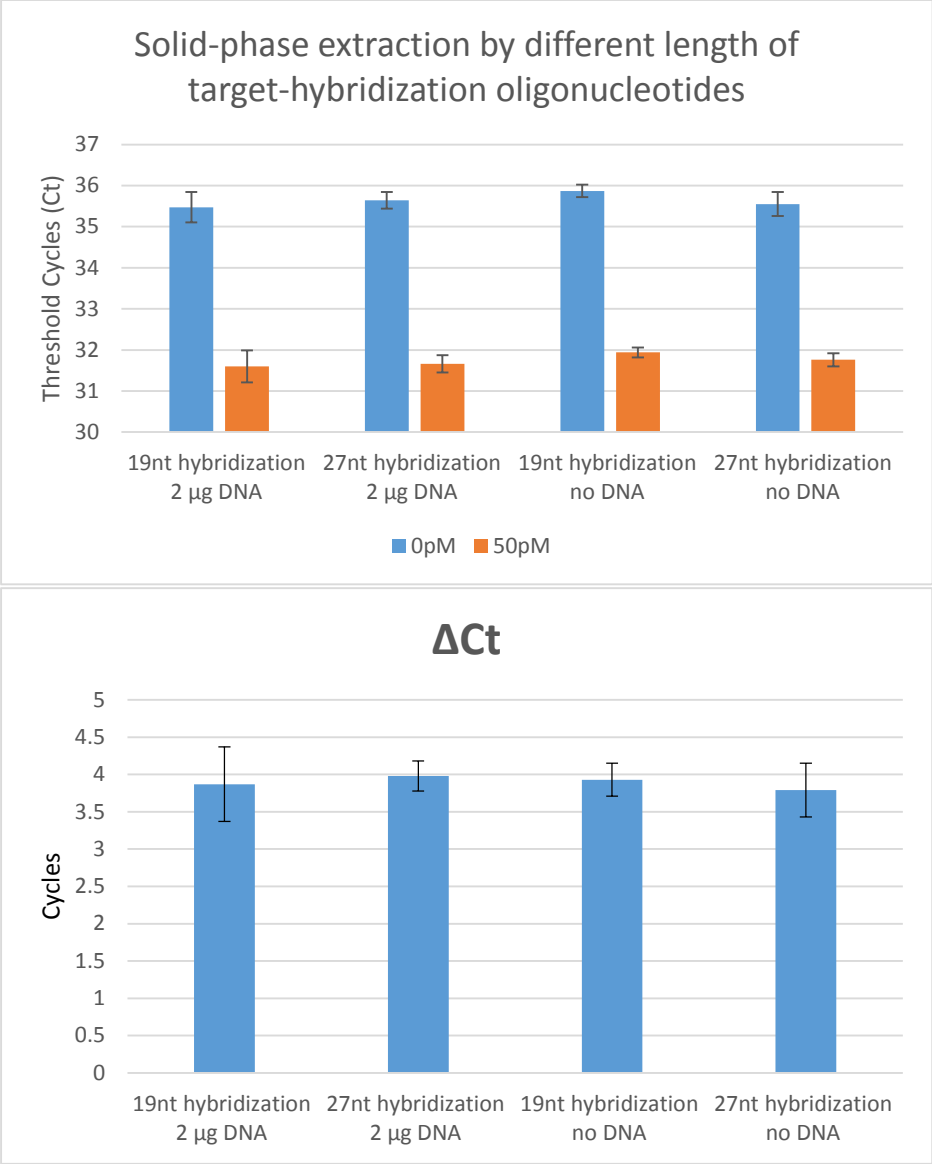

Figure 5.19 Solid phase extraction using different lengths of target hybridization oligonucleotides. Real-time qPCR experiments were carried out in triplicate and values are expressed as mean ± SD.

Longer denaturation time under alkaline conditions might increase the denaturation efficiency but might also decompose the BPDE-*p53*-exon7 adducts. Therefore, optimization for the denaturation of the 19 n.t. and BPDE-*p53*-exon7

hybrid under alkaline conditions was also studied (Figure 5.20). The same concentration of BPDE-*p53*-exon7 was directly analyzed by the assay without the extraction step to compare the extraction efficiency. Figure 5.20 showed that the difference between the three different time points for denaturation was small (ΔCt < 1 cycle). According to Equation (2) in Chapter 4, the extraction efficiencies were 100.6%, 100.0%, 101.5%, and 102.0% for 5 min, 10 min, 20 min, and 20 min without genomic DNA, respectively. The results showed similar efficiencies for the three time points and the genomic DNA interference was minimal. A denaturation time of 10 min was used in the following experiments.

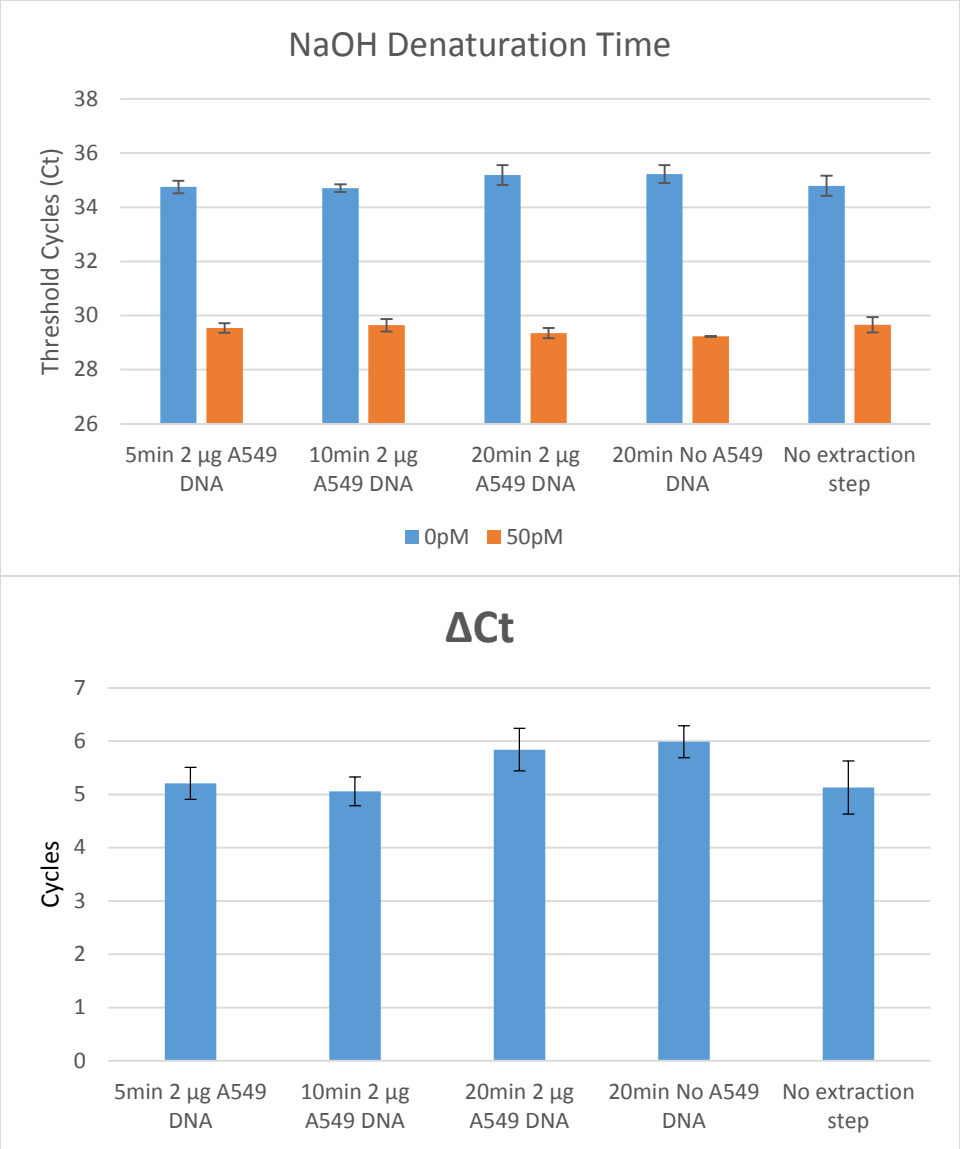

Figure 5.20 Effect of denaturation time in 0.1 M NaOH. Three time points were used: 5 min, 10 min, and 20 min. The sample without genomic DNA was added to examine the genomic DNA interference during the extraction process. The sample without the extraction step was used to calculate the extraction efficiency. Real-time qPCR experiments were carried out in triplicate and values are expressed as mean ± SD.

5.3.4 Coupling of solid-phase extraction with BINDA assays

After development of the solid-phase extraction method, both the homogeneous BINDA assay and the magnetic bead-mediated BINDA assay were used for the analysis of BPDE-*p53*-exon7 adducts in denatured genomic DNA. Four different formats of magnetic bead-mediated BINDA (Figure 5.21) and two formats of homogeneous BINDA (Figure 5.2) were coupled with the solid-phase extraction to detect 50 pM BPDE-*p53*-exon7 in 2 μg denatured genomic DNA (Figure 5.22).

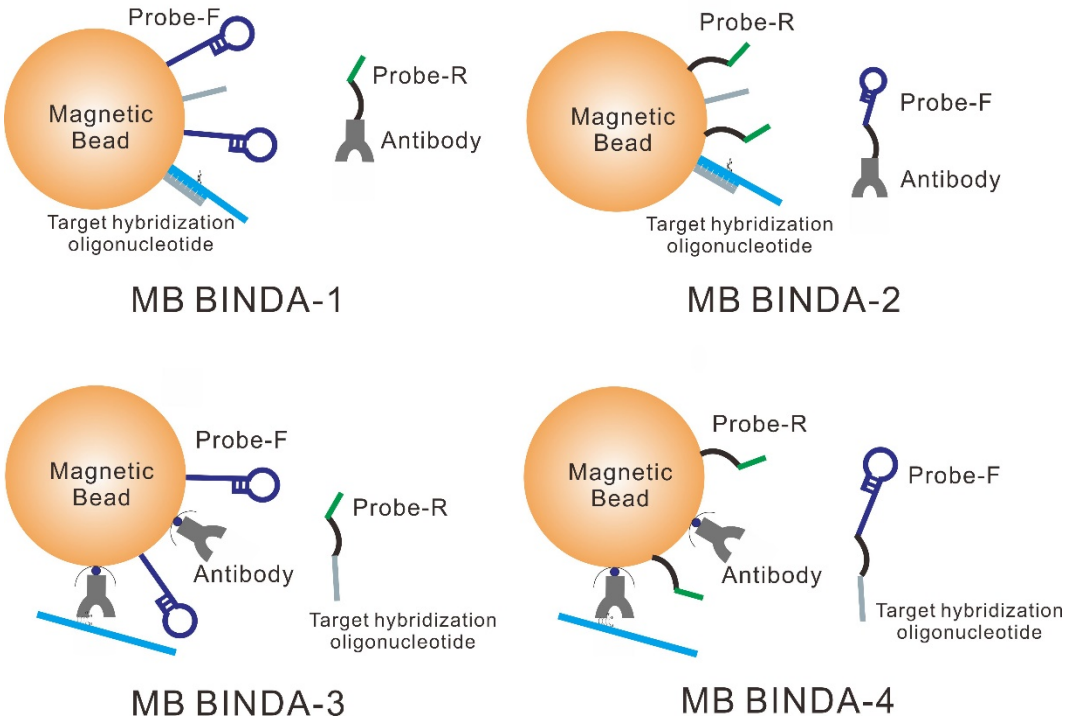

Figure 5.21 Construction of different magnetic beads for different BINDA assay formats. (A) MB BINDA-1: Magnetic bead is conjugated with Probe-F and target hybridization oligonucleotide. Probe-R is in solution and conjugated with BPDE antibody. (B) MB BINDA-2: Magnetic bead is conjugated with Probe-R and target hybridization oligonucleotide. Probe-F is in solution and conjugated with BPDE antibody. (C) MB BINDA-3: Magnetic bead is conjugated with Probe-F and BPDE antibody. Probe-R is in solution and conjugated with target hybridization oligonucleotide. This is the magnetic bead used in Chapter 4. (D) MB BINDA-4: Magnetic bead is conjugated with Probe-R and BPDE antibody. Probe-F is in solution and conjugated with target hybridization oligonucleotide.

Compared to homogeneous BINDA, the magnetic bead-mediated BINDA assay provided much higher ΔCt for the same concentration of target. Among the four formats of magnetic bead-mediated BINDA assays, MB BINDA-2 performed slightly better than the other three formats. The MB BINDA-2 was used to determine the dynamic range and detection limit of the assay in 10 µg denatured A549 DNA (Figure 5.22). A detection limit of less than 1 pM and a dynamic range from 0.5 pM to 250 pM was obtained. A higher concentration of genomic DNA did not compromise the extraction efficiency. High concentration of *p53*-exon7 (10 nM) was included and the specificity of the assay was demonstrated.

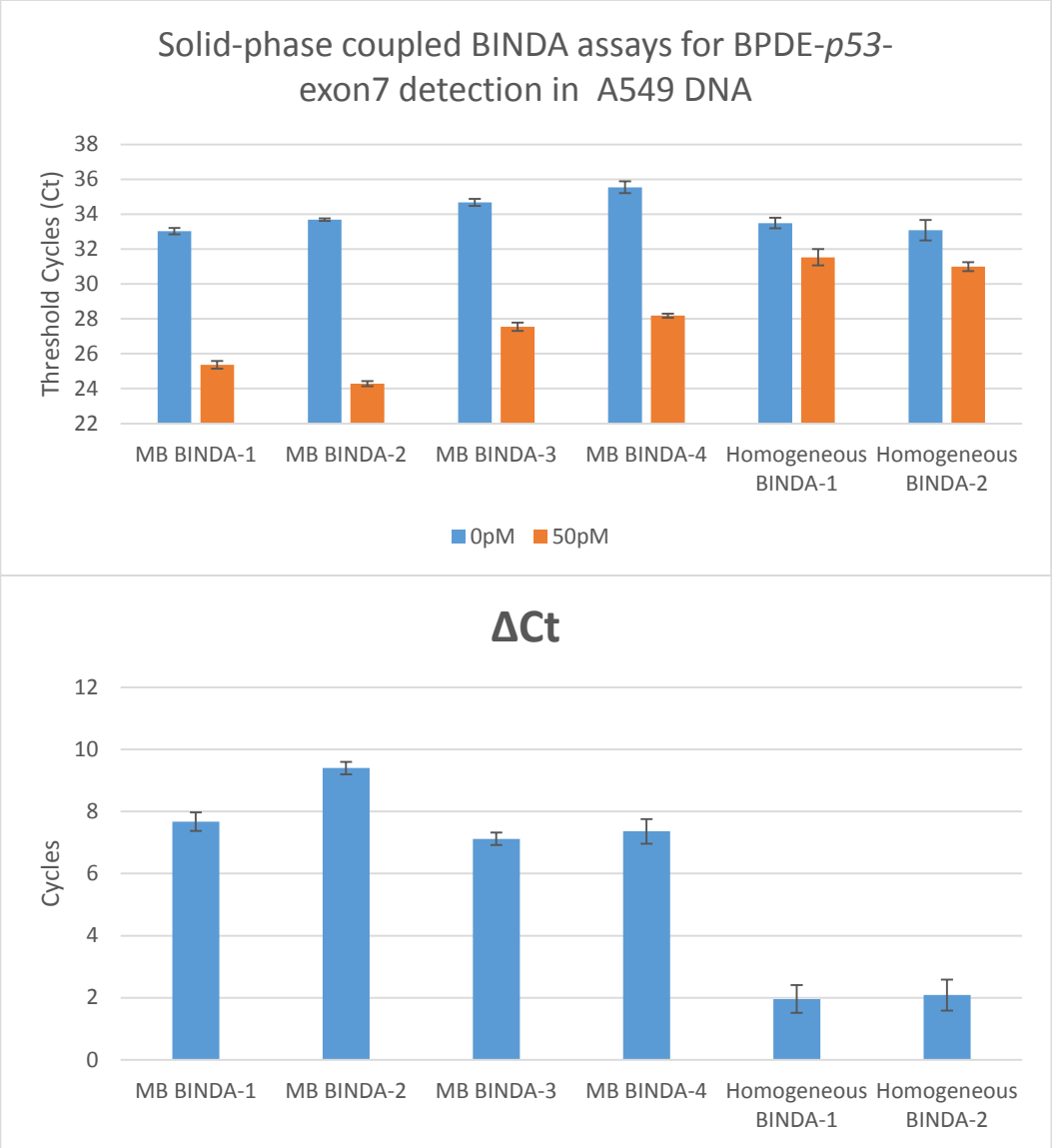

Figure 5.22 Coupling of solid phase extraction to BINDA assays for BPDE-*p53*-exon7 analysis in A549 DNA. The 50pM BPDE-*p53*-exon7 in 2 µg denatured genomic DNA was used as the target sample. Real-time qPCR experiments were carried out in triplicate and values are expressed as mean ± SD.

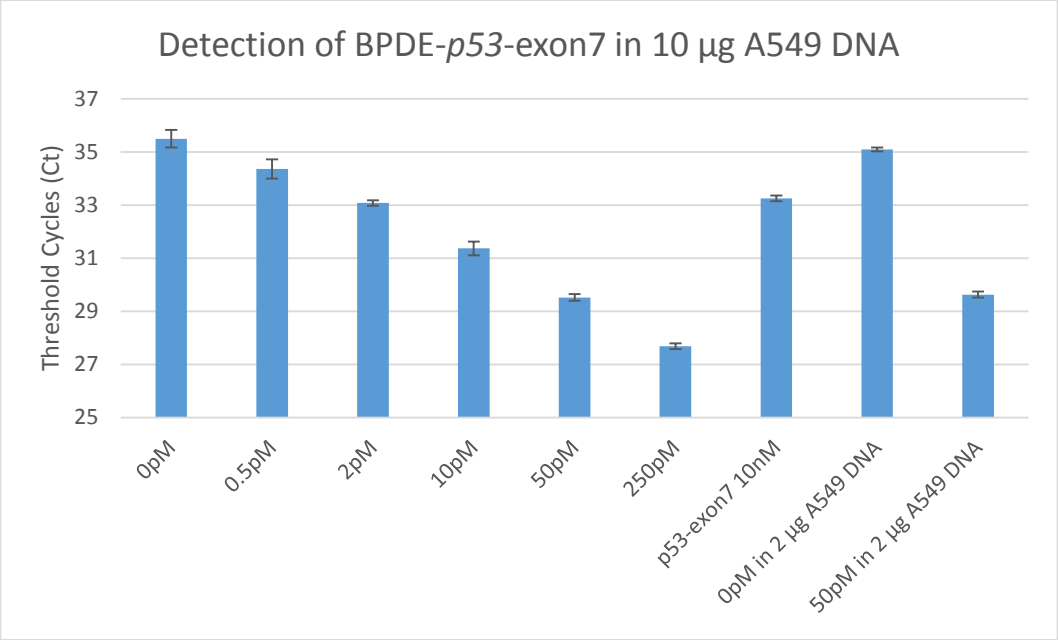

Figure 5.23 Dynamic range of solid phase extraction-coupled MB BINDA-2 assay for BPDE-*p53*-exon7 analysis in 10 µg denatured A549 DNA. Real-time qPCR experiments were carried out in triplicate and values are expressed as mean ± SD.

5.4 Conclusions

In this chapter, the homogeneous BINDA assay and magnetic bead-mediated BINDA assay, developed in Chapter 3 and Chapter 4, were used to detect BPDE-*p53*-exon7 adducts in genomic DNA. The homogeneous BINDA was not able to reduce the interference from genomic DNA and differentiate the BPDE-*p53*-exon7 from the background signal. The magnetic bead-mediated BINDA assay was able to detect BPDE-*p53*-exon7 in double-stranded genomic DNA. However, it could not detect BPDE-*p53*-exon7 in denatured genomic DNA because the genomic DNA non-specifically adsorbed onto the magnetic bead surface and induced target-independent DNA assembly between Probe-F and Probe-R. The

target-independent DNA assembly resulted in high background.

To overcome the interference from denatured genomic DNA adsorbed on the magnetic bead surface, an extra step utilizing solid-phase extraction for BPDE-*p53*-exon7 was incorporated. Another magnetic bead conjugated with the complementary sequence of the target was used to capture the BPDE-*p53*-exon7 The captured BPDE-*p53*-exon7 was then released under alkaline conditions. The released BPDE-*p53*-exon7 could then be analyzed by the BINDA assay.

The coupling of solid-phase extraction with magnetic bead-mediated BINDA assay showed a wide dynamic range (0.5 pM to 250 pM) and low detection limit (less than 1 pM) for the detection of BPDE-*p53*-exon7 in a large amount of denatured genomic DNA. This new assay also provided good specificity as it did not generate a signal for a very high concentration of undamaged *p53*-exon7.

5.5 References

1. International Human Genome Sequencing Consortium, Finishing the euchromatic sequence of the human genome, *Nature* **431**, 931–945 (2004).

Chapter Six

Detection of BPDE-*p53*-exon7 adducts in BPDE-treated cells

6.1 Introduction

In Chapter 5, coupling of solid-phase extraction with magnetic bead-mediated BINDA assay was successfully developed for BPDE-*p53*-exon7 adducts in denatured genomic DNA. This assay will be used for the final goal of the thesis: detection of BPDE-*p53*-exon7 from cells.

In this chapter, we demonstrate the applicability of the assay for real sample analysis by detecting BPDE-*p53*-exon7 from BPDE-treated cells. A549 lung carcinoma cells were treated with three different concentrations of BPDE. After treatment, the cells were lysed and the genomic DNA was extracted. The genomic DNA was then digested by four restriction endonucleases to generate BPDE-*p53*-exon7 and smaller DNA fragments (Figure 6.1 A). Using the magnetic bead solid-phase extraction procedures (Figure 6.1 B-E), the released BPDE-*p53*-exon7 was analyzed by magnetic bead-mediated BINDA assay.

The percentage of adducted *p53*-exon7 could be calculated from the amount of BPDE-*p53*-exon7 divided by the total *p53*-exon7 in treated cells. A dose-damage correlation was obtained through the three BPDE concentration treatments.

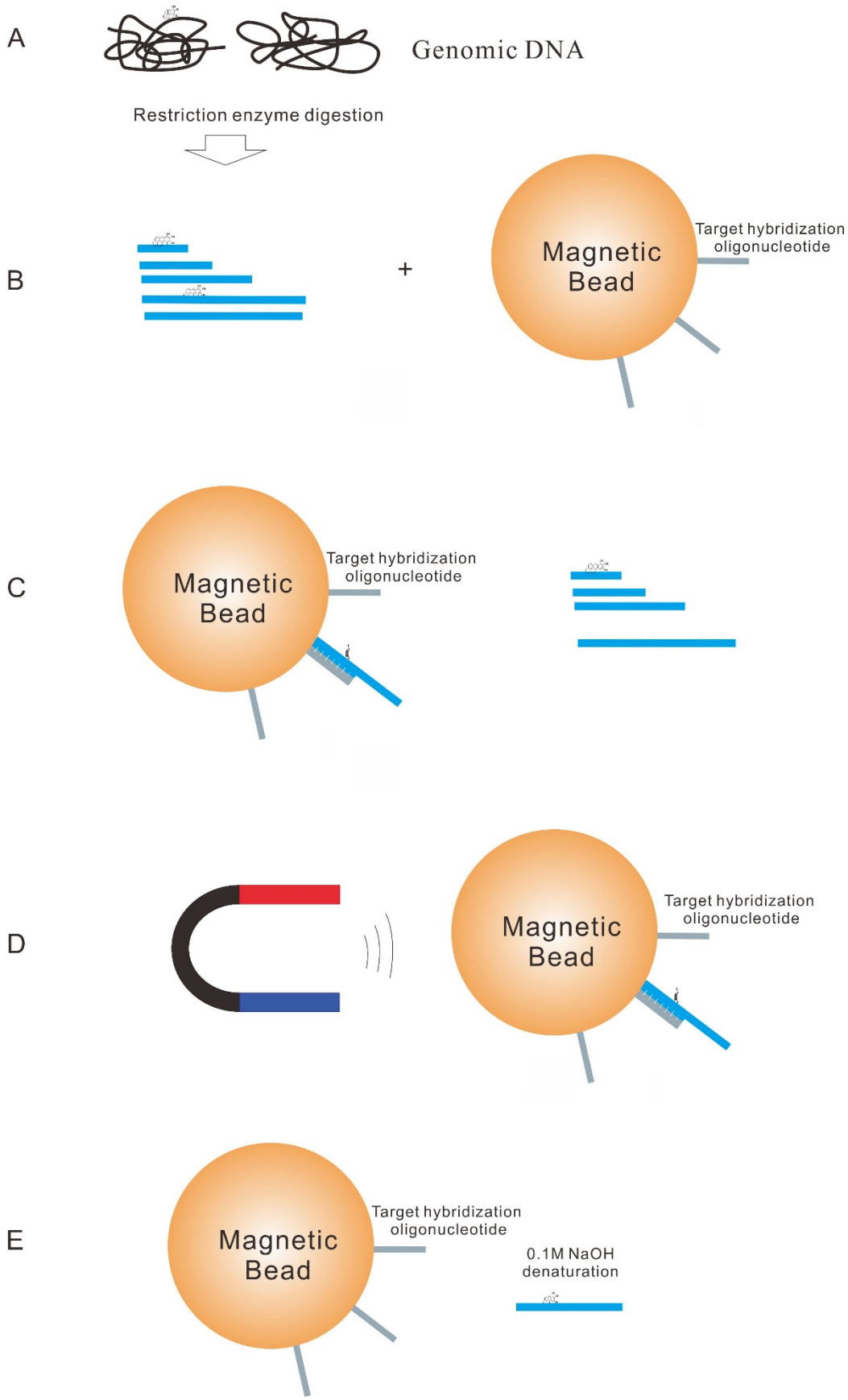
A
Genomic DNA
Restriction enzyme digestion
B
+
Magnetic Bead
Target hybridization oligonucleotide
C
Magnetic Bead
Target hybridization oligonucleotide
D
Magnetic Bead
Target hybridization oligonucleotide
E
Magnetic Bead
Target hybridization oligonucleotide
0.1M NaOH denaturation

Figure 6.1 Schematic for the extraction of BPDE-*p53*-exon7 adducts from cells treated with BPDE. (A) The genomic DNA was digested by four restriction enzymes. (B) Magnetic beads for solid-phase extraction were incubated with the digested genomic DNA. (C) BPDE-*p53*-exon7 was captured by the solid-phase extraction magnetic beads. (D) Other fragments of DNA sequences were removed by magnetic separation. (E) BPDE-*p53*-exon7 was released from the extraction magnetic beads.

6.2 Experimental

6.2.1 Reagents and instruments

(±)-*anti*- Benzo[a]pyrene diol epoxide (BPDE) (MRI No. 477) was supplied by the National Cancer Institute Chemical Carcinogen Reference Standard Repository (Midwest Research Institute, Kansas City, MO). Anhydrous tetrahydrofuran (THF, Cat. No. 401757, ≥99.9%), triethylamine (TEA, Cat. No. 471283, ≥99.5%), and bovine serum albumin (Cat. NO. A7906) were obtained from Sigma-Aldrich (Oakville, ON). Anti-BPDE antibody clone 8E11 (Cat. No. 4360-MC-100) was purchased from Trevigen (Gaithersburg, MD). Biotin-XX microscale protein labeling kit (Cat. No. B30010), Platinum® qPCR SuperMix UDG (Cat. No. 11730), T4 DNA Ligase (Cat. No. 15224), and T4 Polynucleotide Kinase (Cat. No. 18004) were purchased from Invitrogen (Carlsbad, CA). Phosphate buffered saline (10×PBS) and NaOH stock solution (5N) were purchased from Fisher Scientific (Nepean, ON) and were diluted to 1×PBS (137 mM NaCl, 10 mM phosphate, 2.7 mM KCl, pH 7.4) and 0.1 M NaOH by

deionized water, respectively. Tween 20 (Cat. No. BP337500) was also purchased from Fisher Scientific. All other reagents were of analytical grade.

Streptavidin-coupled Dynabeads MyOne C1 (Cat. No. 65001) and DynaMag-Spin Magnet (Cat. No. 12320D) were purchased from Invitrogen Dynal AS (Oslo).

The oligonucleotides (except the TaqMan probe) were custom synthesized, labeled, and purified by Integrated DNA Technologies (IDT, Coralville, IA).

RPMI 1640 with L-glutamine (Cat. No. 11875-093), Penicillin-Streptomycin Solution (10,000 U/mL, Cat. No. 15140-122), fetal bovine serum US Source (Cat. No. 26140-079), and trypsin-EDTA (0.05%, Cat. No. 25300-062) were purchased from Gibco (Burlington, ON). Cellular DNA was extracted by Qiagen DNeasy Blood & Tissue Kit (Cat. No. 69504). The concentrations of genomic DNA were measured by absorption at 260 nm on a NanoVue instrument (GE, Fairfield, CT).

Endonuclease restriction enzymes Hind III (Cat. No.15207-012) and BamH I (Cat. No. 15201-023) were purchased from Invitrogen. CviQ I (Cat. No. R0639) and Bbs I (Cat. No. R0539) were purchased from New England BioLabs Canada (Whitby, ON). All these restriction enzymes are not sensitive to CpG, dam, or dcm methylation.

6.2.2 Cell culture, BPDE treatment and genomic DNA extraction

The lung carcinoma cell line A549 (biosafety level 1) was used in this study. The cells were cultivated in RPMI 1640 supplemented by 10% FBS, 2 mM L-glutamine and 50 U/mL of penicillin and streptomycin. The cells were seeded in 150 mm dishes at a density of 5×10^6 cells per dish and maintained at 37 °C in

humidified air containing 5% CO_2. The cells were grown to approximately 90 % confluence for treatments.

The cells were washed three times with PBS before treatment. BPDE stock solution (10 mM) was freshly prepared by dissolving the powder in 95% THF and 5% TEA. To achieve the final concentration of 1 μM, 5 μM, and 25 μM BPDE in culture medium, 3 μL, 15 μL, and 75 μL of the BPDE stock solution were added to 30 mL of serum-free medium in each dish. Final concentrations of THF/TEA in media were below 0.25%. Control group cells were treated with 0.25% THF/TEA and placed in the incubator for 2 h.

After 2 h treatment, the cells were washed three times by PBS. To harvest the cells, 3 mL of 1×trypsin was added to each dish. After 3 min digestion, 6 mL of cell medium was added to neutralize the trypsin. Cells were collected by centrifugation at 500×g followed by washing with 1× PBS three times.

Cellular DNA was extracted by the Qiagen DNeasy Blood & Tissue Kit standard procedure. Concentrations of genomic DNA were measured by absorption at 260 nm on a NanoVue instrument.

6.2.3 Analysis of BPDE-*p53*-exon7 adducts from extracted genomic DNA by solid-phase extraction-coupled magnetic bead-mediated BINDA assay

Five hundred micrograms genomic DNA was digested by four restriction endonucleases: Hind III, BamH I, CviQ I, and Bbs I. The digestion reaction was carried out at room temperature for 8 h in NEB buffer 2 and 1×BSA. After digestion, the enzymes were deactivated at 65˚C for 20 min. To denature the digested genomic DNA, the tube was placed in a 95˚C water bath for 15 min

followed by chilling on ice for 30 min.

To generate a standard curve for absolute quantification, different concentrations of BPDE-*p53*-exon7 were spiked into 500 µL of genomic DNA elution buffer. The BPDE-*p53*-exon7 spiked samples were analyzed by the same procedures as the digested and denatured cellular genomic DNA samples.

The extraction magnetic beads were added to the denatured genomic DNA. The tube was placed in a mixer to avoid magnetic bead precipitation. After 30 min incubation at room temperature, the aqueous solution was removed by magnetic separation and the beads were washed 3 times by 1×PBS containing 0.01% Tween 20. The beads were then treated with 30 µL 0.1 M NaOH to release captured BPDE-*p53*-exon7 adducts. The 30 µL NaOH solution was collected and neutralized by equal concentration of 0.1 M HCl. The 60 µL 0.05 M NaCl solution obtained was finally applied to the magnetic bead-mediated BINDA assay for quantification of BPDE-*p53*-exon7 adducts.

6.3 Results and Discussion

For absolute quantification of BPDE-*p53*-exon7 adducts from cellular samples, a standard curve was first generated (Figure 6.2). The standard curve was generated as follows: BPDE-*p53*-exon7 was added to the DNA elution buffer for genomic DNA extraction. The BPDE-*p53*-exon7 containing buffer then went through the same procedure as the solid-phase extraction for cellular DNA samples. The released BPDE-*p53*-exon7 was finally analyzed by the magnetic bead-mediated BINDA assay.

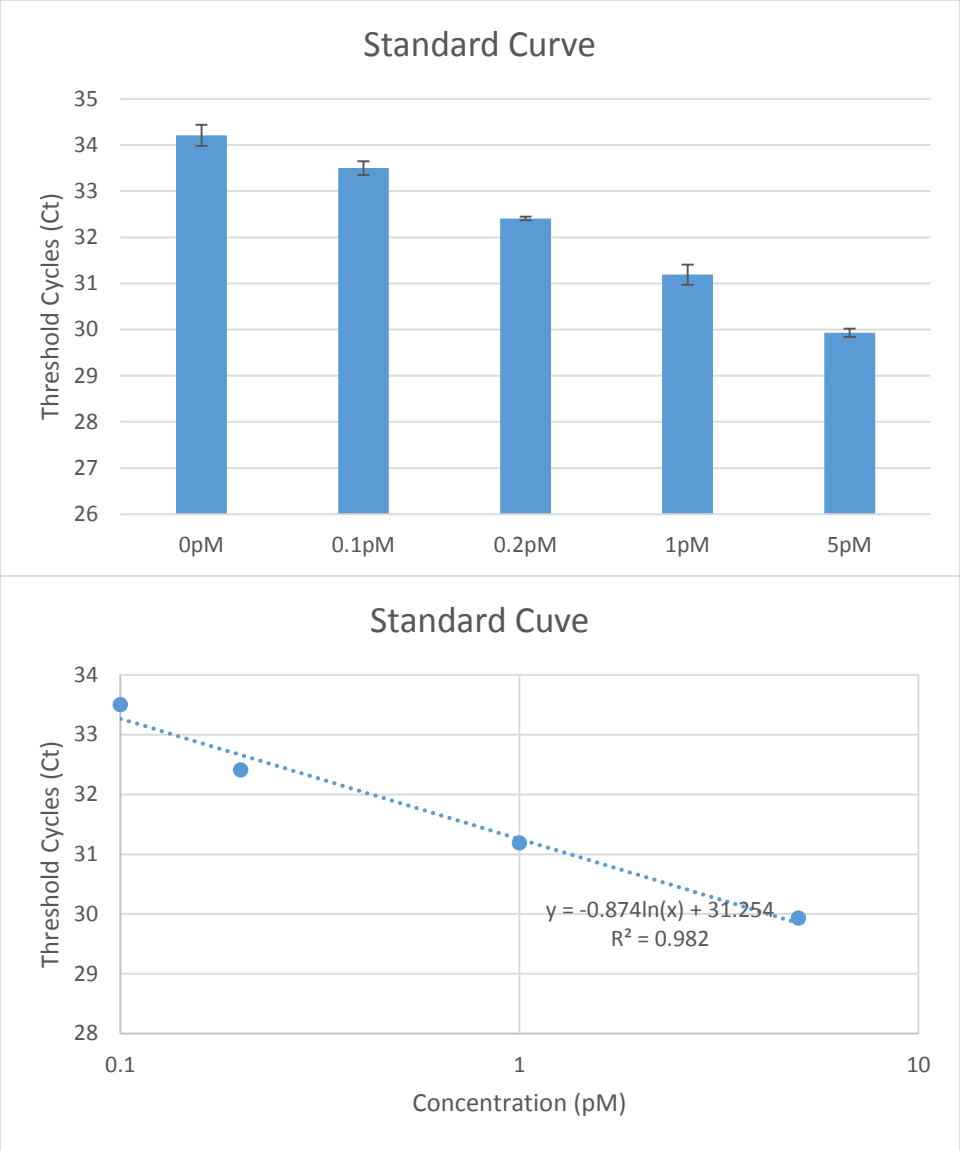

Figure 6.2 Standard curve generated by synthesized BPDE-*p53*-exon7. BPDE-*p53*-exon7 was spiked into the buffer. After using the same procedures for extraction as the cellular DNA samples, the released BPDE-*p53*-exon7 was analyzed by the magnetic bead-mediated BINDA assay. Real-time qPCR experiments were carried out in triplicate and values are expressed as mean ± SD.

Three different concentrations of BPDE were chosen for cell treatment (Figure 6.3). Due to the detection limit of our assay, determined in Chapter 5, the lowest concentration used in this study was 1 µM which is commonly used in research of BPDE-caused DNA damage (*1–4*). Using the standard curve, the number of BPDE-*p53*-exon7 molecules in cells treated with 1 µM, 5 µM, and 25 µM BPDE was 1.9 ± 0.5 $\times 10^7$, 8.3 ± 0.3 $\times 10^7$, and 19.5 ± 3.0 $\times 10^7$, respectively. Approximately 5×10^7 cells were included in each sample for the magnetic bead-mediated BINDA assay. Since there are two copies of *p53* genes in each cell, the total copy number of *p53*-exon7 molecules would be 10^8. Therefore, the percentage of BPDE-adducted *p53*-exon7 was 19 ± 5%, 83 ± 3%, and 195 ± 30% for 1 µM, 5 µM, and 25 µM BPDE treatment, respectively.

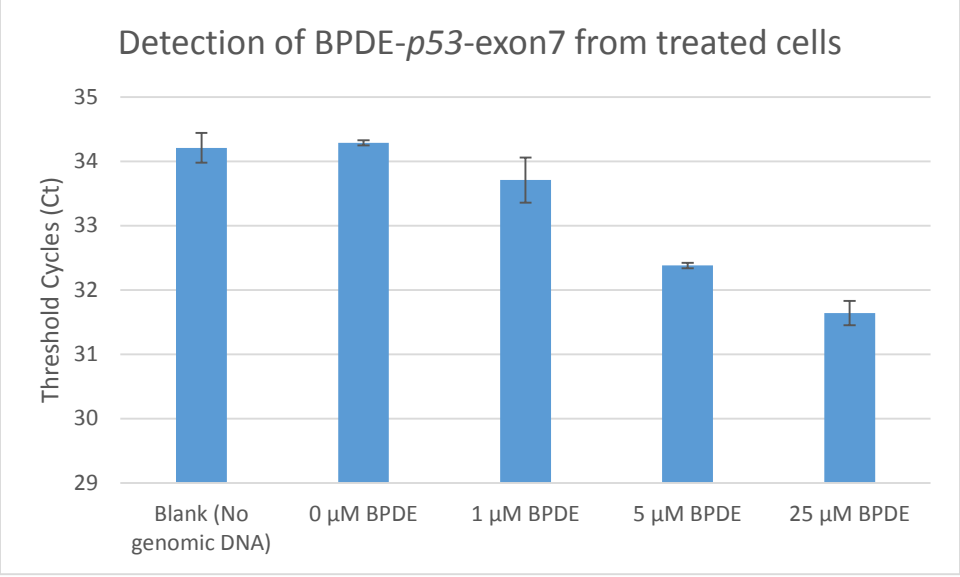

Figure 6.3 Analysis of A549 cells treated with three different concentrations of BPDE: 1 µM, 5 µM, and 25 µM. Real-time qPCR experiments were carried out in triplicate and values are expressed as mean ± SD.

The dose-response is represented in Figure 6.4. The percentage of BPDE-adducted *p53*-exon7 in 25 µM treated cells was more than 100%. One possible reason for this is the formation of multiple adducts on a single *p53*-exon7 sequence. In magnetic bead-BINDA-2 (Figure 5.21 B), the binding of one BPDE-adducted *p53*-exon7 to a magnetic bead will trigger multiple DNA assemblies between Probe-F and Probe-R, generating more than one assembled DNA for signal output. It could be concluded from Figure 6.4 that most *p53*-exon7 formed adducts with BPDE under a high concentration of BPDE (> 5 µM).

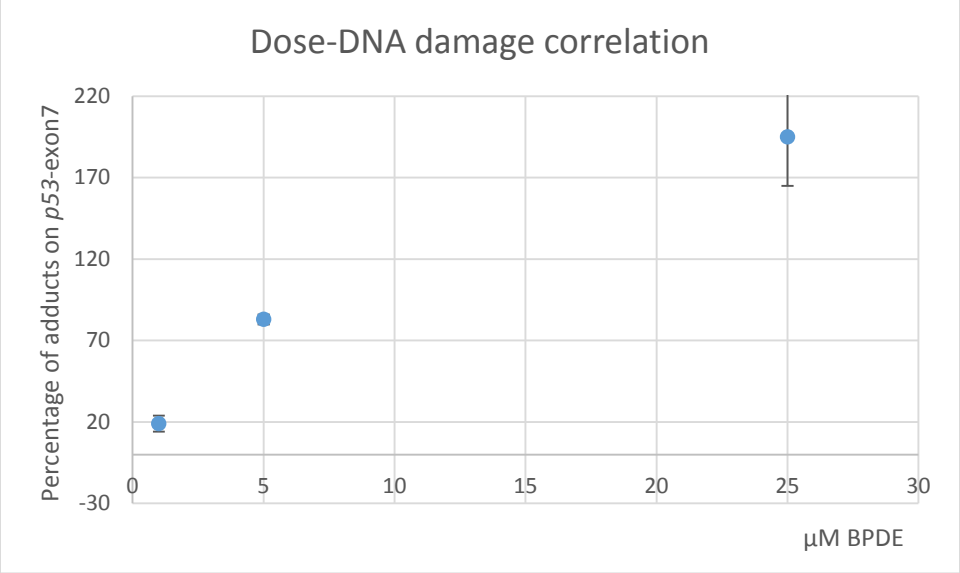

Figure 6.4 BPDE dose-DNA damage correlation. Real-time qPCR experiments were carried out in triplicate and values are expressed as mean ± SD.

6.4 Conclusions

By applying solid-phase extraction coupled with magnetic bead-mediated BINDA assay, the BPDE-DNA adduct formed on *p53*-exon7 was successfully

detected. A dose dependent DNA damage response was obtained by using three different concentrations of BPDE to treat the cells. The lowest concentration of BPDE (1 μM) treatment in this study resulted in 19 ± 5% of the total *p53*-exon7 forming adducts.

This demonstrated that the assay could potentially be used for detecting BPDE-DNA adducts in real samples such as blood and tissue. This assay provided quantitative information on the BPDE-DNA adducts on specific sequences, which is more informative when predicting the possibility of developing a cancer.

Detection of BPDE-DNA adducts using this assay is not limited to the sequence *p53*-exon7; it could be used to detect adducts formed on other important genes, such as *ras* (*5*). To apply the assay for other DNA sequences, the target hybridization sequences need to be designed as discussed in Chapter 3.

6.5 References

1. H. Wang, M. Lu, N. Mei, J. Lee, M. Weinfeld, X. C. Le, Immunoassays using capillary electrophoresis laser induced fluorescence detection for DNA adducts, *Anal. Chim. Acta* **500**, 13–20 (2003).

2. S. Shen, J. Lee, X. Sun, H. Wang, M. Weinfeld, X. C. Le, Elevation of Cellular BPDE Uptake by Human Cells: a Possible Factor Contributing to Co-carcinogenicity by Arsenite, *Environ. Health Perspect.*, 1832–1837 (2006).

3. D. L. Busbee, C. O. Joe, J. O. Norman, P. W. Rankin, Inhibition of DNA synthesis by an electrophilic metabolite of benzo[a]pyrene, *Proc. Natl. Acad. Sci. U. S. A.* **81**, 5300–4 (1984).

4. M. F. Denissenko, A. Pao, M. Tang, G. P. Pfeifer, Preferential Formation of Benzo[a]pyrene Adducts at Lung Cancer Mutational Hotspots in P53, *Science* **274**, 430–432 (1996).

5. M. Malumbres, M. Barbacid, RAS oncogenes: the first 30 years, *Nat. Rev. Cancer* **3**, 459–465 (2003).

Chapter Seven

Conclusions and Synthesis

7.1 Introduction

DNA is crucial for managing normal cell function, including protein synthesis, cellular signaling, and synthesis of metabolites. However, DNA molecules are susceptible to many damaging factors: spontaneous reactions (*1*), endogenous metabolites (*2*), and exogenous physical and chemical agents. Many biological mechanisms have evolved to repair the damage so that the integrity of DNA can be maintained (*3*). It has been suggested that the somatic mutations in cancer genomes might be the consequence of these damaging factors (*4*, *5*). The *p53* gene is one of the most studied genes in somatic cancers (*6*); of its 393 codons, a small number are frequently mutated (Figure 1.1).

Benzo[a]pyrene diol epoxide (BPDE) (a metabolite of benzo[a]pyrene, BP) is a potent carcinogen. Due to its highly electrophilic nature (*7*), BPDE can covalently bind to the N2 position of the guanine base and thus distort DNA structure (*8*). The hotspots of BPDE adduct formed on the *p53* gene were elucidated by Pfeifer and coworkers (*9*). Their investigation showed the similarity of BPDE-*p53* adduct hotspots to those of lung cancer mutation hotspots in the cancer database. In addition, DNA adducts of other polycyclic aromatic hydrocarbons (PAHs) also showed similar adduct profiles to those of BPDE-DNA adducts in *p53* (*10*), suggesting these PAH-DNA adducts might be a direct cause of many cancers. PAH-DNA adducts may serve as good biomarkers for cancer risk assessment.

BPDE-DNA adducts have long been used as a biomarker to monitor human exposure to this carcinogen. However, currently available quantitative analytical methods developed for BPDE-DNA adducts are not able to provide information on which genes or sequences these adducts are formed. Because the genome consists of more than 98% non-coding regions, it is important for better cancer risk assessment to have the capability to specifically quantify the BPDE-adducts that are formed on the functional genes, such as *p53*.

Recently, a set of bio-analytical assays based on the principle of binding induced DNA assembly (BINDA) have been widely applied for protein detection (Section 1.4). They have the advantage of high sensitivity and specificity using dual-recognition strategy. While BINDA assays for protein detection are well-developed, the application of BINDA to DNA adducts has not been demonstrated before this thesis. The BPDE-DNA adduct also consists of two epitopes: the BPDE molecule that can be used for antibody recognition and the DNA sequence that can be recognized by a complementary sequence. Therefore, it was rational to design and develop a BINDA-based assay for quantification and localization of the BPDE-DNA adducts in specific genes.

This thesis has focused on the development of a BINDA-based assay for quantification of BPDE-DNA adducts in specific genes. We have developed and demonstrated the assay using BPDE-*p53*-exon7 as a model system. A brief summary of the contribution of this research is described in the following section.

7.2 Significance of the thesis

The overall objective of this thesis is **to develop a BINDA assay that can quantify the BPDE-*p53*-exon7 adducts in cells**. To achieve this goal, the thesis includes five progressive experimental chapters.

In Chapter 2, a TaqMan-based BINDA assay was developed to broaden the application of the BINDA technique. Previous research has demonstrated sensitive detection of proteins using BINDA, converting the non-amplifiable target to amplifiable DNA. SYBR Green chemistry was used in previous BINDA assays. However, SYBR Green binds to all double-stranded DNA, thus SYBR Green based BINDA assay cannot be used in assays when other DNA is also present in addition to the designed DNA probes. **My research in Chapter 2 integrated TaqMan qPCR with the BINDA assay to enable the specific detection of the target DNA sequence without interference from other DNA sequences**. The TaqMan based BINDA assay was developed and demonstrated with streptavidin as the target and served as the model for further development.

In Chapter 3, the TaqMan based BINDA assay was developed to determine the synthesized BPDE-*p53*-exon7 adducts. The target BPDE-*p53*-exon7 adducts were synthesized based on the sequence of *p53*-exon7. This assay was optimized and demonstrated the successful detection of the synthesized BPDE-*p53*-exon7 adducts. **Chapter 3 demonstrated the proof-of-principle that the BINDA assay can sensitively determine BPDE-DNA adducts in a specific DNA sequence**.

To further improve the sensitivity and specificity of the BINDA assay for determination of BPDE-*p53*-exon7, my research in Chapter 4 explored a magnetic

bead-mediated BINDA assay. **Incorporation of magnetic beads with the BINDA assay enabled further improvement of the target binding on the surfaces of the beads and the combination with the washing step to dramatically reduce background**. Therefore, the magnetic bead-mediated BINDA assay offers an even lower detection limit than the homogeneous assays described in Chapter 3.

In light of the improvement in the detection limit using the magnetic bead-mediated BINDA assay, **in Chapter 5 I explored sample preparation using solid-phase extraction to remove/eliminate non-specific interference**. After solid phase extraction, the samples were determined using both types of BINDA assays for BPDE-*p53*-exon7 in the presence of genomic DNA.

In Chapter 6, the solid-phase extraction coupled with the magnetic bead-mediated BINDA assay was applied to determine the BPDE-*p53*-exon7 adducts in cells. Cellular genomic DNA was extracted and analyzed for the BPDE-*p53*-exon7 adducts. Therefore, quantification of DNA adducts in a specific gene can be achieved. This has not been demonstrated until this study.

The thesis contributed to the research in two aspects: (1) for the first time an assay for the quantification of BPDE-DNA adducts on a specific gene sequence is developed; (2) the applicability of BINDA assays for analysis of a broader range of macromolecules is demonstrated.

7.3 Conclusions and future research

In this thesis, a homogeneous BINDA was first developed for BPDE-*p53*-

exon7. To further improve the sensitivity and specificity, a magnetic bead-mediated BINDA assay for the BPDE-*p53*-exon7 was devised on the basis of homogeneous BINDA. To remove the strong interference from genomic DNA, a solid-phase extraction step was incorporated and successfully applied to the detection of BPDE-*p53*-exon7 from BPDE treated cells. The assay could reach a detection limit of 10^7 BPDE-*p53*-exon7 from treated cells.

The assay is not limited to the analysis of BPDE adducts or adducts formed on *p53*-exon7. It is suitable for detection of other adducts (e.g., pyrimidine (6-4) pyrimidone photoproducts), providing that affinity ligands, such as antibodies, are available for the specific adducts. With proper design of the target hybridization sequence, other important genes containing adducts could also be detected. Multiplexed assays for simultaneous analysis of different adducts or adducts on different genes could be realized using different pairs of Probe-F/R. This assay could be potentially used to investigate the mechanisms of the cellular DNA repair system, for example, the indirect carcinogenetic property of arsenic compounds (*11–13*). In this thesis, real-time qPCR was used for the quantification of assembled DNA Probes. However, many other signal output strategies could also be utilized, such as RCA and FRET. With a highly sensitive isothermal detection method, the assay could potentially be used to achieve in situ imaging and quantification of DNA adducts in the future.

BINDA assays utilize the high sensitivity of amplifiable DNA to detect other non-amplifiable molecules. This powerful strategy has stimulated the development of many ultrasensitive techniques for a wide range of

macromolecules, including proteins, protein–protein interactions and protein modifications, organelles, cells, and protein imaging in fixed cells and tissues (*14*). In this thesis, the strategy was expanded to the detection of DNA adducts. Landegren and coworkers successfully quantified 35 target proteins in a single tube using the DNA assembly strategy combined with PCR amplification and next-generation DNA sequencing (*15*), inspiring us towards a new direction of development of high-throughput analytical assays.

7.4 References

1. T. Lindahl, Instability and decay of the primary structure of DNA, *Nature* **362**, 709–715 (1993).

2. R. De Bont, Endogenous DNA damage in humans: a review of quantitative data, *Mutagenesis* **19**, 169–185 (2004).

3. J. H. J. Hoeijmakers, DNA damage, aging, and cancer, *N. Engl. J. Med.* **361**, 1475–85 (2009).

4. L. B. Alexandrov, S. Nik-Zainal, D. C. Wedge, S. A. J. R. Aparicio, S. Behjati, A. V. Biankin *et al.*, Signatures of mutational processes in human cancer, *Nature* **500**, 415–21 (2013).

5. M. R. Stratton, P. J. Campbell, P. A. Futreal, The cancer genome, *Nature* **458**, 719–24 (2009).

6. M. Olivier, M. Hollstein, P. Hainaut, Origins, Consequences, and Clinical Use, *Cold Spring Harb. Perspect. Biol.* **2**, 1–17 (2010).

7. D. L. Busbee, C. O. Joe, J. O. Norman, P. W. Rankin, Inhibition of DNA synthesis by an electrophilic metabolite of benzo[a]pyrene, *Proc. Natl. Acad. Sci. U. S. A.* **81**, 5300–4 (1984).

8. D. E. Volk, V. Thiviyanathan, J. S. Rice, B. A. Luxon, J. H. Shah, H. Yagi *et al.*, Solution Structure of a Cis-Opened(10R)-N6-Deoxyadenosine Adduct of (9S,10R)-9,10-Epoxy-7,8,9,10-tetrahydrobenzo[a]pyrene in a DNA Duplex, *Biochemistry* **42**, 1410–1420 (2003).

9. M. F. Denissenko, A. Pao, M. Tang, G. P. Pfeifer, Preferential Formation of Benzo[a]pyrene Adducts at Lung Cancer Mutational Hotspots in P53, *Science* **274**, 430–432 (1996).

10. L. E. Smith, M. F. Denissenko, W. P. Bennett, H. Li, S. Amin, M. Tang *et al.*, Targeting of Lung Cancer Mutational Hotspots by Polycyclic Aromatic Hydrocarbons, *J. Natl. Cancer Inst.* **92**, 803–811 (2000).

11. S. Shen, J. Lee, W. R. Cullen, X. C. Le, M. Weinfeld, Arsenite and its mono- and dimethylated trivalent metabolites enhance the formation of benzo[a]pyrene diol epoxide-DNA adducts in Xeroderma pigmentosum complementation group A cells, *Chem. Res. Toxicol.* **22**, 382–90 (2009).

12. S. Shen, J. Lee, M. Weinfeld, X. C. Le, Attenuation of DNA damage-induced p53 expression by arsenic: a possible mechanism for arsenic co-carcinogenesis, *Mol. Carcinog.* **47**, 508–18 (2008).

13. S. Shen, J. Lee, X. Sun, H. Wang, M. Weinfeld, X. C. Le, Elevation of Cellular BPDE Uptake by Human Cells: a Possible Factor Contributing to Co-carcinogenicity by Arsenite, *Environ. Health Perspect.*, 1832–1837 (2006).

14. H. Zhang, F. Li, B. Dever, C. Wang, X.-F. Li, X. C. Le, Assembling DNA through Affinity Binding to Achieve Ultrasensitive Protein Detection, *Angew. Chem. Int. Ed. Engl.* , 10698–10705 (2013).

15. Darmanis, R. Y. Nong, J. Vanelid, A. Siegbahn, O. Ericsson, S. Fredriksson *et al.*, ProteinSeq: high-performance proteomic analyses by proximity ligation and next generation sequencing, *PLoS One* **6**, e25583 (2011).